UNIVERSITÀ DELLA CALABRIA

UNIVERSITÀ DELLA CALABRIA

Dottorato di Ricerca in Scienze e Ingegneria dell'Ambiente, delle Costruzioni e dell'Energia

Department of Environmental and Chemical Engineering - DIATIC

REVERSE ELECTRODIALYSIS FOR ENERGY RECOVERY: MATERIAL DEVELOPMENT AND PERFORMANCE EVALUATION

Cycle: XXX

SSD: CHIM/07

PhD. Supervisor: Prof. Efrem Curcio

PhD. Coordinator: Prof. Salvatore Critelli

PhD. Candidate: Ahmet Halil Avcı

Date and place: 30.04.2018, Rende-Italy

ACKNOWLEDGEMENT

The financial support of The Education, Audiovisual and Culture Executive Agency – EACEA/European Commission within the "Erasmus Mundus Doctorate in Membrane Engineering – EUDIME" (ERASMUS MUNDUS Programme 2009-2013, FPA n. 2011-0014, SGA n. 2014-0970) is kindly acknowledged.

Contents

Summary

Reverse Electrodialysis for Energy Recovery: Material Development and Performance Evaluation

Salinity Gradient Power- Reverse Electrodialysis (SGP-RED), so-called blue energy, is a promising untapped membrane based renewable and sustainable energy generation technology. Salinity gradient energy can be defined as the energy reveals during the mixing of two solution having different concentration. Creating a controlled mixing in a RED stack gives the opportunity to transfer the mixing energy directly to electricity by redox reactions. Alternate arrangement of cation exchange membranes (CEM) and anion exchange membranes (AEM) form the required compartment design for controlled mixing. When high and low concentration solutions are fed from neighboring compartments, electrochemical potential difference of the solutions drive the ions from high to low concentrations. However, only charges opposite to membrane fixed charge can diffuse through, i.e. for an ideal membrane only cations can transport through CEM. Therefore, an ionic flux can be generated inside of the stack.

Understanding the fundamentals of the technology and the present challenges of SGP-RED is very important for the evaluation of the experimental study. Therefore, **Chapter 1** deals with the theory behind SGP-RED, potential of current state of art and challenges on performance and commercialization.

Most of the RED literature investigate RED performance by using artificial solutions that only contains NaCl. In **Chapter 2,** the effect of real river and seawater solutions (collected from river of Amantea, Italy) is experimentally investigated on lab-scale RED stack prototype. Different flow rates and temperature are studied to find an optimized condition. RED effluents are characterized to have a better understanding on transport mechanisms of monovalent and multivalent ions. Ion characterization results indicate multivalent ions tends to transport against their concentration gradient. Moreover, investigations on electrochemical properties concludes Mg^{2+} has the most severe effect on RED performance by causing an order of magnitude reduction on CEM conductivity.

After concluding drastic negative effect of Mg^{2+} on power generation in the second chapter, **Chapter 3** is dedicated to investigate broad range of magnesium content in mixing brine and seawater. Magnesium is known as second most abundant cation in the natural seawater solution and concentration varies from region to region. 0.5 and 4 molal solutions from 0 to 100 % Mg^{2+} content are tested in RED setup. Ionic characterization of outlet solution is completed to see effect of concentration on transport of ions. It is observed that uphill transport is limited to 0 – 30% of $MgCl_2$. Ohmic and non-ohmic resistance of the CEM and AEM characterized in the test solutions. Resistance characterization reveals that cation exchange membrane resistance is critically affected by Mg^{2+} concentration while resistance of AEM remains unaffected.

Due to RED is a non-commercialized technology, there is no commercial ion exchange membranes designed for RED. Therefore, most of the RED studies investigates electrodialysis (ED) membranes because of the similarity. In **Chapter 4**, cation exchange membranes are prepared considering the needs of RED. A well-known polymer, polysulfone, is sulfonated by chlorosulfonic acid to obtain negatively charged polymer. After the characterization of the polymer, CEMs are prepared with an asymmetric porous morphology by wet phase inversion method. Phase inversion parameters, e.g. solvent type, co-solvent ratio, are studied to optimize the membrane resistance and permselectivity. Among the prepared membranes, most promising one is further characterized for different NaCl concentration to estimate the power density. The results encourage to consider wet phase inversion method as a fabrication method for CEM.

Commercial cation exchange membranes are produced as dense homogeneous membranes by functionalized polymeric materials as standalone or into a support to have a mechanical stability. In **Chapter 5**, sulfonated polyethersulfone membranes are prepared by wet phase inversion and solvent evaporation method. In solvent evaporation method, polyethersulfone/sulfonated polyethersulfone blend ratio is optimized considering electrochemical and mechanical properties. In wet phase inversion, effect of co-solvent, evaporation time, coagulation bath composition and concentration are studied to optimize the membrane electrochemical properties. Best performing wet phase inversion membrane, solvent evaporation membrane with corresponding ion exchange capacity and a benchmark commercial membrane CMX (Neosepta, Japan) are characterized to estimate RED performance for different solution concentration. Competitive results point out the possibility of CEM production by wet phase inversion.

Chapter 6 is dedicated to conclude and discuss the achievements of the conducted work. In addition, some outlook for the future works was mentioned based on the deductions of the experimental work

Sommario

Elettrodialisi Inversa per il Recupero di Energia: nuovi materiali e prestazioni.

L'Elettrodialisi Inversa per la produzione di energia da Gradienti Salini (SGP-RED), o "*Blue Energy*", é una promettente e innovativa tecnologia a membrana che consente la generazione di energia rinnovabile ed eco-sostenibile. L'energia da gradienti salini é legata alla miscelazione di due soluzioni aventi diversa concentrazione: quando tale processo è condotto in modo controllato in un'unità RED, l'energia libera di miscelamento è convertita in elettricità tramite lo svolgimento di reazioni redox agli elettrodi. In particolare, l'alternanza di membrane a scambio cationico (CEM) e anionico (AEM) costituisce la soluzione tecnologica attraverso la quale si promuove un flusso controllato di cariche. Quando soluzioni ad alta e bassa concentrazione sono alimentate in due compartimenti adiacenti, la differenza di potenziale elettrochimico indirizza il flusso di ioni dal compartimento più concentrato (HCC) a quello più diluito (LCC). Tuttavia, la presenza di membrane permselettive consente la diffusione solo degli ioni aventi carica opposta (contro-ioni) rispetto alle cariche fisse della membrana: idealmente, le AEM (con cariche fisse positive) consentono esclusivamente il trasporto di anioni e, viceversa, le CEM (con cariche fisse negative) consentono esclusivamente il trasporto di anioni. In ultima analisi, la segregazione delle cariche genera, ai capi degli elettrodi, una differenza di potenziale.

La comprensione dei principi e dei limiti della tecnologia RED costituisce la premessa per l'impostazione dello studio sperimentale. Il **Capitolo 1** del presente lavoro di tesi analizza gli aspetti teorici alla base del processo RED, lo stato dell'arte e le sfide da affrontare per migliorare le attuali prestazioni della tecnologia e renderla commercializzabile.

In molti degli studi presenti in letteratura, le prestazioni della RED sono valutate rispetto a soluzioni artificiali di NaCl. Nel **Capitolo 2,** invece, si analizza sperimentalmente – su un prototipo RED in scala laboratorio – l'effetto di miscelazione di acqua di fiume e di acqua marina naturali (campionati da siti in Amantea, Italia) al fine di ottimizzare le condizioni operative rispetto a portata di alimentazione e temperatura. La caratterizzazione ionica delle correnti in uscita al modulo RED consente una migliore comprensione dei meccanismi di trasporto degli ioni monovalenti e multivalenti: i risultati indicano che gli ioni multivalenti tendono – in alcuni casi - ad essere trasportati contro il gradiente di concentrazione. Inoltre, le indagini sulle proprietà

elettrochimiche del sistema rivelano che gli ioni Mg^{2+} esercitano l'effetto più rilevante sulle prestazioni della RED, determinando una riduzione della conduttività delle CEM fino a un ordine di grandezza.

Acquisita l'evidenza dell'impatto negativo degli ioni Mg^{2+} sulla generazione di potenza in RED, il **Capitolo 3** è dedicato allo studio degli effetti determinati dal contenuto di magnesio in acqua di mare e in salamoia. Il magnesio é, per ordine di abbondanza, il secondo catione presente nelle acque di mare naturali, e la sua concentrazione varia con la localizzazione geografica. I risultati di test sperimentali in RED eseguiti su soluzioni 0.5 and 4 molali con contenuto di Mg^{2+} nell'intervallo 0-100%, e le successive caratterizzazioni delle correnti in uscita dal modulo, consentono di quantificare l'effetto della concentrazione sul trasporto delle specie cariche. In particolare si osserva che il trasporto contro gradiente di concentrazione (fenomeno noto come "uphill transport") è osservato solo entro l'intervallo 0–30% di $MgCl_2$. Inoltre, la caratterizzazione delle resistenze ohmiche e non-ohmiche delle membrane a scambio cationico e anionico mostra che la resistenza elettrica delle CEM è influenzata in maniera significativa dalla concentrazione di ioni Mg^{2+}, mentre la resistenza delle AEM ne rimane sostanzialmente inalterata.

Poiché ad oggi la tecnologia RED non é commercializzata, non sono disponibili sul mercato membrane a scambio ionico che siano progettate in maniera specifica per la RED. Di fatto, la maggior parte degli studi RED fa uso di membrane da elettrodialisi (ED). A tal proposito, nel **Capitolo 4**, l'attività sperimentale é rivolta alla preparazione di membrane a scambio cationico in vista del soddisfacimento dei requisiti della RED. Un polimero ampiamente utilizzato in commercio, il polisolfone, è solfonato mediante acido clorosolfonico al fine di innestare sulla struttura gruppi carichi negativamente. Una volta caratterizzato il polimero solfonato, le membrane CEM sono preparate mediante metodo d'inversione di fase per ottenere una morfologia asimmetrica. I diversi parametri operativi, quali il tipo di solvente, la quantità di co-solvente o il tipo di non solvente etc., sono studiati al fine di ottimizzare la resistenza e la permselettività della membrana. Tra le diverse membrane preparate, le più promettenti sono testate in soluzioni di NaCl per valutare la densità di potenza generata. I risultati incoraggianti indicano come il metodo d'inversione di fase possa essere utilizzato per la fabbricazione di membrane CEM.

Le membrane commerciali a scambio cationico possiedono una struttura densa e omogenea e sono realizzate a partire da materiali polimerici funzionalizzati utilizzati tal quale o integrati in supporti che conferiscono maggiore stabilità meccanica. Nel **Capitolo 5** si descrive la preparazione di

membrane di polietersolfone solfonato mediante inversione di fase in non-solvente oppure con evaporazione di solvente. In quest'ultimo caso, il blending polietersolfone/polietersolfone solfonato é ottimizzato rispetto alle proprietà elettrochimiche e meccaniche della membrana ottenuta. Nel caso di inversione di fase in non-solvente è investigato l'effetto del co-solvente, del tempo di evaporazione e dalla composizione del bagno di coagulo sulle proprietà elettrochimiche delle membrane. Le membrane che mostrano le prestazioni migliori - le cui capacità di scambio ionico sono comparabili con quelle di membrane commerciali CMX (Neosepta, Japan) - sono testate in RED; i risultati comparabili confermano la possibilità di produrre CEM via inversione di fase.

Infine, il **Capitolo 6** é dedicato alla ricapitolazione e alla discussione dei risultati più rilevanti ottenuti nel presente lavoro. In aggiunta, sulla base delle deduzioni del presente lavoro sperimentale, sono tracciate le prospettive di sviluppo della tecnologia RED.

Samenvatting

Omgekeerde Electrodialyse voor energie-terugwinning: Materiaalontwikkeling en prestatie-evaluatie

Zout-gradiënt stroom door middel van omgekeerde elektrodialyse (afgekort SGP-RED), zogenaamde Blue Energy, is een veelbelovende membraan-gebaseerde hernieuwbare en duurzame energie-generatie technologie. Zout gradiënt energie kan gedefinieerd worden als de energie die vrijkomt tijdens het mengen van twee oplossingen met verschillende zoutconcentraties. Een gecontroleerde menging in een RED stack geeft de mogelijkheid om de mixenergie direct om te zetten naar elektriciteit door middel van redox reacties. Alternerende plaatsing van kation uitwissel membranen (CEMs) en anion uitwissel membranen (AEMs) vormen de benodigde compartimenten voor de gecontroleerde menging. Als hoog- en laaggeconcentreerde oplossingen worden gevoed in compartimenten naast elkaar, treedt er een elektrochemisch potentiaalverschil op wat de ionen van de hoge naar de lage concentratie doet willen gaan. Echter, alleen ladingen met een tegenovergestelde lading aan de vaste lading in het membraan kan door het membraan diffunderen. Dat wil zeggen dat voor een ideaal membraan alleen kationen getransporteerd kunnen worden door een CEM. Op deze manier kan een flux van ionen worden gegenereerd in de stack.

In hoofdstuk 1 wordt de theorie achter deze technologie behandeld. In **hoofdstuk 2** wordt het effect van natuurlijk rivier (van de Amantea in Italië) en zeewater experimenteel bestudeerd door middel van labschaal RED stacks. In **hoofdstuk 3** wordt gekeken naar de invloed van Mg^{2+} in zeewater en brijn op RED stroom productie. In **hoofdstuk 4** worden nieuwe CEMs ontwikkeld door polysulfon te sulfoneren met chlorosulfonzuur. Dit polymeer wordt vervolgens gebruikt om een assymetrisch membraan te maken door middel van fase inversie. In **hoofdstuk 5** wordt een

mengsel van commercieel-beschikbaar polyethersulfon en gesulfoneerd polyethersulfon gebruikt om membranen te maken door middel van fase inversie. Deze membranen worden vergeleken met commerciële membranen. In **hoofdstuk 6** wordt deze thesis samengevat en wordt er vooruitgekeken naar toekomstig werk op dit gebied.

CHAPTER 1:

INTRODUCTION

1. Energy and targets

Paris agreement (2016) shows developed countries from all over the world are finally aware that current energy policies are unsustainable. The continuous increase on world surface temperature due to CO_2 emission can be a fatal risk on next generations. An increase of 34% on world energy-related CO_2 emissions, from 32.2 billion metric tons in 2012 to 43.2 billion metric tons by 2040, is expected by the IEO2016 report [1]. To reduce the greenhouse gas emission, many countries/regions have already set their goal for 2030. United States was projected to reduce emissions by 28% in 2025, respectively. China targeted for 2030 to lower the emission per unit of GDP by 60-65% from level of 2005 while European Union target was 40% reduction in total greenhouse gas emission by 2030 compared to 1990 [2]. Implementing energy efficiency standards, increasing electrical or hybrid technologies in transport and increasing renewable energy rate are some of the trends that countries follow for their targets [2].

Regarding energy policies, European Union is one of the leading regions in the world. Their energy policies can be summarize in three main parts;

- The reliable provision of energy must be ensured by secure energy supplies
- Energy providers' operations in a competitive environment must be ensured for affordable energy prices for homes, businesses, and industries
- Energy consumption must be sustainable, through the lowering of greenhouse gas emissions, pollution, and fossil fuel dependence.

Renewable energy was suggested as a key policy by EU to achieve their objectives. By 2020, 20% increase in share of renewable energy is planned compared to 2010 and by 2030, it is projected as 27% [3].

Renewable energy technologies are now a major global industry. Wind and solar PV have led recent growth in renewables-based capacity, though hydropower and bioenergy remain by far the largest source of supply [2]. In 2015, 1820 Mtoe of the 13790 Mtoe total energy production was covered by renewable technologies such as hydo, wind, solar and bio energy (Fig. 1).

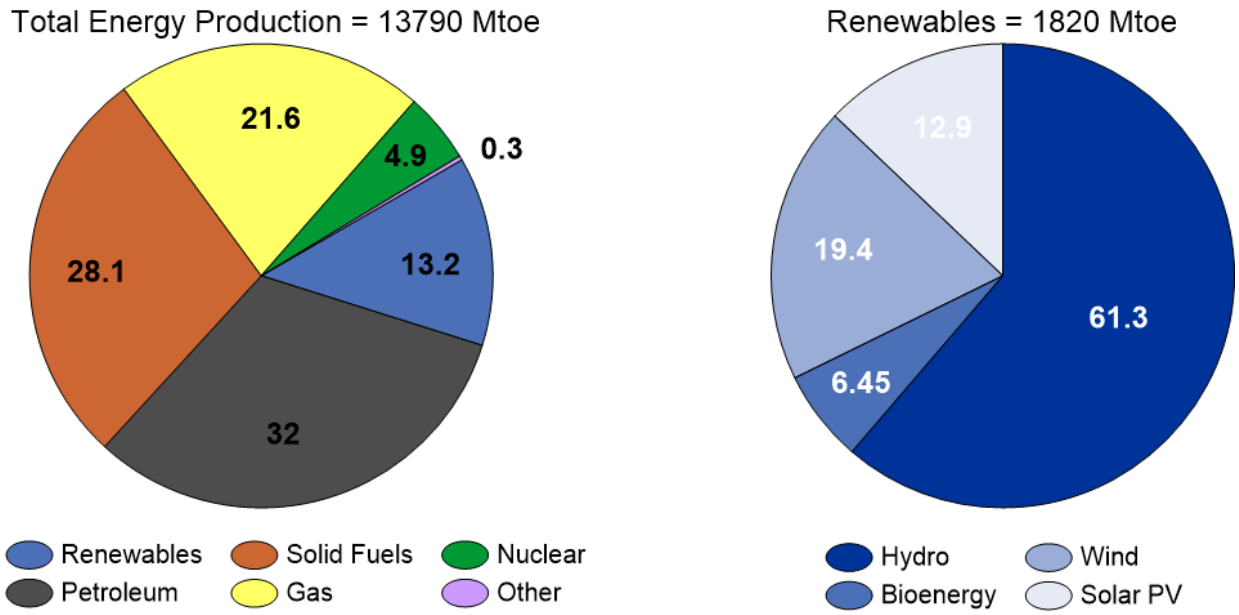

Figure 1. Total energy production and the share of renewables in 2015.

Considering future targets, countries should increase the share of current renewable energies or implement new promising non-commercial renewable energies. In this regard, salinity gradient energy is a promising, renewable, sustainable and environmentally friendly alternative.

2. Salinity gradient energy

Salinity gradient energy (SGE) can be defined as mixing energy of two solutions with different salinity. In 1954, for the first time, Pattle remarked that the free mixing energy of sea and river water is equal to potential energy of 680 ft. high waterfall [4]. This untapped energy is available wherever a river meets with the sea. One of the earliest study, roughly estimated the theoretical SGE potential of equal amount of seawater/river water mixing energy as 2.43 TW by accounting

the total world river flow is 1.08 x 10^6 m^3/s [5]. A more recent study has reported only 57% of the 1.72 TW theoretical potential is technically available due to limitations associated with physical and technical characteristics [6]. A more detailed investigation by Alvarez-Silva et al. (2016) has indicated the extractable global potential of SGE gets decreased to 625 TWh/a when availability of the rivers, extraction factor, capacity factor were taken into consideration [7].

In theory, complete mixing of 1 m^3 seawater (30 kg NaCl/m^3) and 1 m^3 river water (0 kg NaCl/m^3) produces 1.7 MJ energy. This energy can be increased up to 6.1 MJ at 298 K when volumetric ratio of riverwater/sea water is 10 [8].

Mixing energy is available also in other sources than sea and river water. Some of them are;

- anthropogenic brines (salt mines, salt ponds, solar ponds, salt domes of oil wells or natural gas wells), natural sources (hypersaline lakes), geothermal brines or brines of desalination units,
- aqueous waste water with sufficient salinity,
- thermolytic solutions (e.g. Ammonium bicarbonate).

Mixing solutions with a wide range of salinity generates different amount of energy. Fig. 2 illustrates the extractable Gibbs energy of mixing 1 m3 of diluted solution (0.1- 0.5 M NaCl) and 1 m3 of concentrated solution (0.5- 5.4 M NaCl) [9]. Mixing seawater (0.5 M NaCl) and saturated brine solution coming from membrane distillation (5.4 M NaCl) produces approximately 5 MJ energy where mixing seawater and brine solution coming from reverse osmosis (1 M NaCl) produces 0.25 MJ energy.

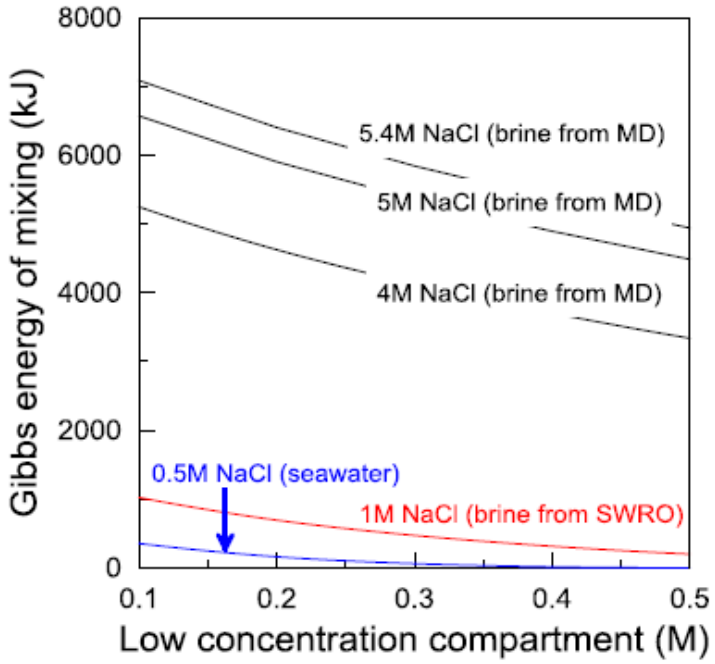

Figure 2. The theoretical Gibbs free energy of mixing for 1 m^3 of NaCl solutions at 293 K [9].

3. Theory

The theoretically available amount of energy obtainable from the controlled mixing of a concentrated salt solution and a diluted salt solution can be calculated from the Gibbs free energy.

$$\Delta G_{mix} = G_m - (G_c - G_d) \quad (1)$$

where ΔG_{mix} is the free energy of mixing ($J \cdot mol^{-1}$), G_m is the Gibbs energy of the mixture, the brackish water ($J \cdot mol^{-1}$), G_c is the Gibbs energy of the concentrated salt solution ($J \cdot mol^{-1}$) and G_d is the Gibbs energy of the diluted salt solution ($J \cdot mol^{-1}$).

The Gibbs energy of an ideal solution is the sum of chemical potentials of the individual chemical components present in that solution:

$$G = \sum \mu_i n_i \quad (2)$$

In this equation, G is the Gibbs energy of the system ($J \cdot mol^{-1}$), μ_i is the chemical potential of component i in the solution ($J \cdot mol^{-1}$), and n_i is the number of moles of component i in the solution. The chemical potential of the component i in an ideal solution can be simplified when no pressure change or charge transport is considered upon mixing of a concentrated and a diluted salt solution:

$$\mu_i = \mu_i^0 + RT \ln x_i \quad (3)$$

where μ_i^0 is the molar free energy under standard conditions ($J \cdot mol^{-1}$), R is the universal gas constant ($8.314\ J \cdot (mol \cdot K)^{-1}$), T is the absolute temperature (K), x_i is the mol fraction of component i. When Equation (3) is substituted in Equation (1) and n is replaced by solution concentration c ($mol \cdot m^{-3}$) and volume V (m^3), the final Gibbs free energy of mixing can be described as follows:

$$\Delta G_{mix} = \sum_i \left[c_{i,c} V_c RT \ln\left(x_{i,c}\right) + c_{i,d} V_d RT \ln\left(x_{i,d}\right) - c_{i,m} V_m RT \ln\left(x_{i,m}\right) \right] \quad (4)$$

Harvesting salinity gradient energy is possible by several membrane based techniques; pressure-retarded osmosis (PRO) [10] and reverse electrodialysis (RED) [11] are the ones close to commercialization stage. Also technologies like capacitive mixing (CapMix) [12] and capacitive reverse electrodialysis (CRED) [13] are gaining attention recently.

Pressure retarded osmosis (PRO) works in an opposite way of reverse osmosis (RO). As in RO, a semi-permeable membrane that only allows the transport of the water and retains the salts were fed in between solutions with different salinity. Due to osmotic pressure water transport through to concentrated compartment and increase the pressure of the compartment. Kinetic energy of pressurized flow can be converted to electrical power by utilizing a turbine and a generator on the effluent of the concentrated solution flow[14,15].

Working principle of reverse electrodialysis (RED) is opposite of electrodialysis (ED). Both technology uses same orientation of alternated cation and anion exchange membrane which allows only transport of positive or negative charges (i.e. cation exchange membranes only let cations permeate and exclude anions). In RED electrochemical potential gradient drives ions from concentrated to diluted compartments. Created ionic flux can be converted to electricity by redox reactions at the electrode compartments in the end.

4. Reverse Electrodialysis

Salinity gradient energy can be harvested in a RED stack where ion exchange membranes were utilized, as demonstrated in Fig. 3. Creating a controlled mixing in a RED stack gives the opportunity to transfer the mixing energy directly to electricity. Alternate arrangement of cation exchange membranes (CEM) and anion exchange membranes (AEM) form the required compartment design for controlled mixing. When high and low concentration solutions are fed from neighboring compartments, electrochemical potential difference of the solutions drive the ions from high to low concentrations. However, only charges opposite to membrane fixed charge can diffuse through, i.e. for an ideal membrane only cations can transport through CEM. Therefore, an ionic flux can be generated inside of the stack. Ionic flux can be converted at the electrodes, by using for example a reversible redox reaction, to power an external electrical circuit [16].

Nernst equation allow is to calculate the membrane potential over an ion exchange membrane:

$$\Delta V^{o} = \frac{\alpha RT}{zF} \ln\left(\frac{a_c}{a_d}\right) \qquad (5)$$

Where ΔV^{o} is the theoretical membrane potential (V), R is the universal gas constant (8.314 J·(mol·K)$^{-1}$), F is Faraday constant (96485 C·mol^{-1}), T is the absolute temperature (K), α is the

membrane permselectivity (-), z is the electrochemical valance (-), α_c is the activity of the concentrated solution (mol·l^{-1}) and α_d is the activity of the concentrated solution (mol·l^{-1}). Overall stack potential can be calculated by adding up the individual membrane potentials.

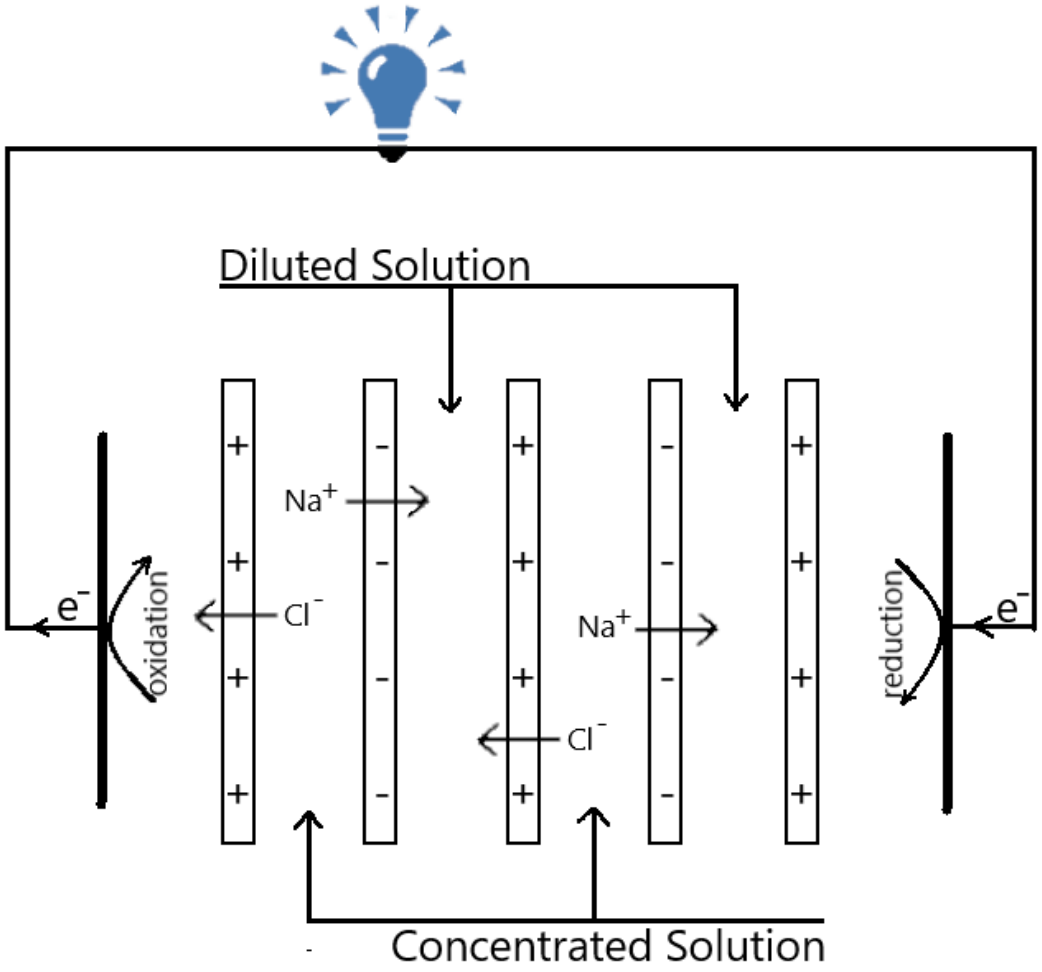

Figure 3. Schematic of reverse electrodialysis.

Every component between two electrodes create a resistance against the transfer of the ions. A RED stack consist of cation exchange membranes, anion exchange membranes, spacers to create channels, high and low concentrated solutions, red-ox electrolyte solution and electrodes . Therefore all these components contribute as ohmic resistance of the stack. In addition to ohmic resistance, non-ohmic resistance is present due to concentration changes in bulk solutions and concentration change in the boundary layer. R_{stack} can be defined as [17];

$$R_{stack} = R_{ohmic} + R_{non-ohmic} \quad (6)$$

where R_{ohmic} is;

$$R_{ohmic} = \frac{N_m}{2}\left(\frac{R_{AEM}}{1-\beta} + \frac{R_{CEM}}{1-\beta} + \frac{h_{HCC}}{\varepsilon^2 \kappa_{HCC}} + \frac{h_{LCC}}{\varepsilon^2 \kappa_{LCC}}\right) + R_{electrodes} \quad (7)$$

in which R_{AEM} and R_{CEM} are the areal resistances of anion and cation exchange membrane ($\Omega \cdot m^2$), respectively, h is the intermembrane distance (m), κ is the electrolyte conductivity ($S \cdot m^{-1}$) and $R_{electrodes}$ is the (ohmic) resistance of both electrodes and electrolyte compartments ($\Omega \cdot m^2$). The spacer porosity ε, and the mask fraction β are dimensionless. $R_{non\text{-}ohmic}$ is;

$$R_{non-ohmic} = R_{\Delta C} + R_{BL} \quad (8)$$

where $R_{\Delta C}$ is resistance due to the concentration change in the bulk solution ($\Omega \cdot m^2$) and R_{BL} is resistance due to concentration gradient ($\Omega \cdot m^2$).

The power can be estimated using Kirchoff's law;

$$W = I^2 R_{load} = \frac{\left(V^o\right)^2 R_{load}}{\left(R_{stack} + R_{load}\right)^2} \quad (9)$$

Here I is the current (A), R_{load} is the resistance of the load (Ω), R_{stack} is the stack resistance (Ω) and V^0 is the stack open circuit potential (V). When R_{stack} is equal to R_{load} maximum power can be obtained analytically [18].

$$W_{\max} = \frac{\left(V^o\right)^2}{4R_{stack}} \quad (10)$$

Calculation of maximum power depends on open circuit voltage and R_{stack}. Therefore for the optimization of RED, these two parameters and related parameters, i.e. permselectivity is related to OCV, must be considered.

Several attempts have been made to extract the mixing energy of solutions in a RED stack. These studies have been conducted with different ion exchange membranes, feed solutions, spacers, operating conditions or number of cells. Table 1 shows the operating conditions, utilized materials and obtained gross power densities for several major studies in the literature. It can be pointed out, in seawater/river water mixing, compartment thickness had a great importance because produced energy is limited by the river water resistance. Importance of salinity ratio was also emphasized in Table 1. High salinity ratio increase the driving force on the ions and enhance the transport.

5. Challenges related to RED components

A RED stack unit compromise cation exchange membranes, anion exchange membranes, spacers, high concentration solution, low concentration solution, electrodes and electrolyte solution. Each component has critical duty in the stack and optimization of these components are possible.

5.1. Ion exchange membranes

A required medium for controlled transport of ions with opposite charges can be created by utilizing ion exchange membranes in RED. According to Strathmann (2014), high permselectivity, low electrical resistance, good mechanical and dimension stability, and high chemical stability are desired properties for an ion exchange membrane [35]. However, regarding the requirements of the process, aforementioned properties can differ. For example, due to milder solutions operated

Table 1. Operating conditions and power densities from the literature.

Producer/ Custom made	CEM	AEM	Spacer thickness (μm)	Flow velocity ($cm \cdot s^{-1}$)	Concentration gradient (M NaCl/M NaCl)	Gross power density ($W \cdot m^{-2}$)	Reference
-	Polyethylene based composite		1000	-	Tap water/0.5	0.20	[4]
Ionics	61CZL	103CZL	1000	15	0.026/0.57	0.34	[5]
Asahi	CMV	AMV	3000	-	0.017/5.03	0.40	[19]
MEGA	CMH	AMH	200	1.7	0.017/0.51	0.60	[20]
Modified commercial PE	JJC-82	JJC-72	550	0.21	0.017/0.56	0.39	[21]
Modified commercial PE	JJC-82	JJC-72	550	0.21	0.55/5.32	0.57	[21]
ACIPLEX	K-502	A-201	1000 and 10000 alternately	1.9 and 0.075 alternately	0.0017/0.60	0.26	[21]
Fumatech	FKS	FAS	200	1.7	0.017/0.51	1.11	[20]
Fumatech	FKS	FAS	100	4.0	0.017/0.51	2.20	[22]
Custom-made	SPEEK65	PECHB2	200	1.7	0.017/0.51	1.28	[20]
Fumatech	FKD	FAD	200	1.2	0.017/0.51	1.17	[23]
Custom-made	CMH-PES	AMH-PES	Profiled membranes-230	21	0.017/0.51	1.00	[24]
Tokuyama	CMX	PECH	100	6.7	0.017/0.51	1.30	[25]
Tokuyama	CMX	AMX	190	0.54	0.0096/0.60	0.46	[25]
Tokuyama	CMX	AMX	320	0.83	0.017/0.50	0.80	[25]
Asahi Glass	CMV	AMV	200	1.16	0.017/0.51	1.18	[26]

Table 1. Operating conditions and power densities from the literature (Continued)

Producer/ Custom made	CEM	AEM	Spacer thickness (μm)	Flow velocity ($cm \cdot s^{-1}$)	Concentration gradient (M NaCl/M NaCl)	Gross power density ($W \cdot m^{-2}$)	Reference
Fujifilm	80050	80045	270	0.62	0.50/5.40	2.4	[9]
Fujifilm	80050	80045	270	0.41	0.50/4.0	1.06	[27]
Neosepta	CMS	ACS	100	0.41	0.01/5.0	3.80	[28]
Fujifilm	80050	80045	270	0.41	0.79/2.67	0.39	[29]
Fujifilm	80050	80045	270	1.00	0.1/5.0	1.95	[30]
Neosepta	CMX	AMX	200	0.12	0.01/2.40	1.86	[31]
Fumasep	FAK-20	FAS-20	270	4.00	0.1/5.0	12.0	[32]
Fujifilm	80050	80045	270	1.00	0.03/4-5	2.70	[33]
Neosepta	CMX	AMX	190	1.32	0.01/1.9	0.87	[34]

in RED, membranes can be designed considering parameters that has crucial effect on power generation and cost of the produced electricity by RED [36,37]. For a RED ion exchange membrane, resistance and the permselectivity has a direct effect on generated power. Even though properties like swelling degree, ion exchange capacity and charge density seems as secondary, they are interrelated with resistance and permselectivity. Other than being interrelated, most of the parameters also have a counteracting relationship (e.g. swelling degree vs. permselectivity and resistance).

When eq. 5, 6, 7, 10 are investigated carefully, resistance and permselectivity can be concluded as performance determining parameters of ion exchange membranes. Table 2 tabulates the properties of some commercial ion exchange membranes tested in RED stack previously [38]. Permselectivity of commercial membranes vary from 86% to 99% where ideal value is 100%. On the other side, areal resistance has a broad range between 0.89 and 11.33 $\Omega \cdot m^2$.

5.1.1. Resistance

Heterogeneous ion exchange membranes are produced by mixing a charged resin and uncharged polymer. In order to have mechanically stable membrane films, thickness of these membranes are higher than homogenous membranes. Thickness together with having local uncharged regions across the membrane cause high areal resistance. Therefore, even though heterogeneous membranes have worthy permselectivity, utilizing them in RED results in low power density.

Most commonly, homogeneous ion exchange membranes are preferred in RED performance tests. Resistance range of these membranes are narrower (0.89-3.70 $\Omega \cdot m^2$). Up to date, the best performing membrane pairs for artificial sea and river water mixing were FKS and FAS provided by Fumatech (Germany). This performance was obtained for 100 μm spacer thickness at 4 $cm \cdot s^{-1}$ flow rate [22].

Electrochemical properties of IEMs can be misleading because characterization conditions may not represent the process solutions accurately. Most common characterization solution for membrane resistance is 0.5 M NaCl while 0.1/0.5 M NaCl solutions are preferred for permselectivity. Membranes in RED, however, are exposed to a concentration gradient, in other words, both face of the membrane are in contact with different concentration. Concentration gradient can be 0.017/0.51 M NaCl (river water/seawater mixing) or 0.5/5.4 M NaCl (seawater/saturated brine mixing). Under these condition, membrane resistance and permselectivity differ from the measured value in 0.5 M NaCl or 0.1/0.5 M NaCl, respectively. Geise et al. (2014) characterized Selemion CMV and AMV membranes in a single concentration (1.0 M NaCl) and in a concentration gradient (0.01/1.0 M NaCl). CMV and AMV resistances measured 15 times and 13 times higher, respectively, when membranes were characterized in gradient solution instead of single solutions. Characterization in single solution for a 0.01-1.0 range also revealed that membrane resistance was dependent to solution concentration at a value lower than 0.5 M NaCl [43].

Dlugolecki et al. (2010) was also noted that at low solution concentrations (<0.1 M NaCl), very sharp increase of commercial AMX, CMX (Neosepta) and FAD, FKD (Fumatech) resistances were observed [44]. A detailed study on resistance of CMX membranes, covering 0.01 to 1.1 M NaCl solutions for single and concentration gradient experiments, was completed by Galama et al. (2014). In that study, 0.3 M NaCl was decided as a critical concentration where membrane resistance depends on external concentration [45].

Table 2. Properties of some commonly used ion exchange membranes

Producer/ Custom made	IEC ($meq \cdot g^{-1}$)	Permselectivity (%)*	Resistance ($\Omega \cdot m^2$)**	Swelling degree (%)	Thickness (μm)	Fixed charge	Reference
Homogeneous CEM							
Fumasep FKD	1.14	89.5	2.14	29.0	113	$-SO_3^{2-}$	[39]
Fumasep FKS	1.54	94.2	1.50	13.5	40	-	[20]
Qianqiu CEM	1.21	82.0	1.97	33.0	205	-	[20]
Neosepta CMX	1.62	99.0	2.91	18.0	164	$-SO_3^{2-}$	[18]
Selemion CMV	2.40	98.8	2.90	25.0	150	$-SO_3^{2-}$	[18]
Heterogeneous CEM							
Ralex CMH-PES	2.34	94.7	11.33	31.0	764	$-SO_3^{2-}$	[18]
Homogeneous AEM							
Fumasep FAD	1.42	86.0	0.89	34	74	-	[18,20]
Fumasep FAS	1.12	89.4	1.03	8.0	33	-	[20]
Neosepta ACS	1.4-2.0	-	2.0-2.5	20-30	150-200	$-N(CH_3)_3^+$	[40]
Neoseopta AMV	1.78-1.90	87.3	3.15	17.0	120-124	-	[20,41]
Neosepta AMX	1.4-1.7	90.7	2.0-3.5	25-30	120-180	$-N(CH_3)_3^+$	[40,42]
Selemion CMV		97	3.7		120	-	***
Qianqiu AEM	1.33	86.3	2.85	35.0	294	-	[20]
Heterogeneous AEM							
Ralex AMH-PES	1.97	89.3	7.66	56	714	-	[18]

* Characterized in 0.1/0.5 M solution.

** Characterized in 0.5 M NaCl solution.

***Information from manufacturer.

Areal solution resistance values was converted from the conductivity values by using Eq. 11 from Galama's study (2016) while CMX and AMX resistance used as it is [46] ;

$$R_{solution} = \frac{\rho L}{A} \tag{11}$$

Where $R_{solution}$ is solution resistance (Ω), ρ is the solution specific resistivity (Ω·cm), L is the thickness (cm), A is the area (cm^2) [30].

Depending on the process conditions, ion exchange membrane resistances can be important. Fig. 4 compares the areal resistances of commercial AMX and CMX in different NaCl concentration with the corresponding areal solution resistance where compartment thickness is 270 μm. In low concentration, up to 0.05 M NaCl, solution resistance is higher than the membranes'. After 0.1 M NaCl solutions membrane resistance remain constant and solution resistance decreases. As a result, seawater/river water mixing in RED is limited by river water resistance. Improving membrane conductivity cannot enhance produced power significantly. On the other hand, power generation is limited by membrane resistance in case of seawater/brine mixing.

Reducing compartment thickness reduces the dominant effect of low concentration compartment on total resistance. In Fig. 5, CMX, AMX and solution areal resistances are compared for 100 μm compartment thickness. For this case membrane and compartment resistance are comparable starting from really low concentration (i.e. 0.001 M NaCl).

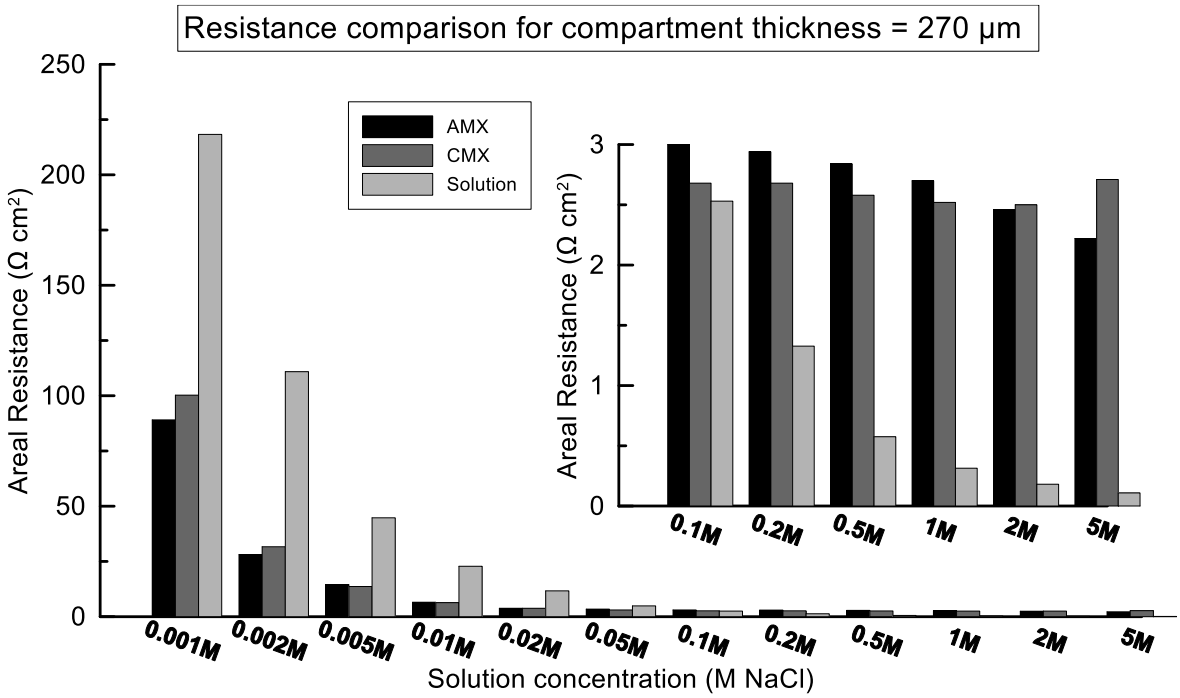

Figure 4. Areal resistance of the solutions, AMX and CMX. 270 μm compartment thickness was assumed for calculation of solution.

Fig. 4 and 5 encourage preparing IEMs designed especially for RED application and for desired process conditions. The comparison also indicates that there is a possibility for membrane engineering to reduce the membrane resistance and generate more energy in return, for the processes where total resistance is dominated by IEMs. Since resistance is proportional to the thickness, reducing membrane thickness can be an opportunity to get benefit from such processes. Considering, also, mechanical properties is related to the thickness, an optimization can be conducted. An alternative to thinner membranes can be a thin active layer membranes with same thickness. Creating dense thin layer that maintain the permselectivity and a porous support that enhance the conductivity can answer the needs of the RED.

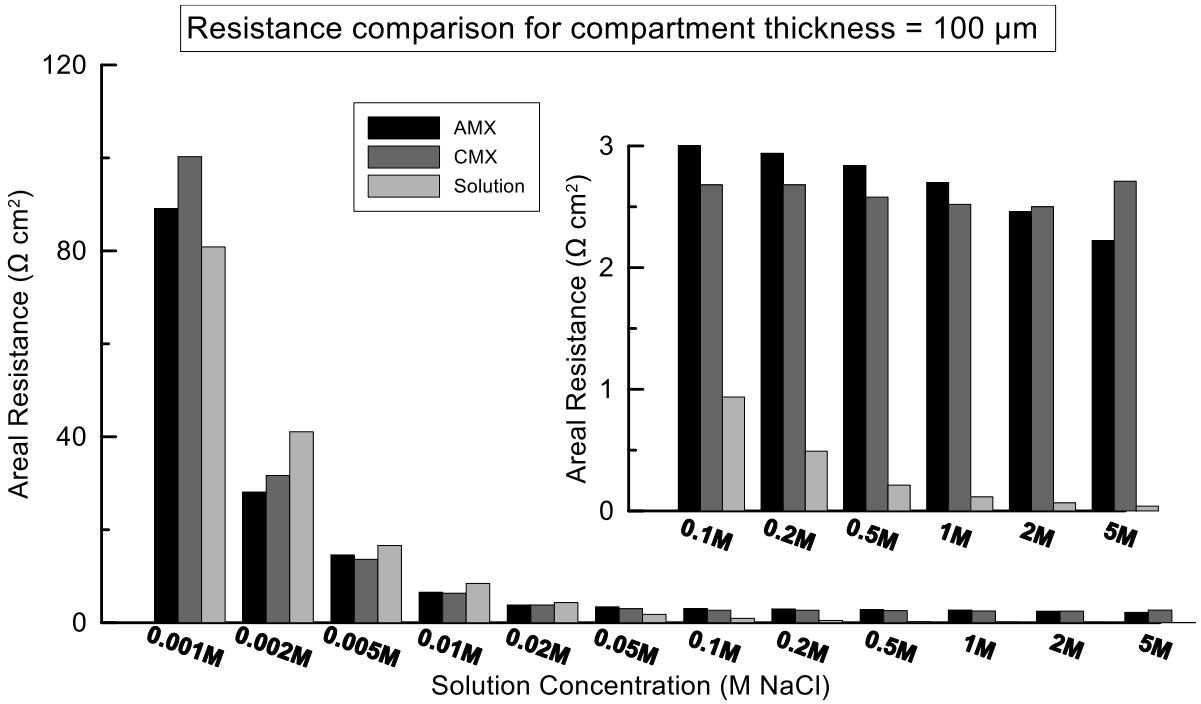

Figure 5. Areal resistance of the solutions, AMX and CMX. 100 μm compartment thickness was assumed for calculation of solution.

Another challenge related to membrane resistance is the mixing solution contains more than NaCl. Most of the RED study so far has been run for the artificial solutions mimicked by NaCl [22,26,28,36]. However, natural solutions are more complex. For example, average real seawater contains 10% of other ions (e.g. Mg^{2+} and SO_4^{2-}) [47]. There are several attempts evaluated the effect of other ions or natural solutions [27,33,48–50]. Evaluation the effect of Mg^{2+}, which is second highest cation in the seawater, for seawater/brine mixing revealed that power reduction was strongly related to increase of the CEM resistance in presence of magnesium [27]. Fig. 6 illustrates the relation between magnesium concentration and IEMs. Introduction of 10% of $MgCl_2$ to the solution (0.5 m NaCl solutions were used for the characterization) resulted in a 3 times higher total CEM resistance, while effect on AEM was insignificant. This drastic effect can be explained by the affinity of the ions. Mg^{2+} has higher affinity to the fixed charged groups (i.e.-SO_3^{2-}) than Na^+ [35]. Due to this high affinity, Mg^{2+} is preferentially selected by the fixed groups

of the membrane and dissociate slower than the Na^+ ions [51]. High affinity and slow dissociation cause charge screening or partial neutralization of charged groups. Ultimately, condensation of counter-ion/fixed-charge pairs takes place, and cause a higher membrane resistance.

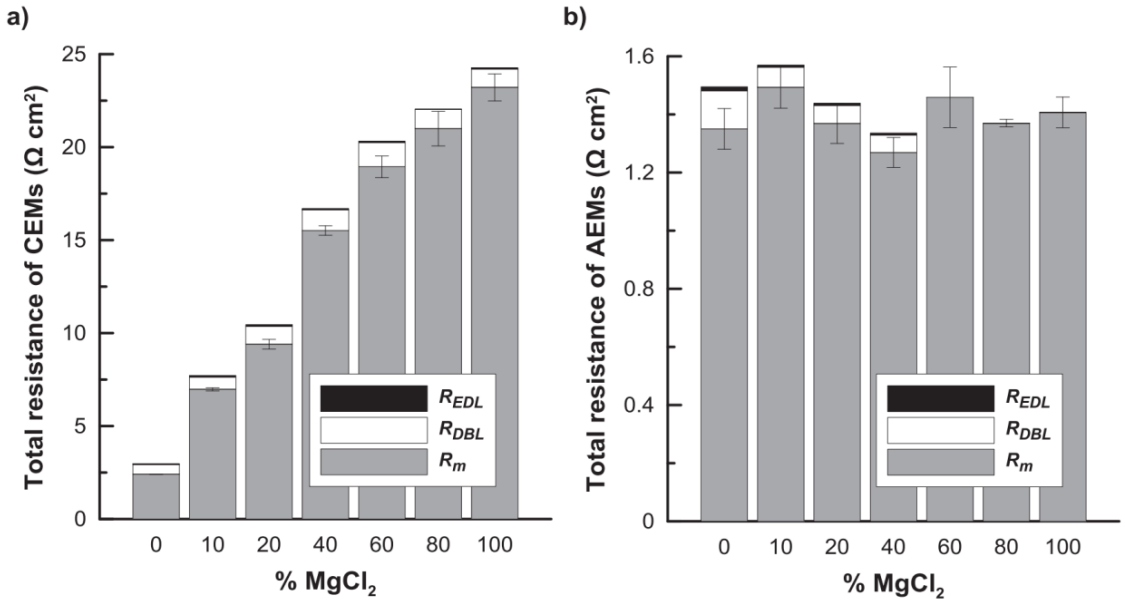

Figure 6. Resistances of membrane (Rm), diffusion boundary layer (RDBL), and electric double layer (REDL) at increasing MgCl2 content for: a) Fuji-CEM-80050 cation exchange membrane; b) Fuji-AEM-80045 anion exchange membrane [27].

One strategy to avoid charge screening can be coating the membrane surface with a very thin layer of charges opposite to the fixed charge sign [52]. This thin layer can prevent Mg^{2+} penetration through the membrane electrostatically. Moreover, because sodium has smaller hydration radius than magnesium, the extra layer create less resistant to sodium ion. Though, the possibility of increasing the resistance due to extra layer must be considered carefully.

5.1.2. Permselectivity

Permselectivity indicates ability to select counter ions over co-ions. Most of the commercial ion exchange membranes has permselectivity higher than 90% while ideal permselectivity is 100%. Although membranes are close to ideal value in characterization solution (0.1/0.5 M NaCl), more realistic process solutions or having different concentrations can alter the permselectivity.

Previous studies showed that permselectivity of a membrane strongly related to concentration of test solutions. Membranes tested in diluted environment resulted in with a permselectivity close to ideal [30,53,54]. Hosseini et al. (2012) measured the permselectivity of the heterogeneous Ralex CMH and AMH membranes in 0.01/0.1, 0.05/0.5, 0.1/1.0 M NaCl by keeping the molar ratio at a constant value 10. AMH permselectivity showed a clear decrease by increasing salt content while insignificant effect was observed on CMH. Moreover, for 0.01/0.1 M, having Ba2+ reduced CEM permselectivity from %91.2 to %65.2 while having SO_4^{2-} reduced it from 84.8% to 43.0% [54]. Similarly, Fontananova et al. (2017) observed a sharp reduction on AEM800 provided by Fujifilm when using 0.5/4 M NaCl for characterization; from 0.93 to 0.68. Furthermore, it reduced to 50% in case 0.473 M NaCl+0.014 M $MgCl_2$/3.78 M NaCl+0.11 M $MgCl_2$ used [30]. Due to divalent ions form stronger bonds, it has a screening effect on polymer fixed charge as it is explained earlier. Therefore, charge density get reduced, so permselectivity. One strategy to overcome this problem can be preparing monovalent selective membranes. Preparation of monovalent selective membranes can be based on the different affinity, hydration radius or electrostatic interaction.

Counter acting effect of membrane properties makes membrane optimization a difficult process. In addition, membrane properties differ depending on concentration and content of ions. Therefore, producing a membrane that can work for all conditions is not possible. Trade-offs and process conditions must be taken into account during the optimization of the RED membranes.

5.2. Spacers

High and low concentration compartments in a RED stack is provided by equipped spacers between cation and anion exchange membranes. They also act as a turbulent flow promoter owing to their meshed geometry.

Total stack resistance is the sum of the resistance of every single component (see eq. 7). In RED processes that is fed with low concentration solutions (<0.3 M NaCl), power production is limited by the low compartment resistance. Since compartment thickness is decided by the spacers, their effect on produced power is significant.

A straightforward strategy to reduce stack resistance and increase gross power density is using thin spacers. Following this strategy, Vermaas et al. (2011) was successful to double the gross power density when using 100 μm thick spacers. On the other hand, when thickness is further reduced to 60 μm, flow rate could only be increased up to some extend because of high shear stress. Moreover, lowering the thickness increased the pump energy loss and reduced the net power density [22].

In a RED stack, after piling up membranes and spacer they are replaced and pressed from both side so feeds cannot leak from the loose parts. In this kind of arrangement spacers contact to membranes and cover a specific area of the membrane depending on their opening. Therefore, ion transport can only occur from the open area. This phenomena is called as "shadow effect" in the literature. There were several attempts to reduce the shadow effect. Dlugolecki et al. (2010) used ion conductive spacers made by cutting CMX and AMX membrane to the desired shape. Ion conductive spacers were compared with non-conductive spacers which has same open area (54%), porosity (73%) and thickness 0.32 mm. Due to enhancement in the conductive medium and reduction in the concentration polarization, 3-4 times higher power density was obtained when ion conductive spacers were used [55].

Spacerless design for RED was suggested by Vermaas et al. (2011) in order to overcome so called shadow effect. On top of one side of the membranes, heterogeneous membranes were hot pressed and desired profiles were formed at 230-245 μm thickness. RED experiments revealed that ohmic

resistance was reduced while non-ohmic resistance was increased in return. Therefore, expected improvement on power could not be achieved [56]. Yet, other attempts with different profile geometry had some achievements [25,57].

5.3. Electrode and electrolyte solution

In a RED stack, electrode compartments are placed at the end of the membrane pile. It consist an anode, a cathode and recirculating electrolyte solution. Most of the time, electrode compartments are separated from inner compartments carefully considering environmental risks. To avoid a possible leakage from electrolyte solution to discharged RED effluents a special membrane (i.e. Nafion) [58] or 2 same kind of ion exchange membranes [59] are used in between. Scialdione et al. (2012) reported that perfluoronated Nafion was impermeable to redox couple while Selemion anionic membranes allowed very slow transport of redox couple to the neighboring compartment [58].

There are a few study that investigated electrodes and electrolyte solutions particularly in RED [58–61]. Lee et al. (2016) prepared a Vulcan coated graphite electrode that resulted in less resistance than the Ir-coated titanium mesh, Pt-coated titanium plate and graphite foil. Lowering electrode resistance helped to increase power density by 5-10%. It is also noted hexacyanoferrate(III) and hexacyanoferrate(II) as redox couple with 1 M Na_2SO_4 showed good reversibility. It is also stated using Na_2SO_4 and Vulcan coated graphite can lower the capital and operational cost [61]. Burheim et al. (2012) tested different red-ox salts and electrode material. They concluded mass transfer in the electrolyte controlled the electrochemical reactions. Therefore, replacing cheap electrodes (i.e. graphite) can be possible [60].

6. Conclusion

Reverse elecrtodialysis is a developing, membrane based, renewable and environmentally friendly technology. The purpose of introduction chapter, was to give a general sense about the theory behind the RED, achievements so far and challenges related to the RED component.

The maximum gross power for artificial seawater/river water mixing was obtained as 2.2 $W \cdot m^{-2}$, up to date [22]. This chapter showed the power density can be increased by some straightforward modification on the membrane components easily (i.e. decreasing thickness of low concentration compartment). It was also noted, membrane components must be design by taking process conditions into account. On the other hand, it was underlined that results reported with artificial solution do not represent the real performance of the RED. In more realistic solutions, electrochemical properties (e.g. permselectivity, resistance) differ significantly from the characterization values.

Due to counteracting behavior of ion exchange membrane properties, optimization of the RED is quite challenging. But, this counter acting effect also gives an opportunity to optimize the properties, for the sake of RED.

7. References

[1] U.S. Energy Information Administration, International Energy Outlook 2016, Washington, USA, 2016.

[2] International Energy Agency, World Energy Outlook 2016, Paris, France, 2016.

[3] European Comission, Communication from the commission to the European parliament, the council, the European economic and social committee and thecommittee of the regions, Brussels, Belgium, 2011.

[4] R.E. Pattle, Production of electric power by mixing fresh and salt water in the hydroelectric pile, Nature. 174

[5] J.N. Weinstein, F.B. Leitz, Electric Power from Differences in Salinity: The Dialytic Battery, Science, 191 (1976) 557–559.

[6] J. Kuleszo, C. Kroeze, J. Post, B.M. Fekete, The potential of blue energy for reducing emissions of CO_2 and non-CO_2 greenhouse gases, J. Integr. Environ. Sci. 7 (2010) 89–96.

[7] O.A. Alvarez-Silva, A.F. Osorio, C. Winter, Practical global salinity gradient energy potential, Renew. Sustain. Energy Rev. 60 (2016) 1387–1395.

[8] J. Veerman, M. Saakes, S.J. Metz, G.J. Harmsen, Reverse electrodialysis: Performance of a stack with 50 cells on the mixing of sea and river water, J. Memb. Sci. 327 (2009) 136–144.

[9] R.A. Tufa, E. Curcio, E. Brauns, W. van Baak, E. Fontananova, G. Di Profio, Membrane distillation and reverse electrodialysis for near-zero liquid discharge and low energy seawater desalination, J. Memb. Sci. 496 (2015) 325–333.

[10] F. Helfer, C. Lemckert, Y.G. Anissimov, Osmotic power with pressure retarded osmosis : theory , performance and trends – a review, J. Memb. Sci. 453 (2014) 337–358.

[11] N.Y. Yip, D.A. Vermaas, K. Nijmeijer, M. Elimelech, Thermodynamic, energy efficiency, and power density analysis of reverse electrodialysis power generation with natural salinity gradients, Environ. Sci. Technol. 48 (2014) 4925-4936.

[12] R.A. Rica, R. Ziano, D. Salerno, F. Mantegazza, R. van Roij, D. Brogioli, Capacitive mixing for harvesting the free energy of solutions at different concentrations, Entropy, 15 (2013) 1388–1407.

[13] D.A. Vermaas, S. Bajracharya, B. Sales, M. Saakes, Environmental science clean energy generation using capacitive electrodes in reverse electrodialysis, Energy Environ. Sci. 6 (2013) 643–651.

[14] S. Loeb, Production of energy from concentrated brines by pressure-retarded osmosis I. preliminary technical and economic correlations, J. Memb. Sci. 1 (1976) 49–63.

[15] K. Gerstandt, K. Peinemann, S. Erik, T. Thorsen, T. Holt, Membrane processes in energy supply for an osmotic power plant, Desalination. 224 (2008) 64–70.

[16] J.W. Post, J. Veerman, H.V.M. Hamelers, G.J.W. Euverink, S.J. Metz, K. Nymeijer, C.J.N. Buisman, Salinity-gradient power: Evaluation of pressure-retarded osmosis and reverse electrodialysis, J. Memb. Sci. 288 (2007) 218–230.

[17] D. a. Vermaas, E. Guler, M. Saakes, K. Nijmeijer, Theoretical power density from salinity gradients using reverse electrodialysis, Energy Procedia. 20 (2012) 170–184.

[18] P. Dlugolecki, K. Nymeijer, S. Metz, M. Wessling, Current status of ion exchange membranes for power generation from salinity gradients, J. Memb. Sci. 319 (2008) 214–222.

[19] R. Audinos, Electrodialyse inverse. Etude de l'energie electrique obtenue a partir de deux solutions de salinites differentes, J. Power Sources. 10 (1983) 203–217.

[20] E. Güler, R. Elizen, D. a. Vermaas, M. Saakes, K. Nijmeijer, Performance-determining membrane properties in reverse electrodialysis, J. Memb. Sci. 446 (2013) 266–276.

[21] J. Jagur-Grodzinski, R. Kramer, Novel process for direct conversion of free energy of mixing into electric power, Ind. Eng. Chem. Process Des. Dev. 25 (1986) 443–449.

[22] D.A. Vermaas, M. Saakes, K. Nijmeijer, Doubled power density from salinity gradients at reduced intermembrane distance., Environ. Sci. Technol. 45 (2011) 2010–2011.

[23] J. Veerman, R.M. de Jong, M. Saakes, S.J. Metz, G.J. Harmsen, Reverse electrodialysis: Comparison of six commercial membrane pairs on the thermodynamic efficiency and power density, J. Memb. Sci. 343 (2009) 7–15.

[24] D.A. Vermaas, M. Saakes, K. Nijmeijer, Enhanced mixing in the diffusive boundary layer for energy generation in reverse electrodialysis, J. Memb. Sci. 453 (2014) 312–319.

[25] E. Güler, R. Elizen, M. Saakes, K. Nijmeijer, Micro-structured membranes for electricity generation by reverse electrodialysis, J. Memb. Sci. 458 (2014) 136–148.

[26] J. Veerman, M. Saakes, S.J. Metz, G.J. Harmsen, Electrical power from sea and river water by reverse electrodialysis: a first step from the laboratory to a real power plant, Environ. Sci. Technol. 44 (2010) 9207–12.

[27] A.H. Avci, P. Sarkar, R.A. Tufa, D. Messana, P. Argurio, E. Fontananova, G. Di, E. Curcio, Effect of Mg^{2+} ions on energy generation by Reverse Electrodialysis, 520 (2016) 499–506.

[28] A. Daniilidis, D.A. Vermaas, R. Herber, K. Nijmeijer, Experimentally obtainable energy from mixing river water, seawater or brines with reverse electrodialysis, Renew. Energy. 64 (2014) 123–131.

[29] E. Farrell, M.I. Hassan, R.A. Tufa, A. Tuomiranta, A.H. Avci, A. Politano, E. Curcio, H.A. Arafat, Reverse electrodialysis powered greenhouse concept for water- and energy-self-sufficient agriculture, Appl. Energy. 187 (2017) 390–409.

[30] E. Fontananova, D. Messana, R.A. Tufa, I. Nicotera, V. Kosma, E. Curcio, W. Van Baak, E. Drioli, G. Di Profio, Effect of solution concentration and composition on the electrochemical properties of ion exchange membranes for energy conversion, J. Power Sources. 340 (2017) 282–293.

[31] K. Kwon, J. Han, B.H. Park, Y. Shin, D. Kim, Brine recovery using reverse electrodialysis in membrane-based desalination processes, Desalination. 362 (2015) 1–10.

[32] M. Tedesco, E. Brauns, A. Cipollina, G. Micale, P. Modica, G. Russo, J. Helsen, Reverse Electrodialysis with saline waters and concentrated brines: a laboratory investigation towards technology scale-up, J. Memb. Sci. 492 (2015) 9–20.

[33] M. Tedesco, C. Scalici, D. Vaccari, A. Cipollina, A. Tamburini, G. Micale, Performance of the first Reverse Electrodialysis pilot plant for power production from saline waters and concentrated brines, J. Memb. Sci. 500 (2015) 33–45.

[34] M. Turek, B. Bandura, P. Dydo, Power production from coal-mine brine utilizing reversed electrodialysis, Desalination. 221 (2008) 462–466.

[35] H. Strathmann, Ion-Exchange Membrane Separation Processes, Elsevier, Amsterdam, The Netherlands, 2004.

[36] E. Guler, Y. Zhang, M. Saakes, K. Nijmeijer, Tailor-made anion-exchange membranes for salinity gradient power generation using reverse electrodialysis, ChemSusChem. 5 (2012) 2262–2270.

[37] J.W. Post, C.H. Goeting, J. Valk, S. Goinga, J. Veerman, H.V.M. Hamelers, P.J.F.M. Hack, Towards implementation of reverse electrodialysis for power generation from salinity gradients, Desalin. Water Treat. 16 (2010) 182–193.

[38] J.G. Hong, B. Zhang, S. Glabman, N. Uzal, X. Dou, H. Zhang, X. Wei, Y. Chen, Potential ion exchange membranes and system performance in reverse electrodialysis for power generation: A review, J. Memb. Sci. 486 (2015) 71–88.

[39] P. Długołecki, A. Gambier, K. Nymeijer, M. Wessling, Practical potential of reverse electrodialysis as process for sustainable energy generation, Environ. Sci. Technol. 43 (2009) 6888–6894.

[40] A. Elattar, A. Elmidaoui, N. Pismenskaia, C. Gavach, G. Pourcelly, Comparison of transport properties of monovalent anions through anion-exchange membranes, J. Memb. Sci. 143 (1998) 249-261.

[41] R.K. Nagarale, G.S. Gohil, V.K. Shahi, Recent developments on ion-exchange membranes and electro-membrane processes, Adv. Colloid Interface Sci. 119 (2006) 97–130.

[42] E. Volodina, N. Pismenskaya, V. Nikonenko, C. Larchet, G. Pourcelly, Ion transfer across ion-exchange membranes with homogeneous and heterogeneous surfaces, 285 (2005) 247–258.

[43] M. Geise, A.J. Curtis, M.C. Hatzell, M.A Hickner, B.E. Logan, Salt concentration differences alter membrane resistance in reverse electrodialysis stacks, Environ. Sci. Technol. Lett. 1 (2014) 36–39.

[44] P. Długołęcki, B. Anet, S.J. Metz, K. Nijmeijer, M. Wessling, Transport limitations in ion exchange membranes at low salt concentrations, J. Memb. Sci. 346 (2010) 163–171.

[45] A.H. Galama, D.A. Vermaas, J. Veerman, M. Saakes, H.H.M. Rijnaarts, J.W. Post, K.

Nijmeijer, Membrane resistance: The effect of salinity gradients over a cation exchange membrane, J. Memb. Sci. 467 (2014) 279–291.

[46] A.H. Galama, N.A. Hoog, D.R. Yntema, Method for determining ion exchange membrane resistance for electrodialysis systems, Desalination. 380 (2016) 1–11.

[47] M. Kennish, (2001), Practical Handbook of Marine Science, 3th ed., Boca Raton, Florida, CRC Press

[48] D.A. Vermaas, J. Veerman, M. Saakes, K. Nijmeijer, Influence of multivalent ions on renewable energy generation in reverse electrodialysis, Energy Environ. Sci. 7 (2014) 1434.

[49] R.A. Tufa, E. Curcio, W. van Baak, J. Veerman, S. Grasman, E. Fontananova, G. Di Profio, Potential of brackish water and brine for energy generation by salinity gradient power-reverse electrodialysis (SGP-RE), RSC Adv. 4 (2014) 42617–42623.

[50] J.W. Post, H.V.M. Hamelers, C.J.N. Buisman, Influence of multivalent ions on power production from mixing salt and fresh water with a reverse electrodialysis system, J. Memb. Sci. 330 (2009) 65–72.

[51] G.M. Geise, H.J. Cassady, D.R. Paul, B.E. Logan, M.A. Hickner, Specific ion effects on membrane potential and the permselectivity of ion exchange membranes, Phys. Chem. Chem. Phys. 16 (2014) 21673–21681.

[52] E. Güler, W. van Baak, M. Saakes, K. Nijmeijer, Monovalent-ion-selective membranes for reverse electrodialysis, J. Memb. Sci. 455 (2014) 254–270.

[53] A. Zlotorowicz, R. V Strand, O.S. Burheim, S. Kjelstrup, The permselectivity and water transference number of ion exchange membranes in reverse electrodialysis, J. Memb. Sci. 523 (2017) 402–408.

[54] S.M. Hosseini, S.S. Madaeni, A.R. Khodabakhshi, The electrochemical characterization of ion exchange membranes in different electrolytic environments: Investigation of concentration and pH effects, Sep. Sci. Technol. 47 (2012) 455–462.

[55] P. Długołęcki, J. Dąbrowska, K. Nijmeijer, M. Wessling, Ion conductive spacers for increased power generation in reverse electrodialysis, J. Memb. Sci. 347 (2010) 101–107.

[56] D.A. Vermaas, M. Saakes, K. Nijmeijer, Power generation using profiled membranes in reverse electrodialysis, J. Memb. Sci. 385–386 (2011) 234–242.

[57] S. Pawlowski, T. Rijnaarts, M. Saakes, K. Nijmeijer, J.G. Crespo, Improved fluid mixing and power density in reverse electrodialysis stacks with chevron-profiled membranes, 531 (2017) 111–121.

[58] O. Scialdone, C. Guarisco, S. Grispo, a. D. Angelo, a. Galia, Investigation of electrode material – Redox couple systems for reverse electrodialysis processes. Part I: Iron redox couples, J. Electroanal. Chem. 681 (2012) 66–75.

[59] J. Veerman, M. Saakes, S.J. Metz, G.J. Harmsen, Reverse electrodialysis: Evaluation of suitable electrode systems, J. Appl. Electrochem. 40 (2010) 1461–1474.

[60] O.S. Burheim, F. Seland, J.G. Pharoah, S. Kjelstrup, Improved electrode systems for reverse

electro-dialysis and electro-dialysis, Desalination. 285 (2012) 147–152.

[61] S.Y. Lee, Y.J. Jeong, S.R. Chae, K.H. Yeon, Y. Lee, C.S. Kim, N.J. Jeong, J.S. Park, Porous carbon-coated graphite electrodes for energy production from salinity gradient using reverse electrodialysis, J. Phys. Chem. Solids. 91 (2016) 34–40.

CHAPTER 2:

REVERSE ELECTRODIALYSIS PERFORMANCE FOR RIVER WATER/SEAWATER MIXING

Abstract

The effectiveness of Salinity Gradient Power - Reverse Electrodialysis (SGP-RE) in real practice is still not clearly defined due to the lack of specific studies in literature, being investigations in large part limited to on pure NaCl solutions or aqueous mixtures of two salts. In this work, we experimentally assessed the impact of natural feed streams (collected from Licetto river and Tyrrenian sea in Amantea - Italy) in terms of Open Circuit Voltage (OCV) and power density (P_d) measured on lab-scale SGP-RE stack prototype; results have been compared to those obtained when using NaCl solutions having equivalent ionic strength. Highest OCV (3.68 V and 4.09 V) and P_d values (0.46 and 1.41 $W \cdot m^{-2}$) were observed at temperature of 60°C for real and synthetic feeds, respectively.

The extent of electrical resistances (ion exchange membrane/electrical double layer/diffusion boundary layer) was elucidated by electrochemical impedance spectroscopy (EIS); in particular, a critical effect of real solution on cation exchange membrane (CEM) resistance was detected. In addition, ionic characterization of process effluents revealed the occurrence of uphill transport of multivalent ions Mg^{2+}, Ca^{2+} and SO_4^{2-}.

1. Introduction

According to US Energy Information Administration, world net electricity generation is expected to increase from 20 trillion to 40 trillion kWh in the coming 30 years; among all sources which presently fulfill the increasing demand of energy, renewable energy is the fastest-growing source of electric power with an annual 2.8% increase [1]. An emerging renewable energy source is Salinity Gradient Power (SGP), originally proposed for sea and river water mixing more than 60 years ago [2]. The total technical potential of SGP is estimated to be around 647 GW, which is 23% of the global electricity consumption [3]. Possible application areas of SGP techniques are estuaries where freshwater rivers run into seawater [4–7], high salinity wastewater (brine from desalination [8–11] or salt mining and saltworks [12–14]) and saltwater lakes [15,16].

There are two common technologies which harvest SGP by utilizing membrane-based processes: Reverse Electrodialysis (RE) – object of the present work - and Pressure Retarded Osmosis (PRO) [17]. In a typical SGP-RE system, cation exchange membranes (CEM) and anion exchange membranes (AEM) are piled up alternately between cathode and anode (Fig. 1). CEMs and AEMs are separated by spacers to allow the diluted and concentrated salt solutions flow through. Due to salinity gradient across the membranes, ions diffuse through the membranes from High Concentration Compartment (HCC) to Low Concentration Compartment (LCC): the ionic flux is converted to electronic flux in the electrode compartments by reduction and oxidation reactions on the electrode surface [10].

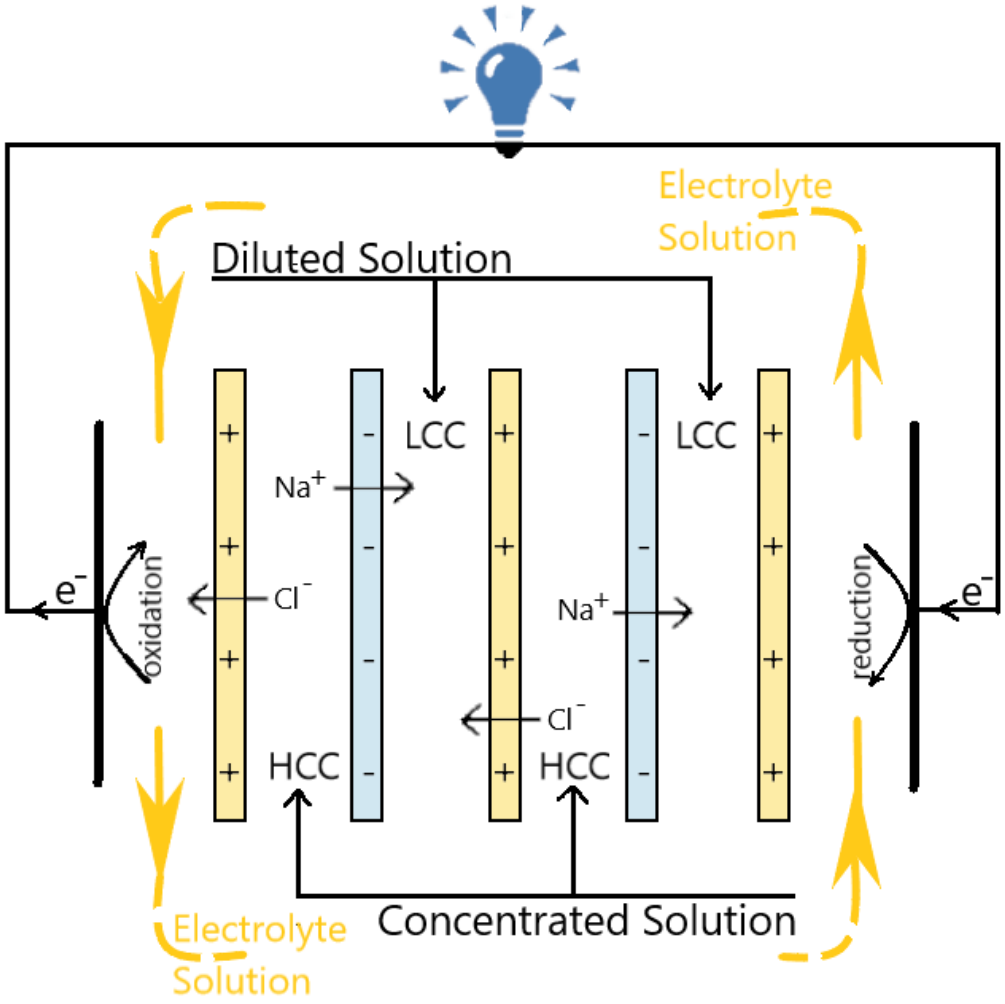

Figure 1. Conceptual scheme of a SGP-RE Unit

The most abundant natural salinity gradient sources are seawater and river water. Theoretically, the generated mixing energy of two solution with different concentration can be calculated by Gibbs free energy equation [6]:

$$\Delta G_{mix} = 2RT\left[V_D C_D \ln\frac{C_D}{C_M} + V_C C_C \ln\frac{C_C}{C_M}\right] \quad (1)$$

$$C_M = \frac{V_D C_D + V_C C_C}{V_D + V_C} \quad (2)$$

where ΔG_{mix} is the Gibbs free energy of mixing, V_D is volume of diluted solution with

concentration C_D, V_C is volume of concentrated solution with concentration C_C, C_M is the concentration of mixed solution, R is the gas constant (R=8.31432 $Jmol^{-1}K^{-1}$) and T is the temperature (K). Eq. 1 assumes entropy change in the water and activity of the solutions having negligible effect on final ΔG_{mix}.

In theory, complete mixing of 1 m^3 seawater (assumed as 30 kg $\cdot m^{-3}$ NaCl) and 1 m^3 river water (assumed as pure water) produces 1.7 MJ energy, that can be increased up to 6.1 MJ at 298 K when volumetric ratio of river water/seawater is 10 [6]. The numerous attempts made to investigate extractable energy of seawater and river water mixing resulted in gross power density between 0.20 - 2.2 $W \cdot m^{-2}$ depending on membrane type, spacer type, spacer thickness, membrane area, number of cells, linear flow velocity, slight difference on concentration gradient and temperature [2,18–27,7,28]. One of the first measurements of power density was reported as 0.20 $W \cdot m^{-2}$ by Pattle (1954). In that study, maximum power was obtained for polyethylene mixed with crosslinked polystyrene resins membranes and 1 mm nonconductive thickness at 39ºC where 0.5 M NaCl solution and tap water were used as feed [2]. After IEM technology had improved, Veerman *et al.* (2009) performed synthetic seawater/river water RE experiments with six commercial membranes pairs; the highest measured power densities were 1.17 and 1.18 $W \cdot m^{-2}$ for Fumasep (FAD and FDK) and Selemion (AMV and CMV) membrane pairs, respectively, and a noteworthy thermodynamic efficiency (35%) was obtained [25]. Guler *et al.* (2013) prepared custom-made sulfonated polyetheretherketone CEM and polyepichlorohydrin AEM designed for RE; utilizing these membrane pairs resulted in 1.28 $W \cdot m^{-2}$ gross power density [20]. Hong *et al.* (2014) conducted RE experiments by pairing a custom-made composite CEM with ASV (Selemion, Japan) AEM; under optimized electrochemical properties, a maximum power density of 1.3 $W \cdot m^{-2}$ was generated [21]. Vermaas *et al.* (2011) investigated the effect of intermembrane

thickness and feed flow rate on the power density for synthetic seawater and river water: the highest recorded gross power density was 2.2 $W \cdot m^{-2}$ for 100 µm intermembrane thickness; moreover, possibility to reach 4 $W \cdot m^{-2}$ was predicted for 60 µm intermembrane thickness [7].

Aforementioned studies were only carried out with synthetic solutions mimicked by NaCl. However, a large spectra of mono- and multivalent ions together with some organic compounds are present in the natural feed solutions. Although previous studies carried out on artificial multi-ion saline solutions revealed a drastic effect of these compounds on the RE performance [10,29–32], investigations on real environment are so far scarcely present in literature [14].

Decrease in Nernst potential, uphill transport, increasing IEM resistance were the most pronounced observations due to presence of multivalent ions. Vermaas *et al.* (2014) and Post *et al.* (2009) investigated effect of divalent ions on stack voltage and resistance for artificial solutions mimicking seawater/river water pair: up to 50% reduction in power density was observed when Mg^{2+} and SO_4^{2-} divalent ions were present [31,32]. For more concentrated solutions and for higher content of multivalent ions, more severe impact has been observed on RED performance. Avci *et al.* (2016) carried out a parametric work on concentration of Mg^{2+} for 0.5 and 4 molal solutions; having 100% Mg^{2+} instead of Na^{+} resulted in more than 50% decrease on OCV, three times higher stack resistance and 90% decrease in produced gross power density [29]. The first RE pilot plant was operated with natural brackish water and almost saturated brine from saltworks and compared with artificial NaCl equivalent solutions by Tedesco *et al.* (2016): the RE unit was able to generate 40 W power with 125 cell pairs and almost 50 m^2 membrane area for real waters whereas artificial NaCl solutions resulted in 65 W [14].

In the present study, the performance of SGP-RE was evaluated in a real environment by testing natural river water and seawater feeds. System performance was evaluated in terms of Open Circuit

Voltage (OCV) and power density (P_d) on a lab-scale SGP-RE stack prototype, and results compared to those obtained when using NaCl solutions with equivalent ionic strength. The extent of electrical resistances (ion exchange membrane/electrical double layer/diffusion boundary layer) was elucidated by electrochemical impedance spectroscopy (EIS). Occurrence of uphill transport due to the presence of multivalent ions (Mg^{2+}, Ca^{2+} and SO_4^{2-}) was investigated by ion chromatography.

2. Materials and Methods

2.1. Solutions

Feed solutions were collected from river Licetto and Tyrrenian Sea in Amantea (Italy). Solutions were microfiltered through 0.20 μm pore size polypropylene membranes (Microdyn®); the ionic composition of the saline feeds, characterized by Ion Chromatography (see 2.3), is reported in Table 1.

Artificial aqueous solutions mimicking river water and seawater (same ionic strength) were prepared by appropriate amounts of NaCl (Sigma Aldrich, Italy). Ionic strength I_m of river and seawater was calculated as:

$$I_m = \frac{1}{2}\sum m_i z_i^2 \qquad (3)$$

where m_i is molality of the i-th ion and z_i its charge.

For SGP-RE operation, the composition of aqueous electrolyte solution was: 0.3 M potassium hexacyanoferrate (II), 0.3 M potassium hexacyanoferrate (III) and 2.5 M sodium chloride (all purchased from Sigma-Aldrich, Italy). For the preparation of synthetic saline solutions and electrolyte solution, deionized water (PURELAB, Elga LabWaters, 0.055 $mS \cdot cm^{-1}$) was used.

Table 1. Ionic Content of river and seawater and equivalent ionic strengths`

	Present Ions (ppm)									Ionic Strength (molal)
	Na^+	K^+	Mg^{2+}	Ca^{2+}	Cl^-	NO_2^-	Br^-	NO_3^-	SO_4^{2-}	
River water	23	4	28	152	16	0.5	-	2	78	0.012
Sea water	17941	671	2121	493	20975	-	117	63	2192	0.958

2.2. Reverse Electrodialysis Setup

The SGP-RED stack prototype provided by REDstack BV (Netherlands) was used in the same arrangement as it is mentioned previously[20]. RED stack was equipped with AEM-80045 and CEM-80050 Ion Exchange Membranes (IEMs) provided by Fujifilm Manufacturing Europe B.V. (The Netherlands). Relevant characteristic of the membranes are illustrated in Table 2.

Table 2. Properties of ion exchange membrane [23]

Membrane code	Thickness (μm)*	Ion exchange capacity (mmol/g membrane)	Density of fixed charge (mol/L)	Membrane areal resistance (Ωcm^2)**
Fuji-AEM-80045	129 ± 2	1.4 ± 0.1	3.8 ± 0.2	1.551 ± 0.001
Fuji-CEM-80050	114 ± 2	1.1 ± 0.1	2.4 ± 0.2	2.974 ± 0.001

*Conditions: NaCl 0.5 M, 20 ° C
**Conditions: NaCl 0.5 M, 20 ° C, 2.8 cm/s

The performance of the SGP-RE unit was investigated at different temperature (20-60 °C) and flow rate (20-40 $L \cdot h^{-1}$). Flowrate of electrolyte solution was fixed to 30 $L \cdot h^{-1}$. Solutions were fed by Masterflex L/S digital peristaltic pumps (Cole-Palmer, US) and conditioned to desired temperature by a refrigerated/heated circulating bath (PolyScience, US) before entering the stack. A high dissipation five-decade resistance box in the range of 0.1–1000 Ω (CROPICO, Bracken Hill, US) was used to load the SGP-RE system. Corresponding voltage drop and current were recorded after altering resistance box in the range of 60–0.1 Ω. DC voltage drop across the stack was measured by a 3½ digital multimeter with accuracy of 70.5% in the range of 200 mV to 200 V (Velleman, DVM760, Belgium), and the current flowing across the load resistors was measured by 6½ digit multimeter (Agilent, 34422A, Italy).

After fitting voltage (V) versus current (I) with a straight line, OCV and the total resistance of stack (R_{stack}) (Ω) were respectively calculated as intercept (I=0) and slope of the equation:

$$V(I) = OCV - R_{stack} I \tag{4}$$

The gross power density P_d follows a parabolic trendline in the form of:

$$P_d = \frac{OCV^2}{4 R_{stack} N_M} \tag{5}$$

in which P_d is the gross power density (in $W \cdot m^{-2}$), OCV is the open circuit voltage, i.e., the stack voltage measured at zero current (V), R_{stack} is the internal resistance of the stack ($\Omega \cdot m^2$) and N_M is the number of membranes contributing to the voltage. P_d reaches its maximum value when external resistance (load resistance) is equal to internal resistance (stack resistance) [7].

2.3. Ion Chromatography

Ion Chromatography was employed to quantify the concentration of ions at the inlet and outlet of SGP-RED unit (Metrohm 861 Advanced Compact Ion Chromatograph) operated under open-circuit configuration and continuous feed flow. In order to reach the steady-state, samples were collected after one hour of operation. 3.2 mM Na_2CO_3 + 1 mM $NaHCO_3$ was used as eluent for anion column Metrosep A Supp 5 - 250/4.0, and 2 mM nitric acid + 0.25 mM oxalic acid was used as eluent for cation column Metrosep C4 – 250/4.0.

2.4. Electrochemical Impedance Spectroscopy

Electrochemical Impedance Spectroscopy (EIS) measurements were carried out using a potentiostat/galvanostat combined with a frequency response analyzer (Metrohm Autolab PGSTAT302N). A home-designed four electrodes impedance cell having 3.14 cm^2 active

membrane area (Fig. 2) was employed. Electro-deposition method was applied to cover working and counter electrodes with a thin layer of AgCl. The sense and reference electrodes were Ag/AgCl electrodes (Gamry Instruments); the Haber–Luggin capillaries were filled with 3 M KCl.

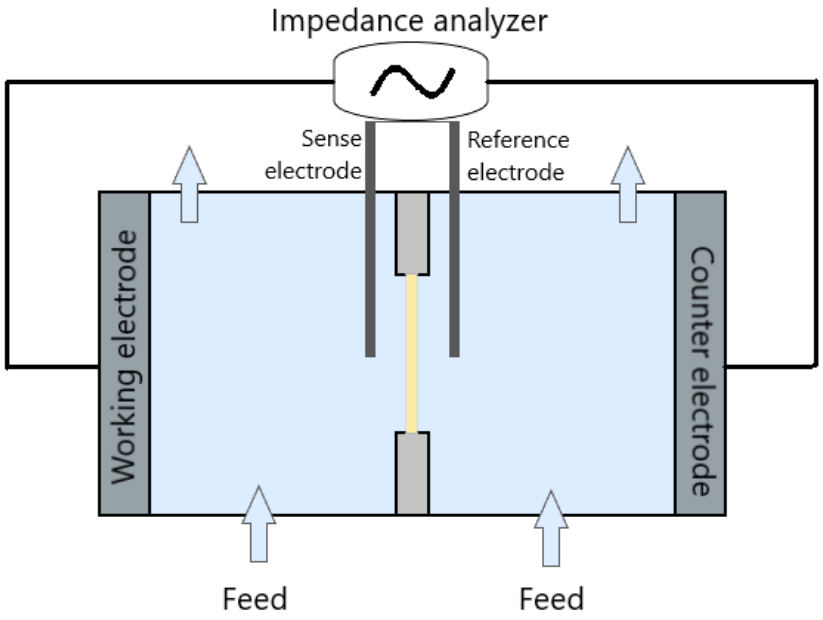

Figure 2. Scheme of four electrode confuguration Electrochemical Impedance Spectroscopy (EIS) cell.

AEM-80045 and CEM-80050 membranes were characterized by EIS for natural sea and river water at 25 °C. Before analysis, virgin membranes were conditioned for 24 h in test solutions, refreshed every 8 h to be sure no residual solutions were present.

Fig. 3 summarizes EIS procedure adopted in this study. AC current in the frequency range of 1000–0.01 Hz with signal amplitude of 10 mV was generated through the cell and response was recorded. Collected data were fitted by the equivalent circuit model shown in Fig. 3c by Nova 1.9.16 by Metrohm Autolab B.V (The Netherlands). Specifically, diffusion boundary layer was represented by a resistor and a constant phase element in parallel, while electric double layer was represented by a parallel combination of a resistor and a capacitor [33]. For each test solution, a blank experiment (without membrane) was carried out in order to measure the solution resistance;

membrane resistance R_m is then calculated by subtracting solution resistance from overall resistance (R_{m+s}).

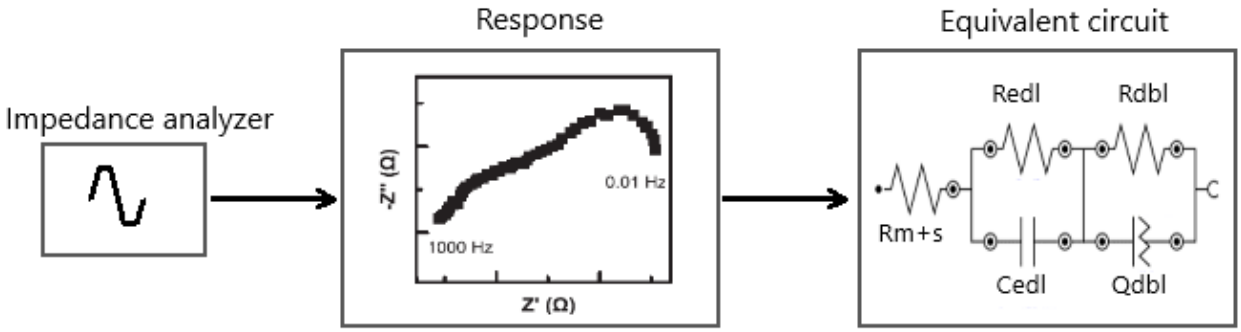

Figure 3. Summary of the EIS procedure: a) impedance analyzer, b) plot of real (Z' (Ω)) and imaginary part (Z'' (Ω)) of impedance, c) illustration of equivalent circuit for membrane and solution resistance, electrical double layer resistance and diffusion boundary layer resistance.

3. Results and discussion

3.1. SGP-RE tests

Natural seawater and river water under investigation contain 44.6 and 0.3 g/L of total dissolved salts, respectively. The ionic content is higher with respect to standard values reported in literature (35 g/L and 0.13 g/L, respectively); however, this salinity variation is an expected situation in restricted basins (i.e. Mediterranean sea) [34].

Fig. 4 illustrates current-voltage and current density-power density curves for natural and artificial solution at constant temperature of 20ºC and at different flow rates. The maximum SGP-RE performance was observed for synthetic NaCl solutions fed at flow rate 40 $L \cdot h^{-1}$: gross P_d reached a maximum of 1.14 $W \cdot m^{-2}$ at current density of 15 $A \cdot m^{-2}$, OCV attained 3.96 V, and R_{stack} was 14.8 Ω. On the other hand, the poorest performance was detected when mixing natural seawater and river water at flow rate 20 $L \cdot h^{-1}$: gross P_d value and current density fell down to 0.29 $W \cdot m^{-2}$ and 5 $A \cdot m^{-2}$, respectively, while OCV decreased to 3.17 V and R_{stack} increased to 34.9 Ω. Use of natural solutions instead of synthetic ones resulted in a reduction of power density higher than

50%; this effect became more visible at higher flow rates. Eq. 5 illustrates the dependence of power density on OCV and R_{stack}. Although OCV is more influential on power density (squared dependence), in our case the dominant decreasing parameter was R_{stack}; in fact, OCV values varied within a quite narrow range (3.1 – 4.0 V), while R_{stack} reduced significantly (from 35 to 14 Ω).

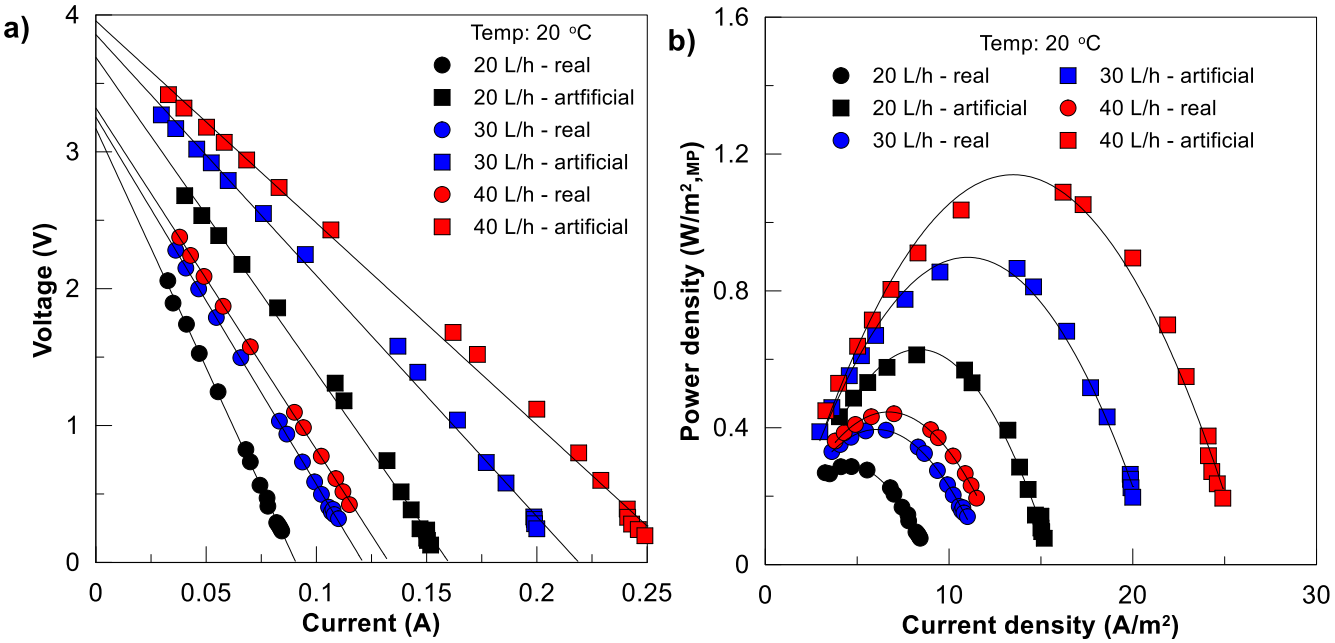

Figure 4. a) Voltage versus current at 20 ° C; b) Gross power density versus current density at 20 ° C.

Average permselectivity α_{ave} of Fuji-AEM-80045 and Fuji-CEM-80050 membranes can be calculated from Planck Henderson equation [5]:

$$OCV = 2N\frac{RT}{F}\frac{\alpha_{ave}}{z}\ln\left(\frac{a_s}{a_r}\right) \quad (6)$$

where N is number of membranes, R is the universal gas constant (J $mol^{-1}\cdot K^{-1}$), T is the absolute temperature (K), F is the Faraday constant ($C\cdot mol^{-1}$), a_s is the activity of seawater solution ($mol\cdot l^{-1}$), a_r is the activity of river water solution ($mol\cdot l^{-1}$), and z is the ion valence (-). Activity coefficients were evaluated by PHREEQC v. 2.18.00 software [35].

Average permselectivity of the Fuji-AEM and CEM in artificial seawater and river water mixing was 68%, assuming a linear variation of solute concentration along the stack. As a comparison,

Fontananova *et al.* (2017) reported permselectivity of Fuji-CEM and Fuji-AEM measured by *ex-situ* method as 96% and 93% (average: 94.5%), respectively, in 0.1//0.5 M pure NaCl solutions [36]. The lower permselectivity can be explained by the higher concentration gradient of feed solutions (from table 1, equivalent ionic strength is 0.012 and 0.958 molal for river water and seawater, respectively, for an HCC/LCC ratio of ~ 80) that enhances the co-ion transport against the chemical potential gradient [36,37]. Accordingly, for 0.1//5.0 M NaCl solutions (HCC/LCC ratio of ~ 50), Fontananova *et al.* (2017) observed a decrease of Fuji-CEM and Fuji-AEM permselectivity to 89% and 73%, respectively [36].

Table 3 summarizes the experimental data for OCV, resistance and P_d. In general, a step increase in flowrate from 20 to 30 $L \cdot h^{-1}$ improved P_d and decreased stack resistance more than a further increment from 30 to 40 $L \cdot h^{-1}$. For natural solutions, in the first case P_d enhanced by 38% while R_{stack} decreased by 23% whereas, in the second step, P_d enhanced by 10% while R_{stack} decreased only by 7%. Likewise, when flowrate of artificial solution was increased from 20 $L \cdot h^{-1}$ to 30 $L \cdot h^{-1}$, P_d increased by 48% and R_{stack} decreased by 24%; these values were limited to 27% and 16% in the case of flowrate enhancement from 30 to 40 $L \cdot h^{-1}$. Vermaas *et al.* (2011) observed that the diffusive boundary layer near the membranes induces a considerable resistance at lower flow rates [7]. Enhancing the non-ohmic resistances by improving fluid-dynamics (higher Reynolds number) is possible up to a certain extent; further increase in flow rate does not promote a significant gain in terms of gross P_d due to increase in pumping energy [38].

An additional reason for increasing power density at higher flow rates is related to the residence time of solutions within the stack. Higher residence time (at lower flowrate) results in a more significant dilution of the HCC solution accompanied by a more significant concentration of the

LCC solution; the consequent decrease of concentration gradient across IEMs causes the decline of SGP-RE performance.

Table 3. Summary of the RED test

		Real Solutions			Artificial Solutions		
Flow rate L/h	**Temp. °C**	**OCV V**	**Resist. Ω**	**P_d W/m²**	**OCV V**	**Resist. Ω**	**P_d W/m²**
20	60	3.68	30.5	0.46	4.09	12.85	1.41
	40	3.54	33.2	0.39	4.10	14.48	1.26
	20	3.17	34.9	0.29	3.69	23.05	0.61
30		3.25	26.8	0.40	3.86	17.61	0.90
40		3.32	25.0	0.44	3.96	14.76	1.14

In natural seawater, more than 10%w of cations were divalent ions (Mg^{2+} and Ca^{+}) and approximately 10%w of anions were divalent SO_4^{2-}. The evidence of the negative impact of divalent ions on the SGP-RE performance, is reported in literature [10,29,31,32,39]; hereafter we show that this effect - intrinsically associated to the ion valence z>1 in equation 6 – is mainly enforced by the increase in IEM resistance and the occurrence of Mg^{2+} and SO_4^{2-} transport against its concentration gradient.

Membrane resistance and permselectivity are significantly affected by the electrical interactions between bi-valent ions and fixed charged groups of IEMs; in particular, an increase in CEM resistance occurs due to crosslinking of two fixed anionic groups when bridged by Mg^{2+}; similarly, SO_4^{2-} ions cause an increase of AEM resistance by attracting each one a pair of fixed cationic groups. Neutralization of some fixed groups reduces the effective charge density of IEMs; consequently, ineffective Donnan exclusion results in a low permselectivity [40]. Ion permselectivity depends on several factors, such as affinity of a specific ion to a given fixed group

on the membrane and mobility of ions. The selectivity order of anions were stated by Sata (2000) [41] as:

$$I^- > NO_3^- \sim Br^- > NO_2^- > Cl^- > OH^- > SO_4^{2-} > F^-$$

while selectivity order for cations were reported by Strathmann (2004) [42] as:

$$Ba^{2+} > Sr^{2+} > Ca^{2+} > Mg^{2+} > H^+ > (Cu^{2+} \sim Zn^{2+} \sim Ni^{2+}) > K^+ > Na^+ > Li^+ > Fe^{3+}$$

According to permselectivity studies, it can be concluded Cl^- is preferred against SO_4^{2-} by AEM whereas Ca^{2+} and Mg^{2+} are preferred against Na^+ by CEM. Coherently, Avci *et al.* (2016) observed that CEM resistance is critically affected by Mg^{2+} concentration.

Fig. 5 shows the results from electrical tests on SGP-RE stack at different temperatures (20, 40 and 60°C) for both natural and artificial seawater and river water. Under the same experimental conditions, mixing artificial NaCl solutions resulted in higher P_d and OCV, and lower R_{stack} than natural solutions. Presence of approximately 10%w multivalent ions reduced OCV due to the screening effect of fixed charge groups on IEMs as discussed before. However, for both natural and artificial solutions, the performance of SGP-RE unit increased with temperature due to higher transport rate of ions. Diffusion coefficients of Na^+ and Cl^- in 0.5 M NaCl were measured for Fuji-CEM-80050 and Fuji-AEM-80045, respectively, at different temperatures by Fontananova *et al.* (2014): a 24% and 80% increase were recorded for chloride and sodium ions, respectively, when increasing temperature from 20 to 40 ℃ [33]. At 60 °C, the maximum power density and OCV were 1.41 $W \cdot m^{-2}$ and 4.09 V, respectively, recorded for artificial feeds. On the other hand, R_{stack} reached its lowest value of 12.8 Ω.

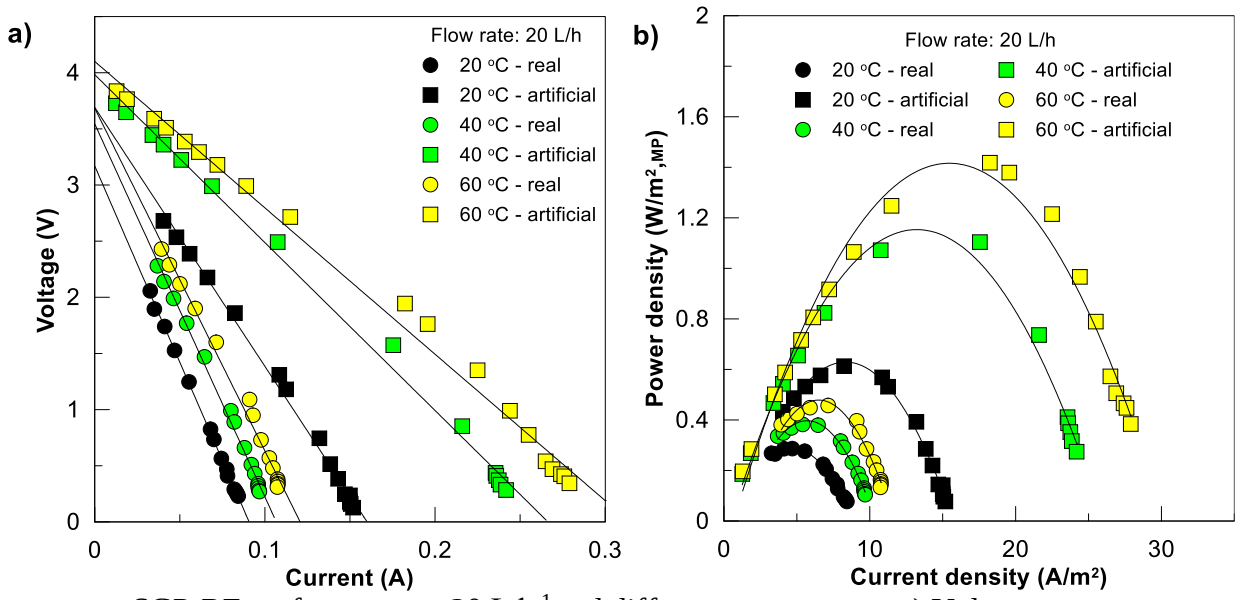

Figure 5. SGP-RE performance at 20 $L \cdot h^{-1}$ and different temperature: a) Voltage versus current; b) Gross power density versus current density.

3.2. Uphill transport

Characterization of ion concentration in the inlet and outlet streams is essential for a deep understanding of mixing process and transport phenomena taking place within the SGP-RE unit. This investigation is important from both chemical and physical point of view, since different ions exhibit a different level of interactions with fixed charge groups located on IEMs. Figure 6 illustrates the influence of flowrate on ion transport at constant temperature (20°C). As expected, increasing flowrate ended up with a decreased number of transported ions for major monovalent species (Cl^- and Na^+) for both artificial and natural solutions due to lower residence time. K^+, a minor monovalent ion, also contributed to the total flux by transporting in the same direction of concentration gradient. On the other hand, multi-valent ions like Mg^{2+}, Ca^{2+} and SO_4^{2-} showed transport along the opposite direction of concentration gradient; this phenomenon is known as "uphill transport" [29,31,32,39].

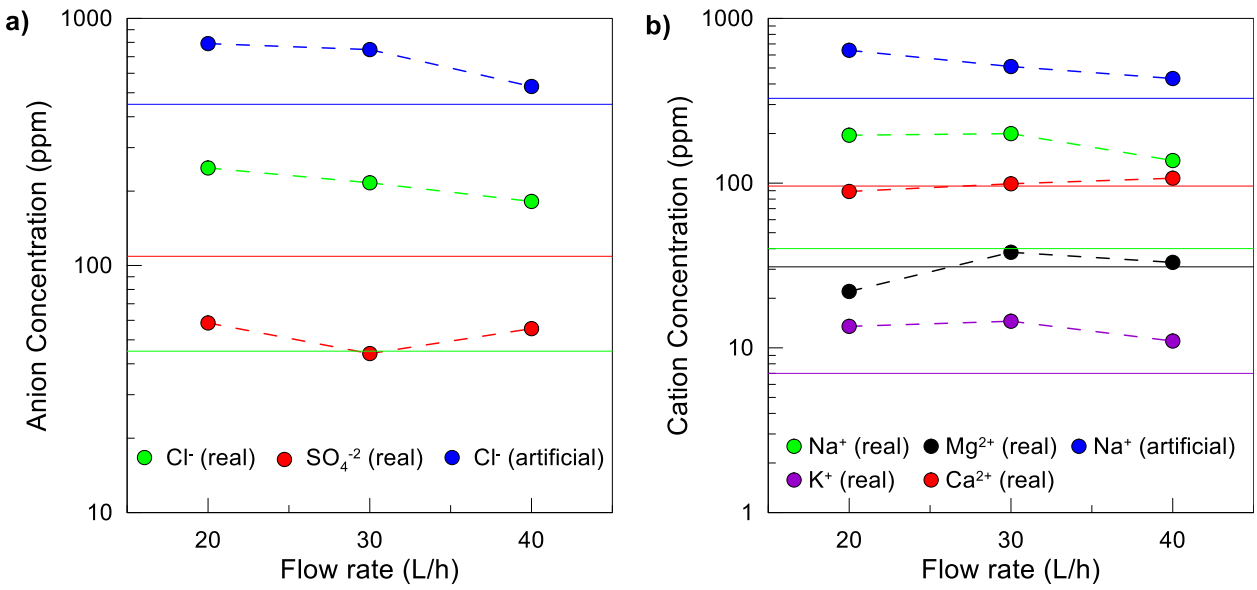

Figure 6. Transport of ions in LCC as a function of flowrate (temperature: 20°C): a) anions Cl^-, SO_4^{2-}; b) cations Na^+, K^+, Ca^{2+} and Mg^{2+}. Solid line with the same color of the symbol represents the inlet concentration of the corresponding ion, symbols are the outlet concentration of ions. Uphill transport occurs when symbols are below the corresponding solid lines.

Inter-diffusion between monovalent and multivalent ions occurs in other systems such as Donnan dialysis, driven by Donnan potential established between the membrane and the adjacent solution to maintain electroneutrality [31,32,39]. In SGP-RE, some previous studies carried out with artificial seawater and river water containing divalent ions, e.g. Mg^{2+} and SO_4^{2-}, reported the occurrence of uphill transport. Rijnaarts *et al.* (2017) theoretically explained the uphill transport over an ideal CEM exposed to 0.5 and 0.017 M saline solutions with 10% mol Mg^{2+}; cations start moving across the ion selective membrane under Donnan potential (0.079 V for Na^+ and 0.039 V for Mg^{2+}), until achieving Donnan equilibrium and maintaining charge neutrality (two Na^+ exchange for one Mg^{2+}) [39]. Investigations of Avci *et al.* (2016) provided evidence of uphill transfer in SGP-RE operated with NaCl-$MgCl_2$ solutions in the range of 0-30% of Mg^{2+} [29]. Fig. 7 shows the transported ions in LCC at temperatures of 20, 40 and 60°C with feed flowrate kept constant at 20 $L \cdot h^{-1}$. At increasing temperature, major monovalent ions exhibit a faster transport

along the concentration gradient, while multivalent ions Ca^{2+}, Mg^{2+} and SO_4^{2-} resulted in uphill transport at increasing mobility.

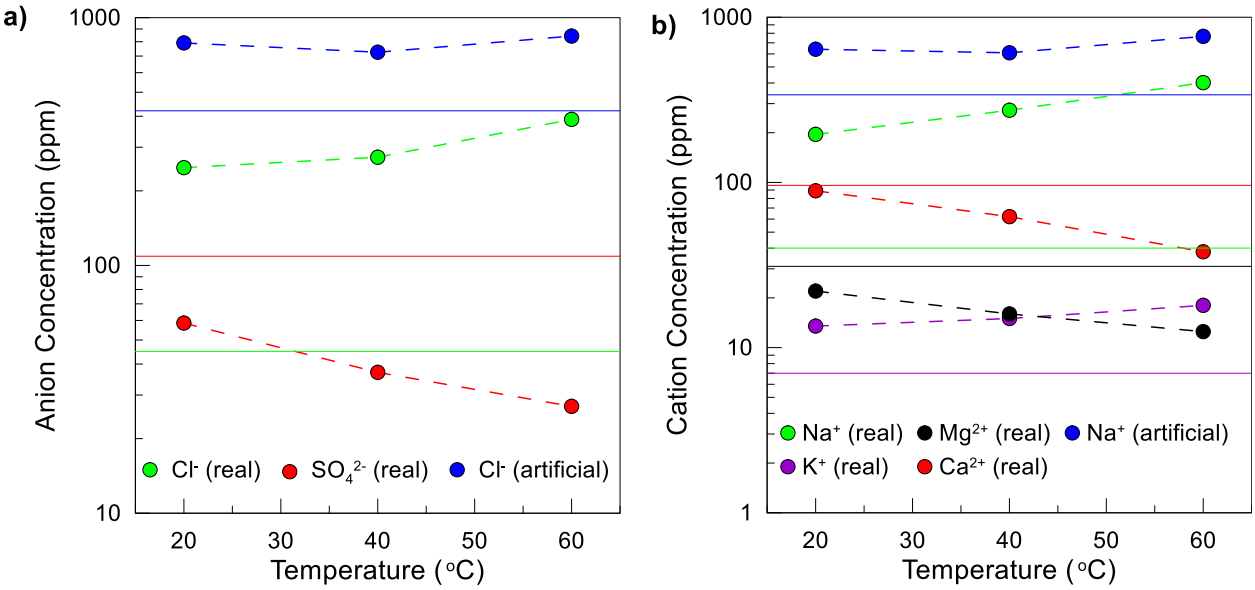

Figure 7. a) Transport of ions in LCC as a function of temperature (flowrate: 20 $L \cdot h^{-1}$): a) anions Cl^-, SO_4^{2-}; b) cations Na^+, K^+, Ca^{2+} and Mg^{2+}. Solid line with the same color of the symbol represents the inlet concentration of the corresponding ion, symbols are the outlet concentration of ions. Uphill transport occurs when symbols are below the corresponding solid lines.

3.3. Electrochemical Impedance Spectroscopy

Characterization of electrical properties of IEMs and their interfaces was done by Electrochemical Impedance Spectroscopy (EIS) [43]. In this study, a range of frequency from 0.01 to 1000 Hz was applied to analyze impedance of the membranes and electrolytes. In such a system, the total resistance is dectermined by ohmic resistances (i.e. membrane and solution resistances) and non-ohmic resistances (i.e. electrical double layer and diffusion boundary layer resistances) as it is shown by the electrical circuit (Fig. 3).

Charged groups fixed on the membrane surface attract the oppositely charged ions via Coulomb forces and create electrical double layer at the solid-liquid interface. Electrical double layer is composed of Stern layer and diffuse layer; strongly bounded ions - due to electrostatic interactions

next to the membrane - form the Stern layer, while diffuse layer is caused by weak electrostatic interactions on the outer shell of electrical double layer [33].

Diffusion boundary layer arises from the difference between transport number of the membrane and the bulk solution. In an ideal IEM, electrical current is transported by counter ions because of the Donnan exclusion. On the other hand, in the bulk solution, univalent ions carry almost the same electrical current, and s a result, excluded ions get polarized as an additional layer [33].

In this work, EIS allowed the quantitative characterization of the different electrical resistances present in the system. Fig. 8 illustrates the impedance characterization of AEM-80045 and CEM-80050 membranes in natural feed streams. As expected, total membrane resistances were an order of magnitude higher when natural river water used. In particular, CEM offers 5-6 times higher resistance than AEM in both seawater and river water, confirming the high impact of divalent cations. The aforementioned charge screening effect by divalent ions cause neutralization of fixed charge groups and, ultimately, increase of membrane resistance. It is worth mentioning that, for all cases, the extent of non-ohmic resistances was negligible with respect to total resistance.

The increase in the stack resistance when feed streams were shifted from artificial to natural solutions can be therefore attributed prevalently to the increase in CEM resistance. When comparing the values of membrane resistance with respect to measurements in standard solutions presented in Table 2, no significant change was observed for AEM, while CEM resistance increased 5 times in natural seawater. A possible explanation is that the affinity of fixed charged groups of a CEM to Na^+ is lower than that of multivalent ions such as Mg^{2+} and Ca^{2+} whereas, for AEM, the affinity to Cl^- is higher than that of SO_4^{2-}, thus determining a limited screening effect.

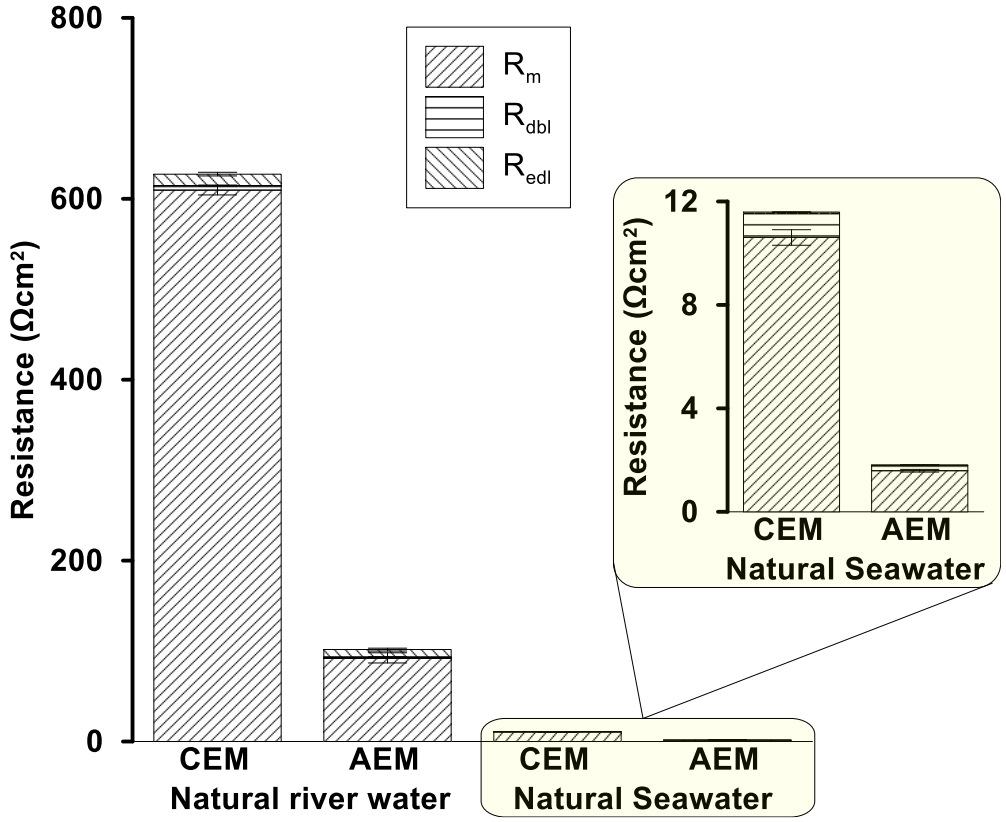

Figure 8. EIS of AEM-80045 and CEM-80050 in natural river water and seawater (R_m: membrane resistance; R_{dbl}: diffusive boundary layer resistance; R_{edl}: electrical double layer resistance).

The high resistance of IEMs in natural river water is coherent with the studies of Galama *et al.* (2014), who noted that membrane resistance mostly depends on the lowest external solution ion concentration and, below 0.3 M, it is limited by the conductivity of ionic solution [44].

Concerning the non-ohmic resistances, electrical double layer and diffusion boundary layer resistances were, respectively, one and two order of magnitude lower than ohmic resistances, for both AEM and CEM. Non-ohmic resistances in river water were about 10 times lower than those measured in seawater. For natural seawater, non-ohmic resistances on CEM were higher than on AEM because of the higher different mobility of chloride with respect to sodium (u_{Cl^-}/u_{Na^+} = 1.5 [45]). Dlugulecki *et al.* (2010) observed that non-ohmic resistances are affected by the

hydrodynamics of the system; on the other hand, ohmic resistances depend on temperature [45]. The values of total stack resistance reported in Table 3 agree with these assumptions: increasing flowrate from 20 to 40 $L \cdot h^{-1}$ resulted in 42% and 36% reduction in R_{stack} for natural and artificial solutions, respectively. Moreover, raising the temperature from 20 °C to 60 °C led to 13% and 44% reduction of R_{stack} for natural and artificial solutions, respectively.

4. Conclusion

Tests with the natural solutions provide reliable data on the realistic potential and current limitation of RE. In this study, energy generation by SGP-RE from natural seawater/river water solutions and equivalent (in terms of ionic strength) NaCl solutions were investigated at different temperatures and flow rates. All artificial solutions resulted in higher power density, higher OCV and lower R_{stack}. At best, 1.41 $W \cdot m^{-2}$ maximum gross power density was extracted when operating with artificial NaCl solutions at 60 ^{o}C, with highest recorded OCV (3.68 V) and lowest R_{stack} (30.5 Ω). On the other hand, SGP-RE performance with natural feeds was significantly reduced as a result of increased IEM resistance (Electrochemical Impedance Spectroscopy detected a noteworthy sensitivity of CEM to the presence of multivalent ions, whose resistance was 6 times higher in river water and 3 times higher in seawater), reduced OCV and occurrence of uphill transport for Ca^{2+}, Mg^{2+} and SO_4^{2-}.

Results revealed the necessity to implement appropriate pretreatment to soften the feed solutions; additionally, further advances on membrane materials and manufacturing strategies are needed in order to enhance both the efficiency of monovalent ions transfer and the rejection of multivalent ions.

5. References

[1] International Energy Outlook 2013, Washington, 2013. doi:EIA-0484(2013). https://www.eia.gov/outlooks/ieo/pdf/0484(2013).pdf. (accessed in 22 February 2018)

[2] R.E. Pattle, Production of electric power by mixing fresh and salt water in the hydroelectric pile, Nature. 174 (1954) 660.

[3] F.N. Ruud Kempener, Salinity gradient energy, Bonn, Germany, 2014. http://eusew.eu/sites/default/files/energy_days/Sal%20Grad%20Background%20doc%20.pdf. (accessed in 22 February 2018)

[4] A. Daniilidis, D. a. Vermaas, R. Herber, K. Nijmeijer, Experimentally obtainable energy from mixing river water, seawater or brines with reverse electrodialysis, Renew. Energy. 64 (2014) 123–131.

[5] J.N. Weinstein, F.B. Leitz, Electric Power from Differences in Salinity: The Dialytic Battery, Science. 191 (1976) 557–559.

[6] J. Veerman, M. Saakes, S.J. Metz, G.J. Harmsen, Reverse electrodialysis: Performance of a stack with 50 cells on the mixing of sea and river water, J. Memb. Sci. 327 (2009) 136–144.

[7] D.A. Vermaas, M. Saakes, K. Nijmeijer, Doubled power density from salinity gradients at reduced intermembrane distance., Environ. Sci. Technol. 45 (2011) 7089–7095.

[8] E. Brauns, An alternative hybrid concept combining seawater desalination, solar energy and reverse electrodialysis for a sustainable production of sweet water and electrical energy, Desalin. Water Treat. 13 (2010) 53–62.

[9] R.A. Tufa, E. Rugiero, D. Chanda, J. Hnàt, W. van Baak, J. Veerman, E. Fontananova, G. Di Profio, E. Drioli, K. Bouzek, E. Curcio, Salinity gradient power-reverse electrodialysis and alkaline polymer electrolyte water electrolysis for hydrogen production, J. Memb. Sci. 514 (2016) 155–164.

[10] R.A. Tufa, E. Curcio, W. Van Baak, J. Veerman, S. Grasman, E. Fontananova, G. Di Profio, Potential of brackish water and brine for energy generation by salinity gradient power-reverse electrodialysis (SGP-RE), RSC Adv. 4 (2014) 42617–42623.

[11] R.A. Tufa, E. Curcio, E. Brauns, W. van Baak, E. Fontananova, G. Di Profio, Membrane distillation and reverse electrodialysis for near-zero liquid discharge and low energy seawater desalination, J. Memb. Sci. 496 (2015) 325–333.

[12] M. Turek, B. Bandura, P. Dydo, Power production from coal-mine brine utilizing reversed electrodialysis, Desalination. 221 (2008) 462–466.

[13] M. Tedesco, E. Brauns, A. Cipollina, G. Micale, P. Modica, G. Russo, J. Helsen, Reverse Electrodialysis with saline waters and concentrated brines: a laboratory investigation towards technology scale-up, J. Memb. Sci. 492 (2015) 9–20.

[14] M. Tedesco, C. Scalici, D. Vaccari, A. Cipollina, A. Tamburini, G. Micale, Performance of the first Reverse Electrodialysis pilot plant for power production from saline waters and

concentrated brines, J. Memb. Sci. 500 (2016) 33–45.

[15] A. Emdadi, P. Gikas, M. Farazaki, Y. Emami, Salinity gradient energy potential at the hyper saline Urmia Lake - Zarrineh Rud River system in Iran, Renew. Energy. 86 (2016) 154–162.

[16] G.L. Wick, Power from salinity gradients, Energy. 3 (1978) 95–100.

[17] J.W. Post, J. Veerman, H.V.M. Hamelers, G.J.W. Euverink, S.J. Metz, K. Nymeijer, C.J.N. Buisman, Salinity-gradient power: Evaluation of pressure-retarded osmosis and reverse electrodialysis, J. Memb. Sci. 288 (2007) 218–230.

[18] P. Długołęcki, J. Dąbrowska, K. Nijmeijer, M. Wessling, Ion conductive spacers for increased power generation in reverse electrodialysis, J. Memb. Sci. 347 (2010) 101–107.

[19] E. Güler, R. Elizen, M. Saakes, K. Nijmeijer, Micro-structured membranes for electricity generation by reverse electrodialysis, J. Memb. Sci. 458 (2014) 136–148.

[20] E. Güler, R. Elizen, D.A. Vermaas, M. Saakes, K. Nijmeijer, Performance-determining membrane properties in reverse electrodialysis, J. Memb. Sci. 446 (2013) 266–276.

[21] J.G. Hong, Y. Chen, Nanocomposite reverse electrodialysis (RED) ion-exchange membranes for salinity gradient power generation, J. Memb. Sci. 460 (2014) 139–147.

[22] J. Jagur-Grodzinski, R. Kramer, Novel process for direct conversion of free energy of mixing into electric power, Ind. Eng. Chem. Process Des. Dev. 25 (1986) 443–449.

[23] F. Suda, T. Matsuo, D. Ushioda, Transient changes in the power output from the concentration difference cell (dialytic battery) between seawater and river water, Energy. 32 (2007) 165–173.

[24] M. Turek, B. Bandura, Renewable energy by reverse electrodialysis, Desalination. 205 (2007) 67–74.

[25] J. Veerman, R.M. de Jong, M. Saakes, S.J. Metz, G.J. Harmsen, Reverse electrodialysis: Comparison of six commercial membrane pairs on the thermodynamic efficiency and power density, J. Memb. Sci. 343 (2009) 7–15.

[26] J. Veerman, J.W. Post, M. Saakes, S.J. Metz, G.J. Harmsen, Reducing power losses caused by ionic shortcut currents in reverse electrodialysis stacks by a validated model, J. Memb. Sci. 310 (2008) 418–430.

[27] J. Veerman, M. Saakes, S.J. Metz, G.J. Harmsen, Electrical power from sea and river water by reverse electrodialysis: a first step from the laboratory to a real power plant, Environ. Sci. Technol. 44 (2010) 9207–9212.

[28] D.A. Vermaas, M. Saakes, K. Nijmeijer, Enhanced mixing in the diffusive boundary layer for energy generation in reverse electrodialysis, J. Memb. Sci. 453 (2014) 312–319.

[29] A.H. Avci, P. Sarkar, R.A. Tufa, D. Messana, P. Argurio, E. Fontananova, G. Di Profio, E. Curcio, Effect of Mg2+ ions on energy generation by Reverse Electrodialysis, J. Memb. Sci. 520 (2016) 499–506.

[30] E. Farrell, M.I. Hassan, R.A. Tufa, A. Tuomiranta, A.H. Avci, A. Politano, E. Curcio, H.A. Arafat, Reverse electrodialysis powered greenhouse concept for water- and energy-self-sufficient agriculture, Appl. Energy. 187 (2017) 390–409.

[31] D.A. Vermaas, J. Veerman, M. Saakes, K. Nijmeijer, Influence of multivalent ions on renewable energy generation in reverse electrodialysis, Energy Environ. Sci. 7 (2014) 1434–1445.

[32] J.W. Post, H.V.M. Hamelers, C.J.N. Buisman, Influence of multivalent ions on power production from mixing salt and fresh water with a reverse electrodialysis system, J. Memb. Sci. 330 (2009) 65–72.

[33] E. Fontananova, W. Zhang, I. Nicotera, C. Simari, W. van Baak, G. Di Profio, E. Curcio, E. Drioli, Probing membrane and interface properties in concentrated electrolyte solutions, J. Memb. Sci. 459 (2014) 177–189.

[34] M.J. Kennish, Practical Handbook of Marine Science, 3th ed., CRC Press LLC, Boca Raton, FL, 2001.

[35] D.L. Parkhurst, C.A.J. Appelo, User's Guide To PHREEQC (version 2) — a Computer Program for Speciation, and Inverse Geochemical Calculations, Water-Resources Investig. Rep. 99-4259. D (1999) 312.

[36] E. Fontananova, D. Messana, R.A. Tufa, I. Nicotera, V. Kosma, E. Curcio, W. Van Baak, E. Drioli, G. Di Profio, Effect of solution concentration and composition on the electrochemical properties of ion exchange membranes for energy conversion, J. Power Sources. 340 (2017) 282–293.

[37] A. Zlotorowicz, R. V Strand, O.S. Burheim, S. Kjelstrup, The permselectivity and water transference number of ion exchange membranes in reverse electrodialysis, J. Memb. Sci. 523 (2017) 402–408.

[38] S. Pawlowski, T. Rijnaarts, M. Saakes, K. Nijmeijer, J.G. Crespo, Improved fluid mixing and power density in reverse electrodialysis stacks with chevron-profiled membranes, J. Memb. Sci. 531 (2017) 111–121.

[39] T. Rijnaarts, E. Huerta, W. Van Baak, K. Nijmeijer, Effect of Divalent Cations on RED Performance and Cation Exchange Membrane Selection to Enhance Power Densities, Environ. Sci. Technol. 51 (2017) 13028–13035.

[40] G.M. Geise, D.R. Paul, B.D. Freeman, Fundamental water and salt transport properties of polymeric materials, Prog. Polym. Sci. 39 (2014) 1–42.

[41] T. Sata, Studies on anion exchange membranes having permselectivity for specific anions in electrodialysis - effect of hydrophilicity of anion exchange membranes on permselectivity of anions, J. Memb. Sci. 167 (2000) 1–31.

[42] H. Strathmann, Ion-Exchange Membrane Separation Processes, Membrane S, Elsevier B.V, Amsterdam, The Netherlands, 2004.

[43] E. Barsoukov, J.R. Macdonald, Impedance Spectroscopy Theory, Experiment, and Applications, Second, Wiley-Interscience, Hoboken, New Jersey, 2005.

[44] A.H. Galama, D.A. Vermaas, J. Veerman, M. Saakes, H.H.M. Rijnaarts, J.W. Post, K. Nijmeijer, Membrane resistance: The effect of salinity gradients over a cation exchange membrane, J. Memb. Sci. 467 (2014) 279–291.

[45] P. Długołęcki, P. Ogonowski, S.J. Metz, M. Saakes, K. Nijmeijer, M. Wessling, On the resistances of membrane, diffusion boundary layer and double layer in ion exchange membrane transport, J. Memb. Sci. 349 (2010) 369–379.

CHAPTER 3:

EFFECT OF Mg^{2+} IONS ON ENERGY GENERATION BY REVERSE ELECTRODIALYSIS

Abstract

Reverse Electrodialysis is today recognized as one of the most promising technology to harvest Salinity Gradient Power (SGP-RE). However, the effectiveness of SGP-RE in real practice is still not clearly defined due to the lack of specific studies in literature, being in large part limited to investigations on pure NaCl solutions. In this work we experimentally investigated the effect of Mg^{2+}, the most abundant cation in natural water after Na^{+}, on SGP-RE performance by power measurements on a lab-scale stack prototype. Maximum power density ranged from 1.06 W/m^2_{MP} (MP: membrane pair) - generated when feeding SGP-RE prototype with 0.5 molal//4 molal NaCl, to 0.06 W/m^2_{MP} - measured when using 0.5 molal//4 molal $MgCl_2$ solutions. Likewise, open circuit voltage decreased from 1.70 to 0.72 V. Evidence of uphill transport in the range of 0–30% $MgCl_2$ was confirmed by Ion Chromatography analysis carried out on inlet and outlet streams of SGP-RE stack. Electrochemical Impedance Spectroscopy analysis revealed that cation exchange membrane resistance was critically affected by Mg^{2+} concentration: membrane resistance, from a value of 2.41 $\Omega \cdot cm^2$ in pure NaCl solution, increased tenfold in pure $MgCl_2$ solution.

1. Introduction

Generation of power from mixing saline solutions at different concentrations by Salinity Gradient Power – Reverse Electrodialysis (SGP-RE) is a sustainable answer to the intensive energy production by fossil fuels [1–5]. The total technical potential of SGP has been estimated around 647 GW, which is 23% of global electricity consumption [6].

In a typical SGP-RE system, two aqueous streams having different salinity (High Concentration Compartment: HCC; Low Concentration Compartment: LCC) are fed between alternately stacked cation exchange membranes (CEM) and anion exchange membranes (AEM). Under the driving force of an electrochemical potential gradient, a selective transport of ions (cations through CEMs and anions through AEMs) takes place. This ion current activates a flux of electrons by redox reactions occurring in the electrode compartments [2].

The effectiveness of SGP-RE in real practice (i.e. using natural feeds containing several ionic species) is still not clearly defined due to the lack of specific studies in literature, being in large part limited to investigations on artificial aqueous solutions contain only NaCl. Power density values in the range of 0.8–2.2 W/m^2_{MP} (MP: membrane pair) are reported for "seawater" (0.5 M NaCl)// "river water" (0.015 M NaCl)" combination [7–11]. Nevertheless, real solutions contain - in a wide range of concentration – a large spectra of mono and multivalent ions that negatively affect the SGP-RE performance. Among them, magnesium is the most abundant cation present in real water (Mg^{2+} concentration in typical seawater is around 1200 mg/L [12]) and brines. In one of the first experiments carried out on real solutions, Jagur-Grodzinski and Kramer [13] observed that SGP-RE tests on brine from Dead Sea resulted in a low power density due to high membrane resistivity caused by the huge Mg^{2+} content. Recently, Vermaas et al. [14] investigated the effect of multivalent ions on different commercial cation and anion exchange membranes; overall, the

presence of Mg^{2+} and SO_4^{2-} caused a reduction in power density between 29% and 50%. Moreover, uphill transport of Mg^{2+} and SO_4^{2-} against their concentration gradient reported by Post et al. [15] resulted in a decrease of the Open Circuit Voltage (OCV) of the stack.

The impact of multivalent ions is further exacerbated whenever highly concentrated brines are used as possible option to increase power density by decreasing the internal resistance [16–22].

Tedesco et al. [22] measured a maximum P_d of 1.6 W/m^2_{MP} when mixing natural brackish water and saturated brine in a SGP-RE pilot plant, whereas tests with pure NaCl solutions resulted in a 60% increase of power density.

Tufa et al. (2014) carried out experiments using brackish water and brine from solar ponds in Sicily (Italy): 3.04 W/m^2_{MP} was obtained for 0.1 M//5M artificial NaCl solutions; on the other hand, up to 60% decrease in P_d was caused by the presence of Mg^{2+} (0.083M NaCl + 0.017M $MgCl_2$//3.25M NaCl + 1.75M $MgCl_2$) [4].

The objective of this study is to systematically investigate the impact of Mg^{2+} ions present in feed solutions on the reduction of power density generated by SGP-RE operated with multi-ion solutions having a total concentration typically associated to seawater and brines.

The possibility to integrate SGP-RE technology with seawater desalination practice is now becoming of interest: the potential to recovery electrochemical energy from Reverse Osmosis retentate further concentrated by Membrane Distillation has been explored by Tufa et al. [20]. Moreover, since the use of brine as feed solution reduces the internal electrical resistance stack in the high concentrated compartment thus increasing the power output [18,21], brines from oil and natural gas fields, flooding of salt domes, salt lakes and solar ponds – showing a large variety of composition - are today emerging as alternative saline sources [2–4].

Systematic experimental tests were carried out by feeding the Low Concentration Compartment (LCC) and the High Concentration Compartment (HCC) with binary NaCl-$MgCl_2$ solutions at different composition.

Due to the complexity of electrochemical phenomena taking place through membranes and their interfaces, the depth knowledge of electrical and mass-transport properties is essential to understand the impact of multivalent ions on SGP-RE performance. Therefore, the effect of multi-ion solution composition on the extent of membrane, electrical double layer and diffusion boundary layer resistances [23, 24] was studied by Electrochemical Impedance Spectroscopy (EIS), an analytical technique able to measure the resistance to the charges transfer through the bulk and interfacial regions of solid and liquid electrolyte materials. A quantitative characterization of the impact of divalent ions on the membrane resistance is decisive to develop ion exchange membranes able to reduce the overall electrical resistance of the stack and to sustain the power generation. The generated power also suffers limitations in ion exchange occurring between the membrane, the electrical double layer (mostly sensitive to charge density of the membrane) and the diffusive boundary layer (influenced by the fluid-dynamics of the system). In particular, even a modest transfer of ions through the membrane due to uphill transport is sufficient to bring the concentration in the electrical double layer to equilibrium, so determining the voltage over the membrane [14, 15]. The extent of ionic interactions is specifically sensitive to the nature of charged species and to the solution composition. At the best of our knowledge, for the first time electrochemical properties are systematically investigated as a function of multi-ion electrolyte composition (Na^+/ Mg^{2+} /Cl^-) by EIS with the aim to identify the most sensitive step to the presence of Mg^{2+}.

Additionally, Atomic Absorption Spectrometry and Ion Chromatography were used to quantify the effect of Mg^{2+} on ion exchange capacity of CEM, and to investigate the transport of ions within SGP-RE stack by measuring the variation of ionic composition in LCC and HCC compartments, respectively.

2. Materials and methods

2.1. Solutions

Feed solutions were prepared by dissolving appropriate amount of NaCl and $MgCl_2 \cdot 6H_2O$ (Sigma-Aldrich, Italy) in deionized water (PURELAB, Elga LabWaters, 0.055 $mS \cdot cm^{-1}$). Experiments were carried out by keeping constant the total molal concentration, expressed in $mol \cdot kg^{-1}$ of solvent and conventionally indicated as m, in both LCC and HCC (0.5m and 4m, respectively) and varying the $MgCl_2$ content in the range of 0–100% (with respect to molal composition). The composition of aqueous electrolyte solution was: 0.3M potassium hexacyanoferrate(II), 0.3M potassium hexacyanoferrate(III) and 2.5M sodium chloride (Sig- ma-Aldrich S.r.l., Italy).

2.2. Salinity gradient power-reverse electrodialysis setup

The SGP-RE stack prototype (Fig. 1), provided by REDstack BV (The Netherlands), was equipped with 25 cell pairs having each one an active membrane area of 0.01 m^2 (10 cm x 10 cm) and operated in cross-flow mode. Relevant characteristics of AEM-80045 and CEM-80050 Ion Exchange Membranes (IEMs), provided by Fujifilm Manufacturing Europe B.V. (The Netherlands), are reported in Table 1. Each cell pair was supported with 270 mm polyethylene gaskets and PET spacers (Deukum GMBH, Germany). The electrode compartments include anode and cathode made of inert Ti–Ru/Ir mesh with dimension of 10 cm x 10 cm (MAGNETO Special Anodes B.V., The Netherlands).

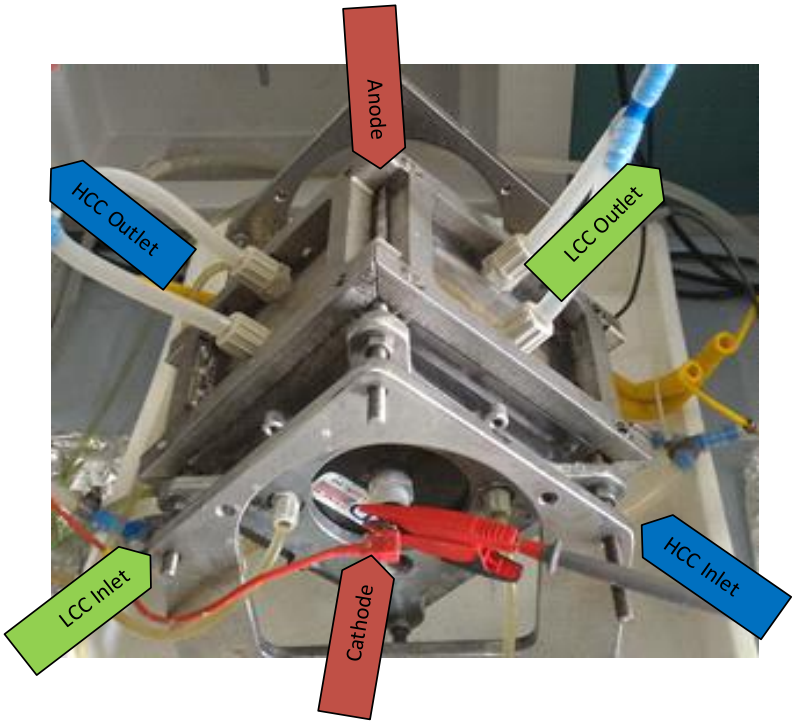

Figure 1. Lab-scale RE stack unit (25 cell pairs)

Table 1. Properties of ion exchange membrane [23]

Membrane code	Thickness (mm)*	Ion exchange capacity (mmol/g membrane)	Density of fixed charge (mol/L)	Membrane areal resistance ($\Omega \cdot cm^2$)**
Fuji-AEM-80045	129 ± 2	1.4 ± 0.1	3.8 ± 0.2	1.551 ± 0.001
Fuji-CEM-80050	114 ± 2	1.1 ± 0.1	2.4 ± 0.2	2.974 ± 0.001

*Conditions: NaCl 0.5 M, 20 º C
**Conditions: NaCl 0.5 M, 20 º C, 2.8 cm/s

Masterflex L/S digital peristaltic pumps (Cole-Palmer, US) were used to feed the stack in continuous mode with NaCl-$MgCl_2$ solutions and electrolyte at flow rates of 20 and 30 L h^{-1}, respectively. Before and after each experiment, the stack was washed with osmotized water for 60 min. Reverse Electrodialysis experiments were carried out at feed flow velocity of 0.7 cm s^{-1} in conformity with our recent studies [20, 25]. This value is not far from the optimal flow velocity of 0.46 cm s^{-1} found by Weiner et al. [26] after an optimization procedure aiming at the maximization of the net power density in a form that includes the pumping power required to drive solutions through the SGP-RE stack and to pre-treat feed by coarse media filtration.

A high dissipation five-decade resistance box in the range of 0.1–1000Ω (CROPICO, Bracken Hill, US) was used to load the SGP- RE system (Fig. 2). Corresponding voltage drop and current were recorded after altering resistance box in the range of 60–0.1Ω.DC voltage drop across the SGP-RE stack was measured by a 3½ digital multimeter with accuracy of 70.5% in the range of 200mV to 200 V (Velleman, DVM760), and the current flowing across the load resistors was measured by Agilent 34422A 6½ digit multimeter.

After fitting voltage (V) versus current (I) with a straight line, the open circuit voltage (OCV) and the total resistance of stack R_{stack} (Ω) were respectively calculated as intercept (I=0) and slope of the equation:

$$V(I) = OCV - R_{stack} I \tag{1}$$

The gross power density P_d plotted versus the current density i (A/m^2) follows a parabolic trendline in the form of:

$$P_d(i) = ai^2 + bi \tag{2}$$

and reaches its maximum value for:

$$P_{d,\max} = -\frac{b^2}{4a} \tag{3}$$

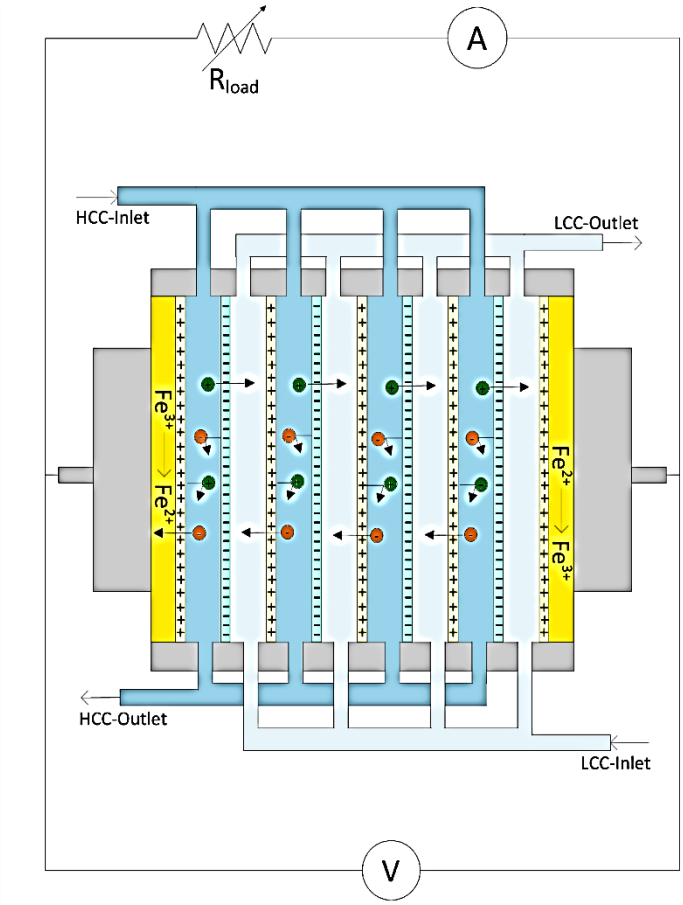

Figure 2. RED setup: scheme of the electric circuit.

2.3. Electrochemical impedance spectroscopy setup

Electrochemical Impedance Spectroscopy (EIS) measurements were carried out using a potentiostat/galvanostat combined with a frequency response analyzer (Metrohm Autolab PGSTAT302N). A home-designed four electrodes impedance cell having 3.14 cm^2 active membrane area (Fig. 3a) was employed. Electro-deposition method was applied to cover working and counter electrodes with a thin layer of AgCl. The sense and reference electrodes were Ag/AgCl electrodes (Gamry Instruments); the Haber–Luggin capillaries were filled with KCl 3 M Milli-Q water (18.2 M Ω cm). In each EIS test, identical NaCl-$MgCl_2$ solutions were recirculated to both compartments of the impedance cell at 25 °C and 0.7 cm s^{-1} flow velocity by gear pumps. Before

analysis, virgin AEM-80045 and CEM-80050 membranes were conditioned for 24 h in test solutions, refreshed every 8 h to be sure no residual solvents or chemical agents were present.

AC current in the frequency range of 1000–0.01 Hz with signal amplitude of 10 mV was generated through the cell and response recorded. Collected data were fitted by the equivalent circuit model showed in Fig. 3b by Nova 1.9.16 by Metrohm Autolab B.V. According to previous investigations, diffusion boundary layer was represented by a resistor and a constant phase element in parallel, while electric double layer was represented by a parallel combination of a resistor and a capacitor [23]. For each test solution, a blank experiment (without membrane) was carried out in order to measure the solution resistance; membrane resistance R_m is then calculated by subtracting solution resistance from overall resistance (R_{m+s}).

2.4. Ion transport analysis

Ion Chromatography was employed to quantify the concentration of ions at the inlet and outlet of SGP-RE unit (Metrohm 861 Advanced Compact Ion Chromatograph) operated under open circuit configuration and continuous feed flow. In order to reach the steady-state, samples were collected after one hour of operation. 3.2mM Na_2CO_3 + 1mM $NaHCO_3$ was used as eluent for anion column Metrosep A Supp 5 - 250/4.0, and 2 mM nitric acid + 0.25 mM oxalic acid was used as eluent for cation column Metrosep C4 – 250/4.0. In order to quantify the ion exchange capacity (IEC) of CEM in presence of Mg^{2+}, membrane samples were immersed in a known volume of NaCl/$MgCl_2$ solutions at different composition (total concentration: 0.5 molal) and equilibrated over 72 h at 25°C. The liquid phase was collected and analyzed by High-Resolution Continuum Source atomic absorption spectrometer (HR-CS AAS) by means of ContrAA 700 (Analytik Jena AG, Germany) with a high- intensity Xe short-arc lamp as continuum source, calibrated with ICP multi-element IV standard solution Merck (Germany). Samples and standards, acidified with 1% HCl, were fed

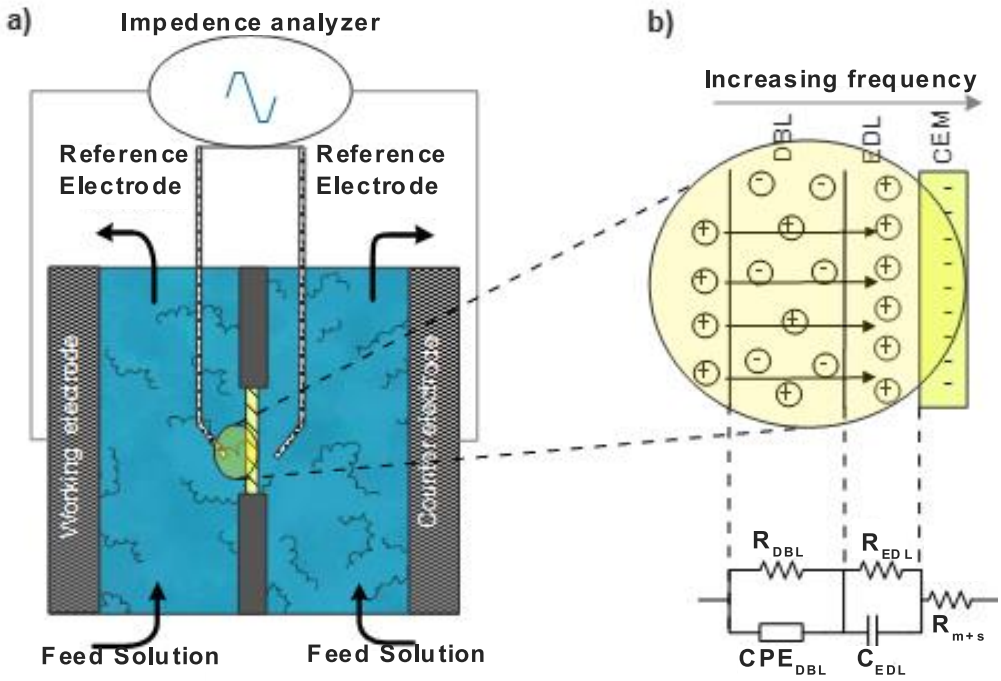

Figure 3. a) Scheme of the four electrodes EIS cell; b) Resistance layers and equivalent circuit model utilized to fit EIS data (DBL: Diffusion Boundary Layer; EDL: Electric Double Layer; CEM: Cation Exchange Membrane; R: resistance; C: Capacitor; CPE: Constant Phase Element; m: membrane; s: solution)

to the air-acetylene flame by an Injection Module (SFS 6), which allowed washing or continuous aspiration of the carrier solution. Method parameters (i.e. fuel flow and burner height) obtained by the flame automatic optimization procedure for the determination of Na and Mg were applied, the absorbance measurements being performed using the spectral lines for Mg at 202.58 nm and for Na at 330.24 nm.

2.5. Statistic

Experimental data were averaged over three repeated measurements; the standard error, calculated by dividing the standard deviation by the square root of number of measurements that make up the mean (i.e.: 3), is graphically represented by error bars. Systematic errors are typically associated to the accuracy of instrumental devices for voltage and current measurement

3. Results and discussion

3.1. Salinity Gradient Power-Reverse Electrodialysis performance

Fig. 4 illustrates the results from electrical tests on SGP-RE stack for NaCl-$MgCl_2$ solutions at seven different molal compositions as detailed in Table 2.

The best performance of SGP-RE stack was observed for pure NaCl solutions (HCC: 4m NaCl//LCC: 0.5m NaCl). Gross P_d reached a maximum of 1.06 W/m^2 at current density of 30 A/m^2; measured OCV attained 1.70 V, while shortcut current was 0.61 A. The progressive addition of $MgCl_2$ resulted in a significant decrease of stack performance: P_d, max and OCV were reduced by 60% and 20%, respectively, already at 10% $MgCl_2$ (representative for typical seawater and river water). In general, a reduction of P_d, max by 0.01 W/m^2 and OCV by 0.0098 V per %$MgCl_2$ was observed.

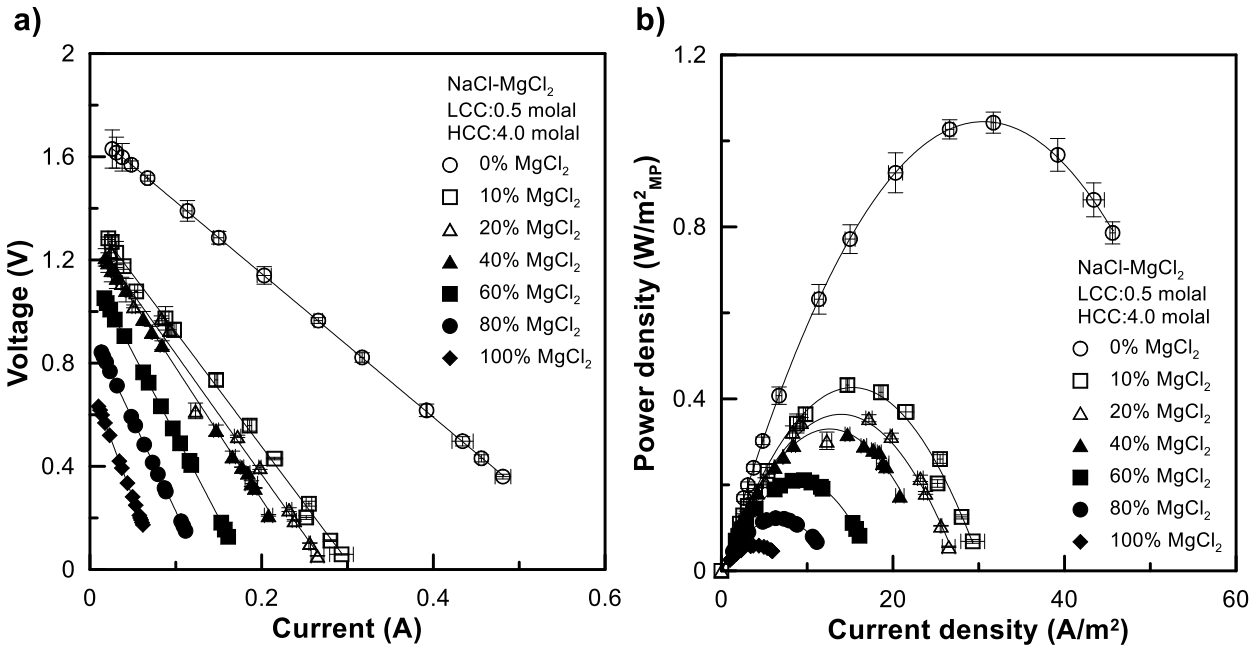

Figure 4. a) Voltage vs. current and b) gross power density vs. current density

Minimum SGP-RE performance was detected when using pure $MgCl_2$ solutions, with P_d, max almost approaching zero, OCV falling down to 0.72 V (-58% with respect to pure NaCl solutions)

and shortcut current at 0.081 A. R_{stack} varied from 2.78 Ω for pure NaCl solutions to 8.92 Ω for pure $MgCl_2$ solutions, increasing by 0.06 Ω per %molal $MgCl_2$.

Table 2 Composition of HCC/LCC solutions expressed as molality (m), and summary of main electrical parameters of SGP-RE system

Soln #	**Composition HCC**	Composition LCC	**OCV (V)**	**R_{stack} (Ω)**	**$P_{d,max}$ (W/m^2_{MP})**
1	4.00 m NaCl	0.50 m NaCl	1.70	2.78	1.06
2	3.60 m NaCl+ 0.40 m $MgCl_2$	0.45 m NaCl+ 0.05 m $MgCl_2$	1.36	4.44	0.43
3	3.20 m NaCl+ 0.80 m $MgCl_2$	0.40 m NaCl+ 0.10 m $MgCl_2$	1.30	4.67	0.36
4	2.40 m NaCl+ 1.60 m $MgCl_2$	0.30 m NaCl+ 0.20 m $MgCl_2$	1.29	5.11	0.32
5	1.60 m NaCl+ 2.40 m $MgCl_2$	0.20 m NaCl+ 0.30 m $MgCl_2$	1.15	6.38	0.21
6	0.80 m NaCl+ 3.20 m $MgCl_2$	0.10 m NaCl+ 0.40 m $MgCl_2$	0.93	7.08	0.12
7	4.00 m $MgCl_2$	0.50 m $MgCl_2$	0.72	8.92	0.06

Overall, our findings are coherent with literature results. Vermaas et al. [14] working on artificial seawater (0.508M)//river water (0.017 M) solutions both containing 10% $MgCl_2$,observed an OCV decrease of 5–15% for single Ralex, Neosepta and Fujifilm CEMs, while the performance of single AEMs exhibited an almost stable behavior.

In a previous work, Tufa et al. [4] detected a 20% decrease in OCV, 64% reduction in power density and 75% increase in total stack resistance in SGP-RE tests when mixing artificial brackish water and brine having $[Na^+]/[Mg^{2+}]$ molar ratio of 4.99 and 1.86, respectively.

Experimental data collected from a full-scale SGP-RE pilot plant, equipped with about 50 m^2 of IEMs and operated with natural brackish water/solar pond brine solutions (sodium and magnesium were the two prevalent cations in solar pond brine with 40% Mg^{2+} concentration) generated a maximum power density of 1.6 W/m^2_{MP} [22]. On the other hand, when using corresponding artificial solutions (LCC=0.03M $NaCl_{equivalent}$, HCC: 4– 5M $NaCl_{equivalent}$) prepared using sea-salt still containing 3–5% of non NaCl ions, it was observed an increase of about 30% in power density

(2.1 W/m^2_{MP}). Power output reached 2.7 W/m^2_{MP} (+60%) when the stack was operated with artificial solutions prepared using 99.5% purity NaCl, so confirming that even a low amount of magnesium has a severe impact on the system performance. The significant power reduction was mainly attributed to the drastically increased IEMs resistance in presence of Mg^{2+} [22].

Evidence for reduction of OCV in presence of multivalent ions has been also reported by Post et al. [8] in experimental studies carried out with a concentrated sodium chloride solution of 0.45 mol/L +with 0.05 mol/L of added chemicals (NaCl, Na_2SO_4, $MgCl_2$, $MgSO_4$) and with a diluted 3 mmol/L sodium chloride solution progressively enriched with previously mentioned salts [15]. Interestingly, for standard-grade IEMs, it was observed that each addition of charge carriers had the same lowering effect on OCV (e.g. 10 meq/L of dosed salt to diluted solution resulted in a decrease of about 25%); monovalent-selective IEMs were able to slightly mitigate this detrimental effect when adding magnesium salts (e.g. 10 meq/L of $MgCl_2$ dosed to diluted solution resulted in a OCV decrease of 20% c.a). Impact of Mg^{2+} on generated voltage is anticipated by Planck-Henderson equation [27]:

$$OCV = 2N\frac{RT}{F}\sum_i \frac{\alpha_i}{z_i}\ln\left(\frac{a_{i,HCC}}{a_{i,LCC}}\right) \quad (4)$$

where α is the membrane permselectivity for the ionic species i-th, N is number of membrane pairs, R is the universal gas constant (J mol^{-1} K^{-1}), T is the absolute temperature (K), F is the Faraday constant (C eq^{-1}), α_i is the activity of ionic species i-th in solution, and z_i is the valance of the diffusion ion (eq mol^{-1}). Eq. 4 shows that, assuming an ideal condition of $\alpha=1$, divalent ions ($z_i=2$) generate half voltage with respect to monovalent ions. In real applications, OCV is proportional to permselectivity, and ionic interactions between counter-ions and fixed charged groups in ion exchange membranes can differ. Binding affinity of Mg^{2+} is relatively higher than Na^+ [28];

therefore, Mg^{2+} may neutralize fixed charge groups leading to a remarkable decrease of ion exchange capacity and permselectivity [29].

An additional contribution to the reduction of OCV comes from the difference between the hydrated atomic radii of Na^+ and Mg^{2+}. The atomic radius of Na^+ (0.98 Å) is larger than Mg^{2+} (0.78 Å); however, in aqueous solutions, the situation is reversed due to the higher propensity of magnesium ion to be covered by water molecules (hydrated atomic radii of Na^+ and $Mg^{2+}$are 3.58 Å and 4.28 Å, respectively [30]). The resulting lower diffusion coefficient of Mg^{2+} in water (0.706 x 10^{-9} m^2/s) with respect to Na^+ (1.334 x 10^{-9} m^2/s) exacerbates the loss of permselectivity [31]. Higa et al. [32] stated that, under certain circumstances, the simultaneous presence of multivalent ions and monovalent co-ions results in a Donnan potential which increases co-ions permeation even against the concentration gradient, so reducing permselectivity. In our work, evidence for uphill transport of Mg^{2+} is discussed in Section 3.3.

3.2. Electrochemical Impedance Spectroscopy test results

Electrochemical impedance spectroscopy is a powerful technique to enlighten electrochemical phenomena in membranes, allowing to quantitatively estimate resistances related to membrane, diffusion boundary layer and electric double layer [23, 24, 33–35]. In order to distinguish resistance of solution layers, alternate current is supplied in different ranges of frequency. A three resistance mechanism is sketched in Fig. 3b. At low frequency, resistance of diffusion boundary layer (R_{DBL}), caused by different ion transport number between bulk solution and membrane, is prevalent. In the equivalent circuit used in this work, R_{DBL} is modelled by a parallel connected resistance and a constant phase element. Single membrane and electrolyte solution, modelled in the equivalent circuit by a resistor (R_{m+s}), respond at high frequency. Analysis carried out at medium frequency allows at detecting the resistance of electrical double layer (R_{EDL}), determined

by fixed counter ions on the membrane surface, and modelled by a parallel resistance and capacitance pair.

Nyquist plots of the real and imaginary parts of the impedance for Fuji-CEM-80050 membrane (the most sensitive to Mg^{2+} extent) in LCC solution at three different compositions are shown in Fig. 5. At increasing Mg^{2+} content, Z′ value measured at 1000 Hz shifted from 2.3 Ω (0.5 m NaCl) to 7.1 Ω (0.2 m NaCl+0.3 m $MgCl_2$), resulting in a 7-fold increase of the membrane resistance. At low frequency, the moderate differences among -Z" values (maximum values were comprised within 0.045–0.065 Ω) reflect the relatively low contribution of diffusion boundary layer resistances. On the other hand, impedance curves were broadened at increasing Mg^{2+}, indicating that the resistances of electrical double layer and diffusion boundary layer moderately increase their relevance compared to pure NaCl solution.

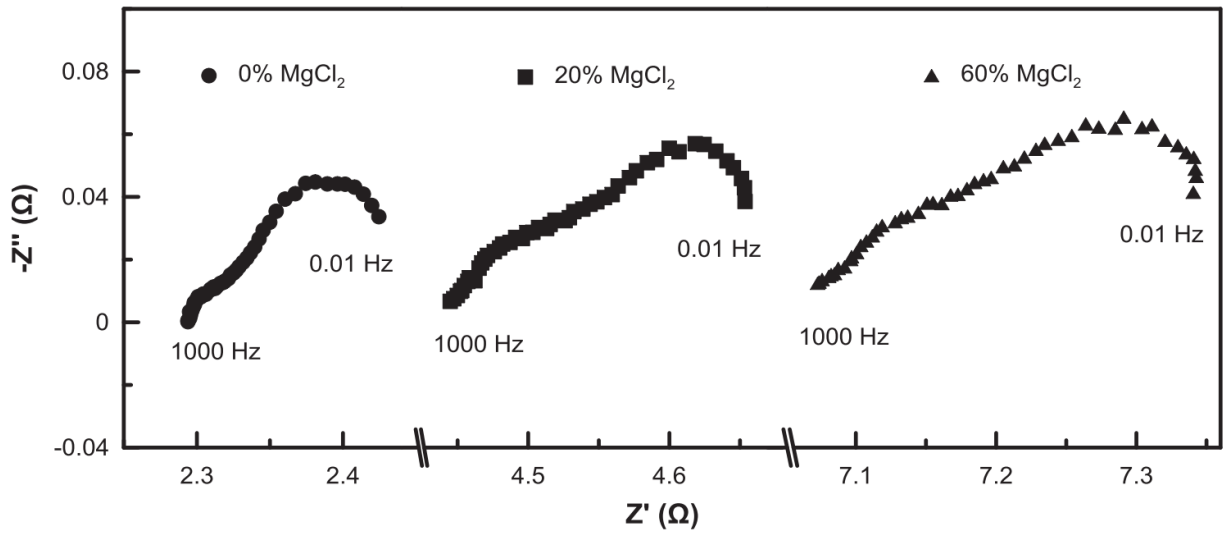

Figure 5. Nyquist plots of the Fuji-CEM-80050 membrane at increasing $MgCl_2$ content in LCC solution. Z′ (Ω) and Z″ (Ω) are the real and imaginary parts of the impedance, respectively.

Bar charts in Fig. 6 summarize the results of resistance analysis after fitting impedance spectroscopy data to equivalent circuits. Results indicate that, for both AEM and CEM, Rm was the dominant resistance over R_{EDL} and R_{DBL}. These findings are coherent with previous EIS

investigations on ion exchange membranes [23, 24]. Values of 2.41 $\Omega \cdot cm^2$ for Fuji-CEM-80050 membrane resistance and 1.35 $\Omega \cdot cm^2$ for Fuji-AEM-80045 membrane resistance, detected with 0.5 m NaCl solution, agree with those (2.97 and 1.55 $\Omega \cdot cm^2$, respectively) reported by Fontananova et al. [23].

For CEM, membrane resistance increased with increasing $MgCl_2$ concentration, while not changing significantly for AEM (R_m varying between 1.27 and 1.49 $\Omega \cdot cm^2$). A 3-fold increase in CEM resistance was observed for 10% $MgCl_2$ content; moreover, CEM resistance in pure 0.5 m $MgCl_2$ solution was one order of magnitude greater than the one measured in pure 0.5 m NaCl solution.

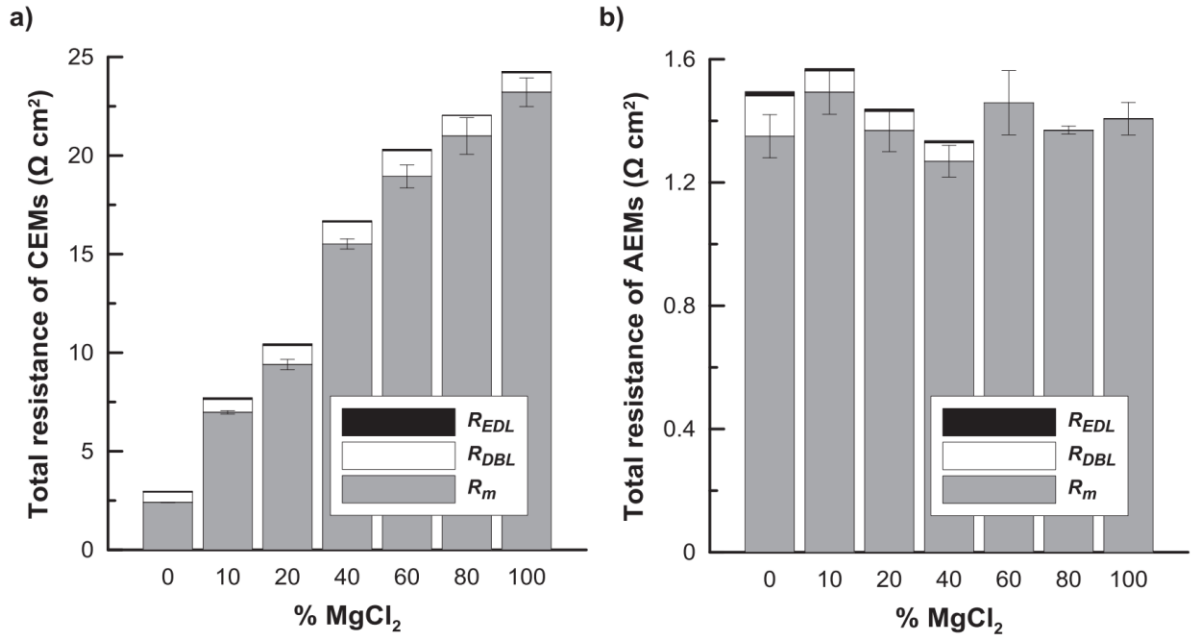

Figure 6. Resistances of membrane (R_m), diffusion boundary layer (R_{DBL}), and electric double layer (R_{EDL}) at increasing $MgCl_2$ content for: a) Fuji-CEM-80050 cation exchange membrane; b) Fuji-AEM-80045 anion exchange membrane.

Although the existence of a plateau due to possible CEM saturation is not evident, the rate of R_m increase at $\%MgCl_2$>60 appears substantially lower with respect to measurements carried out at low $MgCl_2$ concentration.

For CEM, the extent of R_{EDL} was in the range of 0.008– 0.014 $\Omega \cdot cm^2$, about two order of magnitude lower than R_{DBL}, whose values were comprised between 0.52 and 1.30 $\Omega \cdot cm^2$. The slight decrease of R_{DBL} at higher Mg^{2+} concentration, under constant flow velocity, is attributable to a little enhancement of Reynolds number as a result of the increasing density of the saline solution. The negligible impact and the relative contribution of R_{EDL} and R_{DBL} on the overall resistance agrees with our previous investigations [23].

No notable changes were observed on the total resistance of AEM.

3.3. Ion transport

With the aim to better understand the effect of the presence of divalent Mg^{2+} cations, the ion exchange capacity (IEC) of FujiCEM-80050 has been evaluated for different NaCl/$MgCl_2$ solution compositions total concentration: 0.5 molal). Generally, IEC data reported in literature are provided for NaCl solutions; however, the nature of the different co-ions present in feed solution significantly influences the performance of ion exchange membranes as a result of the different ion affinities. Results are illustrated in Fig. 7. Coherently with expectations, Mg^{2+} ions are preferentially exchanged by CEM. For a molar concentration of $MgCl_2$ greater than 30%, the amount of exchanged divalent ions prevails over the transferred Na^+.

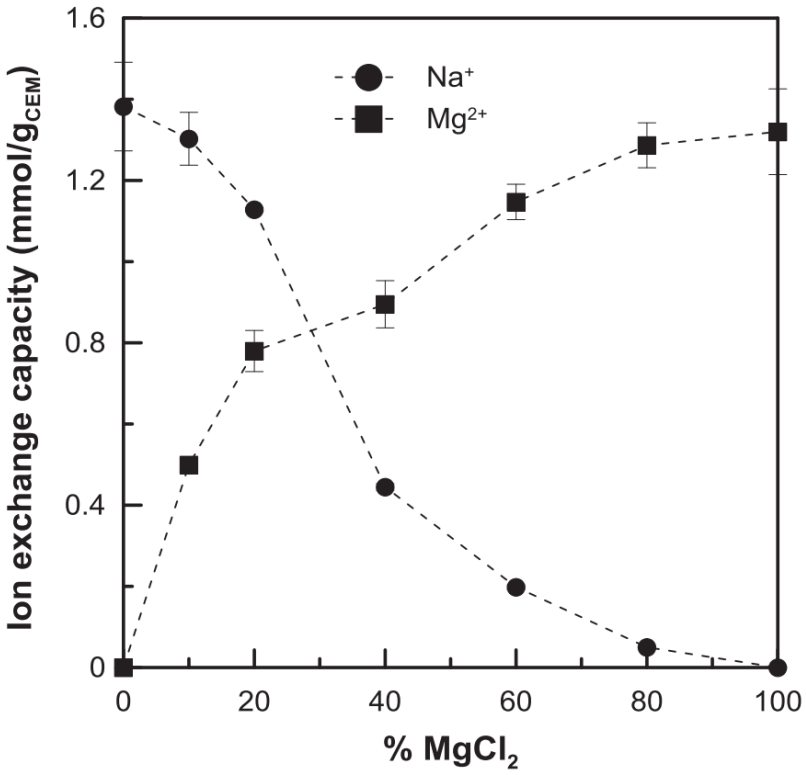

Figure 7. Ion exchange capacity of Fuji-CEM-80050 as a function of NaCl/ $MgCl_2$ solution composition (total concentration: 0.5 m).

As known from literature, in cation exchange membranes (CEM), divalent ions typically bind more strongly to sulfonate groups than monovalent ions. Geise et al. [36] reported that the affinity constant of magnesium ion with respect to sulfonate group is almost twice with respect to Na^+.

This larger affinity may effectively reduce the polymer's fixed charge concentration through a phenomenon so-called “charge screening” or partial neutralization of charged groups. Ultimately, condensation of counter-ion/fixed-charge pairs takes place, divalent ions weaken Donnan exclusion of mobile ions thus leading to a loss in CEM permselectivity [37] and resulting in a higher membrane resistance [28, 38].

The extent of transported cations (Na^+ and Mg^{2+}) and chlorine (Cl^-) from HCC to LCC is illustrated in Fig. 8a and b; data are reported as a function of the molal percentage of $MgCl_2$.

Fig. 8a indicates that transport of Na^+ ions was in the same direction of its concentration gradient over the whole range of $MgCl_2$ concentration, whereas transport of Mg^{2+} against its concentration gradient occurred at $MgCl_2$ concentration below 30% molal. Since the transport of charged species through ion exchange membranes is driven by concentration and electrical potential gradients, both mechanisms need to be taken into consideration. The electrochemical potential of magnesium is low at low concentration, and it is further reduced by its double valence. On the contrary, the electrochemical potential of Na^+ is high for opposite reasons. The higher transfer rate of Na^+ ions breaks electroneutrality around CEM and, if the extent of unbalanced positive charges is sufficiently high, uphill transport of magnesium takes place. Since Cl^- contribution of $MgCl_2$ is double than NaCl, the concentration gradient driving anions becomes more significant at increasing $MgCl_2$ content, and more Cl^- ions are expected to diffuse across AEM. Overall, Fig. 8b is coherent with this expectation; the presence of a minimum in correspondence of 10% $MgCl_2$ is caused by the uphill transport of magnesium that reduced the amount of anions required to preserve the electroneutrality of the solution.

So far, the incidence of this phenomenon in SGP-RE was marginally reported in literature [14, 15, 39].

Uphill transport of magnesium and sulfate was observed by Post et al. [15] through standard-grade Neosepta CMX/AMX ion exchange membranes under open-circuit conditions, feeding LCC and HCC with 3 mM NaCl + 2 mM $MgSO_4$ and 0.45 M NaCl + 0.05 M $MgSO_4$, respectively. Batch tests carried out by recycling feed solutions over about 6 h revealed that the exchange of monovalent Na^+ ions in HCC with multivalent Mg^{2+} ions in LCC occurs in a ratio of 1:2 like in Donnan dialysis to sustain the electroneutrality of compartments [15]. Moreover, it was observed that, at the beginning of the tests, the sodium flow was counterbalanced by back-diffusion of

magnesium and diffusion of chloride; at the end of the experiment, the sodium flux was simply counterbalanced by diffusion of chloride.

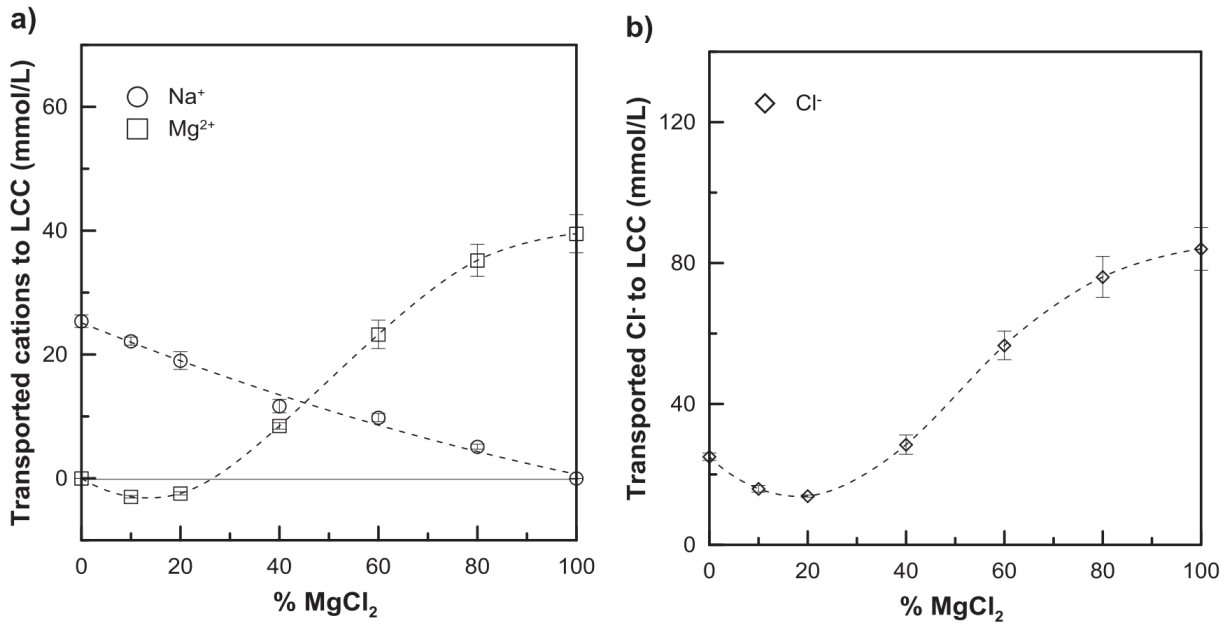

Figure 8. Transport of ions from HCC to LCC in SGP-RE stack operated under open-circuit and continuous feed flow: a) Na^+ and Mg^{2+}; b) Cl^-.

Vermaas et al. [14] reported a significant decrease of power density (by approximately 50%) due to uphill transport using Ralex CMH/AMH membranes $MgSO_4$ (10%)/NaCl(90%) solutions with total salt concentrations of 0.508 M (artificial seawater) and 0.017 M (artificial river water) in HCC and LCC, respectively. Theoretical calculations showed that uphill transport occurs for a molar fraction of $MgSO_4$ lower than 20% [14].

4. Conclusion

In this work, energy generation by SGP-RE from saline solutions containing both Na^+ and Mg^{2+} is investigated; the total concentration of dilute (LCC) and concentrated (HCC) solutions was 0.5 and 4 molal, respectively. 1.06 W/m^2_{MP} maximum gross power density was produced when operating SGP-RE with pure NaCl solutions. The presence of magnesium ions significantly

affected the performance of the system, even at low content: solutions with 10% molal $MgCl_2$ resulted in a 20% decrease of OCV and in a 60% reduction of power density. Furthermore, extracted maximum power density was only 0.06 W/m^2_{MP} in experimental tests carried out with LCC and HCC fed by pure $MgCl_2$ solutions, as a consequence of halved OCV and tripled total stack resistance.

This drastic decrease in power density, mainly caused by a decline in open circuit voltage, is intrinsically associated to the bivalence of Mg^{2+} ion (Planck-Henderson equation), to occurrence of Mg^{2+} transport against its concentration gradient occurring up to 30% molal $MgCl_2$ content, and – to a lesser extent - to the higher cation exchange membrane resistance as quantified by EIS analysis.

In order to limit the uphill transport of divalent Mg^{2+} ions, a new generation monovalent-selective ion exchange membranes need to be developed. Since the larger affinity of Mg^{2+} with respect to Na^+ determines the charge screening the polymer's fixed charges, ultimately weakening Donnan exclusion of mobile ions, highly permselective CEM with low internal electrical resistance are also necessary to increase the extractable power density by SGP-RE up to reliable level. The improvement of fluid-dynamics within the stack through geometry optimization of channels and spacers, aimed at reducing the resistance of the diffusive boundary layer, is also expected to have beneficial effects [40].

Upstream SGP-RE stack, mitigation of the negative effect of multivalent ions present in real solutions, and particularly of Mg^{2+} (the most abundant cation after Na^+) requires appropriate softening of feed streams. Due to the high operating costs associated to an energetically intensive pretreatment, the possibility to integrate SGP-RE technology within desalination practice is crucial to open viable and realistic perspectives, also in terms of valorization of the discharged brine.

5. Acknowledgments

The financial support of the Education, Audiovisual and Culture Executive Agency (EACEA-EU) within the programme EUDIME "Erasmus Mundus Doctorate in Membrane Engineering" (FPA 2011–0014, SGA 2014–0970, http://eudime.unical.it) is kindly acknowledged.

6. References

[1] R.E. Pattle, Production of electric power by mixing fresh and salt water in the hydroelectric pile, Nature 174 (1954), 660–660.

[2] R.E. Lacey, Energy by reverse electrodialysis, Ocean Eng. 7 (1980) 1–47.

[3] G.L. Wick, J.D. Isaacs, Salt domes: is there more energy available from their salt than from their oil?, Science. 199 (1978) 1436–1437.

[4] R.A. Tufa, E. Curcio, W. van Baak, J. Veerman, S. Grasman, E. Fontananova, G. Di Profio, Potential of brackish water and brine for energy generation by salinity gradient power-reverse electrodialysis (SGP-RE), RSC Adv. 4 (2014) 42617–42623.

[5] M. Migliori, A. Aloise, G. Giordano, Methanol to dimethyl ether on H-MFI catalyst: the influence of the Si/Al ratio on kinetic parameters, Catal. Today 227 (2014) 138–143.

[6] R. Kempener, F. Neumann, Salinity gradient energy, Int. Renew. Energy Agency (2014), www.irena.org.

[7] P. Długołecki, A. Gambier, M. Wessling, Practical potential of reverse electrodialysis as process for sustainable energy generation, Environ. Sci. Technol 43 (2009) 6888–6894.

[8] J.W. Post, C.H. Goeting, J. Valk, S. Goinga, J. Veerman, H.V.M. Hamelers, P.J.F. M. Hack, Towards implementation of reverse electrodialysis for power generation from salinity gradients, Desalin. Water Treat. 16 (2010) 182–193.

[9] J. Veerman, M. Saakes, S.J. Metz, G.J. Harmsen, Reverse electrodialysis: performance of a stack with 50 cells on the mixing of sea and river water, J. Membr. Sci. 327 (2009) 136–144.

[10] J. Veerman, M. Saakes, S.J. Metz, G.J. Harmsen, Electrical power from sea and river water by reverse electrodialysis: a first step from the laboratory to a real power plant, Environ. Sci. Technol. 44 (2010) 9207–9212.

[11] D.A. Vermaas, M. Saakes, K. Nijmeijer, Doubled power density from salinity gradients at reduced intermembrane distance, Environ. Sci. Technol. 45 (2011) 7089–7095.

[12] K.E. Chave, Chemical reactions and the composition of sea water, J. Chem. Educ. 48/3 (1971) 148–150.

[13] J. Jagur-Grodzinski, R. Kramer, Novel process for direct conversion of free energy of mixing into electric power, Ind. Eng. Chem. Process Des. Dev. 25 (1986) 443–449.

[14] D.A. Vermaas, J. Veerman, M. Saakes, K. Nijmeijer, Influence of multivalent ions on renewable energy generation in reverse electrodialysis, Energy Environ. Sci. 7 (2014) 1434–1445.

[15] J.W. Post, H.V.M. Hamelers, C.J.N. Buisman, Influence of multivalent ions on power production from mixing salt and fresh water with a reverse electrodialysis system, J. Membr. Sci. 330 (2009) 65–72.

[16] M. Tedesco, P. Mazzola, A. Tamburini, G. Micale, I.D.L. Bogle, M. Papapetrou, A. Cipollina, Analysis and simulation of scale-up potentials in reverse electrodialysis, Desalin. Water Treat. (2014) 1–13.

[17] A. Daniilidis, D.A. Vermaas, R. Herber, K. Nijmeijer, Experimentally obtainable energy from mixing river water, seawater or brines with reverse electrodialysis, Renew. Energy 64 (2014) 123–131.

[18] M. Tedesco, A. Cipollina, A. Tamburini, G. Micale, J. Helsen, M. Papapetrou, REAPower: use of desalination brine for power production through reverse electrodialysis, Desalin. Water Treat. 53 (2014) 3161–3169.

[19] E. Brauns, Towards a worldwide sustainable and simultaneous large-scale production of renewable energy and potable water through salinity gradient power by combining reversed electrodialysis and solar power? Desalination 219 (2008) 312–323.

[20] R.A. Tufa, E. Curcio, E. Brauns, W. Van Baak, E. Fontananova, G. Di Profio, Membrane distillation and reverse electrodialysis for near-zero liquid discharge and low energy seawater desalination, J. Membr. Sci. 496 (2015) 325–333.

[21] M. Tedesco, E. Brauns, A. Cipollina, G. Micale, P. Modica, G. Russo, J. Helsen, Reverse electrodialysis with saline waters and concentrated brines: a laboratory investigation towards technology scale-up, J. Membr. Sci. 492 (2015) 9–20.

[22] M. Tedesco, C. Scalici, D. Vaccari, A. Cipollina, A. Tamburini, G. Micale, Performance of the first reverse electrodialysis pilot plant for power production from saline waters and concentrated brines, J. Membr. Sci. 500 (2015) 33–45.

[23] E. Fontananova, W. Zhang, I. Nicotera, C. Simari, W. van Baak, G. Di Profio, E. Curcio, E. Drioli, Probing membrane and interface properties in concentrated electrolyte solutions, J. Membr. Sci. 459 (2014) 177–189.

[24] P. Długołęcki, P. Ogonowski, S.J. Metz, M. Saakes, K. Nijmeijer, M. Wessling, On the resistances of membrane, diffusion boundary layer and double layer in ion exchange membrane transport, J. Membr. Sci. 349 (2010) 369–379.

[25] R.A. Tufa, E. Rugiero, D. Chanda, J. Hnat, W. van Baak, J. Veerman, E. Fontananova, G. Di Profio, E. Drioli, K. Bouzek, E. Curcio, Salinity gradient power-reverse electrodialysis and alkaline polymer electrolyte water electrolysis for hydrogen production, J. Membr. Sci. 514 (2016) 155–164.

[26] A.M. Weiner, R.K. McGovern, J.H. Lienhard V, A new reverse electrodialysis design strategy which significantly reduces the levelized cost of electricity, J. Membr. Sci. 493 (2015) 605–614.

[27] J.N. Weinstein, F.B. Leitz, Electric power from differences in salinity: the dialytic battery, Science 191 (1976) 557–559.

[28] G.M. Geise, Water and Salt Transport Structure/Property Relationships in Polymer Membranes for Desalination and Power Generation Applications (PhD Thesis), The University of Texas at Austin, US, 2012.

[29] G.M. Geise, H.J. Cassady, D.R. Paul, B.E. Logan, M.A. Hickner, Specific ion effects on membrane potential and the permselectivity of ion exchange membranes, Phys. Chem. Chem. Phys. 16 (2014) 21673–21681.

[30] R. Nightingale, Phenomenological theory of ion solvation. Effective radii of hydrated ions, J. Phys. Chem. 63 (1959) 1381–1387.

[31] E. Samson, J. Marchand, K.A. Snuder, Calculation of ionic diffusion coefficients on the basis of migration test results, Mater. Struct. 36 (2003) 156–165.

[32] M. Higa, A. Tanioka, K. Miyasaka, A study of ion permeation across a charged membrane in multicomponent ion systems as a function of membrane charge density, J. Membr. Sci. 49 (1990) 145–169.

[33] J.S. Park, J.H. Choi, K.H. Yeon, S.H. Moon, An approach to fouling characterization of an ion-exchange membrane using current–voltage relation and electrical impedance spectroscopy, J. Colloid Interface Sci. 294 (2006) 129–138.

[34] J.S. Park, J.H. Choi, J.J. Woo, S.H. Moon, An electrical impedance spectroscopic (EIS) study on transport characteristics of ion-exchange membrane systems, J. Colloid Interface Sci. 300 (2006) 655–662.

[35] E. Barsoukov, J.R. Macdonald, Impedance Spectroscopy, John Wiley & Sons Inc., New Jersey, 2005.

[36] G.M. Geise, D.R. Paul, B.D. Freeman, Fundamental water and salt transport properties of polymeric materials, Prog. Polym. Sci. 39 (2014) 1–42.

[37] H.J. Cassady, E.C. Cimino, M. Kumar, M.A. Hickner, Specific ion effects on the permselectivity of sulfonated poly (ether sulfone) cation exchange membranes, J. Membr. Sci. 508 (2016) 146–152.

[38] O.D. Bonner, A selectivity scale for some monovalent cations on Dowex 50, J. Phys. Chem. 58 (1954) 318–320.

[39] M. Higa, A. Kira, Theory and simulation of ion transport in nonstationary states against concentration gradients across ion-exchange membranes, J. Phys. Chem. 96 (1992) 9518–9523.

[40] S. Pawlowski, P. Sistat, J.G. Crespo, S. Velizarov, Mass transfer in reverse electrodialysis: flow entrance effects and diffusion boundary layer thickness, J. Membr. Sci. 471 (2014) 72–83.

CHAPTER 4:

ASYMMETRIC CATION EXCHANGE MEMBRANE PREPARATION BY SULFONATED POLYSULFONE FOR REVERSE ELECTRODIALYSIS

Abstract

In this study, asymmetric porous cation exchange membranes were prepared by wet phase inversion of sulfonated polysulfone (sPSf) solutions. sPSf with different degree of sulfonation (DS) obtained by variating PSf/chlorosulfonic acid ratio where chlorosulfonic acid was used as sulfonating agent. Characterization of SPSf samples were completed by using FTIR and H-NMR techniques. sPSf with 0.31 DS and 0.67 meq/g corresponding ion exchange capacity was chosen to prepare membranes due to polymers with SD higher than 0.31 resulted in low mechanical properties and high swelling degree. Effect of two different phase inversion parameters, solvent type and co-solvent ratio, were investigated by morphological and electrochemical characterization. The best performance was obtained as 0.84 permselectivity and 4 $\Omega \cdot cm^2$ for the membrane prepared with 20/80: IPA/NMP ratio. This membrane and CMX (Neosepta) were further characterized in different solution concentration to estimate the RED performance. Although the generated power was less than commercial CMX membrane, home-made membrane was considered as a cost-effective alternative where the biggest limitation is the membrane price against the commercialization of Reverse Electrodialysis.

1. Introduction

Being limited of conventional energies and increasing environmental problems impel researchers to investigate alternative renewable energies. During last decade, Salinity Gradient Power – Reverse Electrodialysis (SGP-RED) has regained considerable attention in parallel with developments in material science. Considering estimated SGP potential is around 2.4 TW [1], it can be a promising renewable and sustainable solution to energy related problems e.g. environmental pollution caused by greenhouse gaseous.

A typical RED stack consists alternately arranged cation exchange membranes (CEM) and anion exchange membranes (AEM) which are separated by spacers to create channels for concentrated and diluted solutions. A CEM contains negatively charged groups on its polymer backbone that gives the ability of exclusion of positively charged ions while an AEM has positively charged fixed groups and excludes negatively charged ions. The salinity difference between two adjacent channels drives ions from concentrated to diluted compartment. However, due to fixed charged groups on ion exchange membranes (IEM), cations can transport only across the CEM while anions through the AEM. Thus, an ionic flux can be created through IEMs. Utilization of electrodes at the end of compartments allows to convert the ionic flux to electronic flux which later can be used to power an electrical circuit [2].

IEMs play a key role in the RED technology when both technical and economic problems towards the commercialization considered. However, there is lack of membrane designed for the needs of RED. Most of the RED investigations were carried out by utilizing commercial IEMs designed for electrodialysis (ED) due to their similarities. A good IEMs must have high permselectivity, low electrical resistance, decent mechanical stability over long term and low price [3–6]. For a feasible

RED operation, envisaged membrane lifetime is between 7-10 years whereas a competitive membrane price must be less than 5 €/m^2 [7,8].

Permselectivity of an IEM indicates the ability of the membrane to discriminate between opposite charges (anions against cations in case of AEM and cations against anions in case of CEM). Commercial membranes tested in RED have permselectivity more than 0.95 for CEMs and more than 0.85 for AEMs where ideal permselectivity is 1.00 [3]. In recent years, necessity of tailor-made membranes for RED has been realized. Guler et al. (2013) prepared first tailor made SPEEK (sulfonated polyetheretherketone) CEMs which had permselectivity greater than 0.89, while tailor-made PECH-PAN-DABCO blend AEMs had permselectivity more than 0.79 [9]. Later, Hong et al. (2014) characterized iron (III) oxide (Fe_2O_3-SO_4^{2-})/ poly(2,6-dimethyl-1,4-phenylene oxide) (sPPO) composite membranes for different iron (III) oxide load. Composites resulted in minimum 0.68 and maximum 0.88 permselectivity [10]. Kim et al. (2015) reported homemade pore filling CEMs (KIER-CEM1) and AEMs (KIER-AEM1) have 0.97 and 0.91 permselectivity, respectively [11].

Since SGP-RED harvest Gibbs free mixing energy of solutions, enhanced mixing rate promotes the generated power. Electric resistance of IEMs oppose to the transport of ions, so the mixing. Therefore, an ideal RED membrane must have low resistance which allows faster ion transport. Dlugolecki et al. (2008) scanned potential of various ED membranes for RED. Resistance of homogeneous membranes varied between 0.68-2.91 Ω·cm^2 while heterogeneous membranes have resistance an order of magnitude higher [3]. Tailor-made SPEEK CEMs and PECH-PAN-DABCO blend AEMs with different thickness characterized by Guler et al. (2013) resulted in resistance of 0.82-2.05 Ω·cm^2 [9]. Areal resistance of sPPO/ Fe_2O_3-SO_4^{2-} organic/inorganic composites, investigated by Hong et al. (2014), measured between 0.87 to 2.05 Ω·cm^2 [10]. Ultrathin pore

filling CEMs (KIER-CEM1) and AEMs (KIER-AEM1) resulted in 0.34 and 0.28 $\Omega \cdot cm^2$, respectively [11].

Although resistance and permselectivity are the most important membrane properties, ion exchange capacity (IEC), swelling degree (SD) and charge density (CD) also play effective role. Most of these membrane properties are related to each other and most of the time they have a counteracting effect on each other. For example, swelling degree increases with increasing ion exchange capacity because more water molecules get attracted by elevated fixed charge content of membrane. On the other hand, resistance and permselectivity decrease with higher IEC because water channels will be created across the membrane and these channels favor ion transport and decline ion exclusion ability.

CEMs contain negative fixed charged moieties on their backbone to be able to exclude co-ions present in the facing electrolyte solution. These fixed charges can be $–SO_3^-$, $-COO^-$, $-PO_3^{2-}$, $-PHO_2^-$, $-AsO_3^{2-}$, $-SeO_3^-$ [12]. Among all, sulfonation is one of the most accepted functionalization because sulfonate groups are easy to introduce into aromatic groups. Moreover, they dissociate easier than carboxylic acid moieties and formation of anhydrides on dehydration is easier and faster than phosphonic acids [13]. Hydrophobic nature of polysulfone (PSf) makes it an attractive candidate as CEM material. Moreover, it is cheap, commercially available and well established. Regarding desired end-product, various sulfonation agents are reported to obtain sulfonated polysulfone (sPSf). Chlorosulfonic acid (CSA) has been classified as inexpensive, strong sulfonation agent for PSf, while sulfur trioxide/triethylphosphate and trimethylsilyl chlorosulfonate (TMSCS) are relatively expensive and less reactive [14,15]. Although, previous researchers noted easiness of the chlorosulfonation in a chlorinated solvent, they also mentioned chain cleavage and non-homogenous reaction medium as drawbacks of the reaction [14–19].

In this study, chlorosulfonation of PSf carried out by changing CSA/sPSf ratio in the reaction medium. Asymmetric membrane formation abilities of obtained SPSf with different DS studied and most convenient polymer was chosen to investigate various phase inversion parameters such as solvent and co-solvent. Finally, electrochemical characterization in different solutions was carried out to predict RED performance of the membranes.

2. Experimental

2.1. Materials

Polysulfone (PSf Udel® P-1700) was provided by Solvay and was kept at 100^{o}C for overnight before using. Chlorosulfonic acid (CSA, 99%), deuterated dimethyl sulfoxide (DMSO-d_6, %99.9) were purchased from Sigma-Aldrich. Dichloromethane (DCM, HPLC grade), 1-Methyl-2-pyrrolidinone (NMP, 99%), dimethylformamide (DMF, extra pure), 2-propanol (IPA, %99.5) were supplied by Acros Organics. All solvents were used as it is, without further purification.

Neosepta CMX cation exchange membranes were purchased from Takuyama Soda Co. (Japan).

2.2. Sulfonation

DCM was used as sulfonation reaction medium. First, 10 g of PSf was dissolved in 90 ml of DCM and solution was cooled down to 0^{o}C in an ice bath. CSA was diluted to 10 w/v% in DCM and then added dropwise into polymer solution over 30 min. CSA amount was changed from 1.58 g to 3 g which correspond to theoretical maximum degree of sulfonation 0.60 to 1.14, respectively. Following the addition of CSA solution, reaction medium was allowed to increase room temperature by removing ice bath and reaction continued 3 h more. At the end of reaction, brownish slurry polymer, sPSf, precipitated because it is not soluble in DCM. Then, excess DCM was decanted and 90 ml of DMF introduced to obtain a clear polymer solution again. Following

this, polymer was precipitated into 500 ml technical ethanol. Obtained polymer was dried at 70^{o}C under vacuum overnight.

2.3. Polymer Characterization

2.3.1. Fourier Transform Infrared (FTIR)

Chemical structure of dry powder PSf and sPSf were characterized by Bruker Alpha II FTIR spectroscopy. Characteristic peaks belong to sulfonate group were studied qualitatively between 4000 to 400 cm^{-1} wavelength.

2.3.2. Nuclear Magnetic Resonance (NMR)

sPSf samples with different degree of sulfonation were prepared for NMR by dissolving samples in DMSO-d_6. After complete dissolution, samples analyzed by Bruker Avance 400 spectrometer protons. Quantitative calculation known as Kopf's formula was applied to obtain sulfonation degree [20,21].

2.3.3. Membrane preparation

In this study, asymmetric porous membranes were prepared by using wet phase inversion method. Two main solvent, DMF and NMP, and one co-solvent, IPA (also act as non-solvent) were used in the dope solution of asymmetric membranes. Both NMP/IPA and DMF/IPA solvent pairs were varied in solvent/co-solvent ratio from 100/0 to 70/30. Asymmetric membrane films were prepared with 250 µm casting thickness on a glass plate. Following casting, glass plates immersed into coagulation bath which contains technical IPA. After keeping membranes in technical IPA at least 10 min, membranes transferred into distilled water in which peeling of was easier. Membranes kept in distilled water until further use.

2.4. Membrane characterization

2.4.1. Permselectivity

Membrane potential was determined in a two compartment cell as it is illustrated in Fig. 1. Prior to measurement, solutions were heated up to 25 ^{o}C and membranes were conditioned overnight in low concentrated test solution. Then, membrane was fitted in between compartments and 0.1/0.5, 0.1/1.0 or 0.5/1.0 M NaCl were recirculated through the compartments at a flow rate 900 ml/min. Potential difference over the electrodes was recorded until constant values were obtained. Finally, membrane permselectivity was calculated from the ratio between the measured membrane potential (V) to theoretical membrane potential (V) which represents 100% permselectivity.

$$\alpha(\%) = \frac{\Delta V_{measured}}{\Delta V_{theoretical}} 100\% \quad (1)$$

$\Delta V_{theoretical}$ can be calculated by the Nernst equation:

$$\Delta V_{theoretical} = \frac{RT}{zF} \ln\left(\frac{C_2\gamma_2}{C_1\gamma_1}\right) \quad (2)$$

In which R is the gas constant ($J \cdot mol^{-1}K^{-1}$), T the temperature (K), z the electrochemical valence (-), F the Faraday constant (96485 $s \cdot A \cdot mol^{-1}$), C_1 and C_2 the concentrations of the two solutions ($mol \cdot l^{-1}$) and γ_1 and γ_2 the activity coefficients of the two solutions. Table 1 presents calculated theoretical membrane potentials for different solution pairs by using eq. 2.

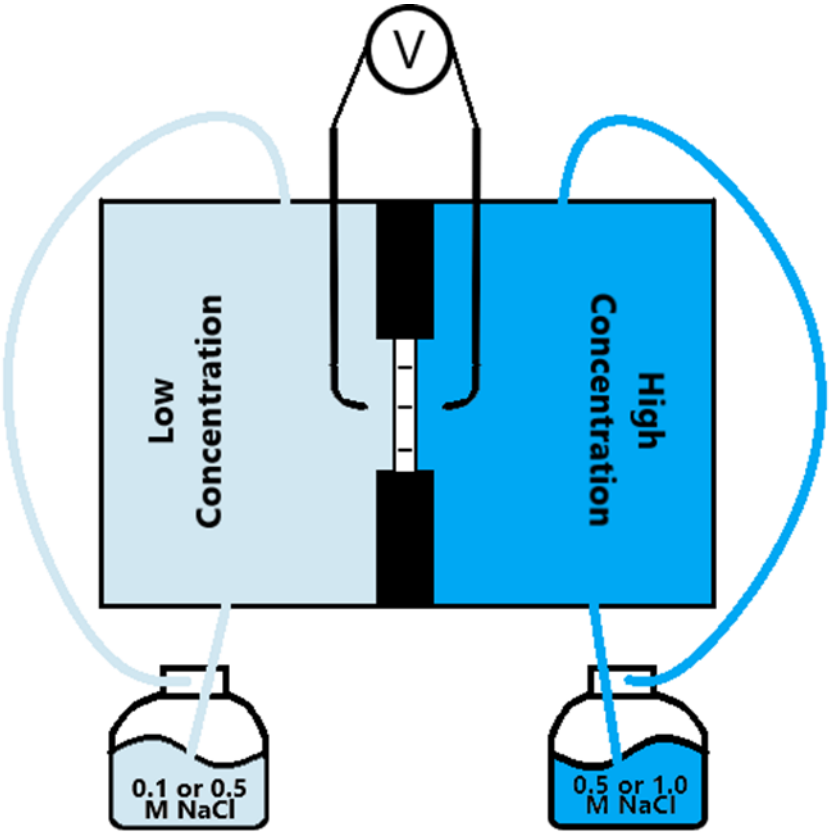

Figure 1. Two compartment permselectivity characterization setup

Table 1. Activity coefficient and theoretical membrane potential of test solution pairs[22].

Concentration (M NaCl)	Activity coefficient (-)	Test solution pair (M NaCl/M NaCl)	Theoretical ΔP (mV)
0.1	0.778	**0.1/0.5**	37.9
0.5	0.681	**0.1/1.0**	54.8
1.0	0.657	**0.5/1.0**	16.9

2.4.2. Resistance

Ionic resistance of sPSf membranes were characterized in various NaCl solutions by using six compartment cell as it was described elsewhere [3]. Fig. 2 illustrates resistance measurement setup supported with 2 calomel electrodes in the compartment 3, 4 and two working electrodes in the compartment 1, 6. Prior to measurement, membranes were conditioned overnight in the test solution which has lower concentration. Electrolyte, shielding and test solutions were warmed up to 25°C. Membrane under investigation was fitted between compartment 3 and 4 while four CMX

membranes were utilized to separate other compartments. CMX membranes which has 99% permselectivity for 0.1/0.5 M NaCl solution were preferred to reduce possible co-ion leakage from neighboring compartments. 1.0 M Na_2SO_4 electrolyte solution was fed into compartment 1 and 6 to avoid dangerous chemical production, i.e. Cl_2 in use of NaCl, on the electrode surface. In compartment 2 and 5, fed shielding solution was at same concentration of electrolyte solution due to inconsistent results were obtained at low concentration (i.e. 0.1 M NaCl solution in use of 0.1 M test solution) in compartment 3 and 4.

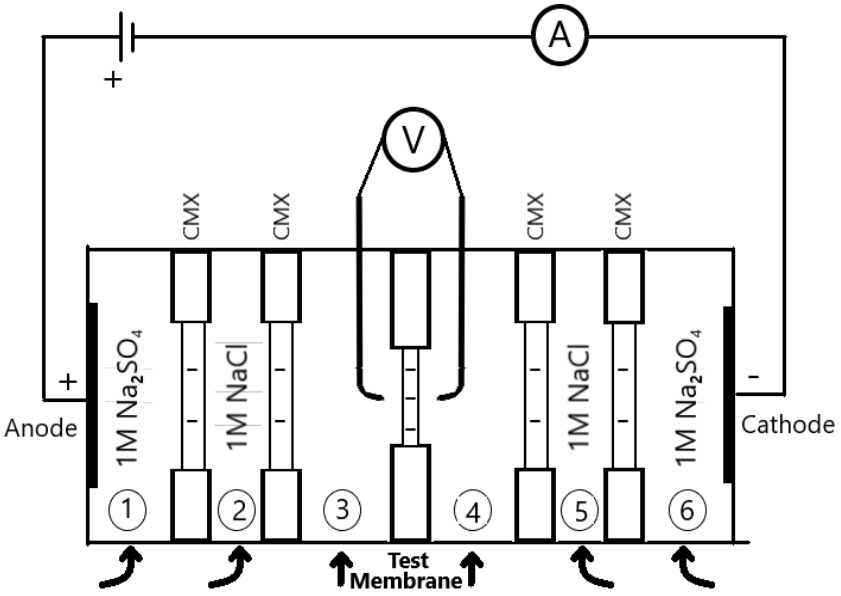

Figure 2. 6-compartment resistance characterization cell

In the first part of the experiments, compartment 3 and 4 was fed with the same concentration: 0.1/0.1, 0.5/0.5, 1.0/1.0 M NaCl. This mode will be called as non-gradient resistance characterization later on. In the second mode, concentration gradient has been created around the membrane by using different feed solutions in compartment 3 and 4. The second mode will be called as gradient resistance characterization from now on. Gradient resistance characterization feed solutions were 0.1/0.5, 0.1/1.0 and 0.5/1.0 M NaCl. For the second mode, test membranes

were flipped to see if membrane orientation has an effect on resistance. Masterflex peristaltic pump with CT numbers 19347 were operated to feed the solutions at 270 ml/min flowrate.

Membrane resistance characterization were carried out for DC and AC current mode.

Resistance in DC mode

DC current ranged between 0-15 mA applied through working electrodes and corresponding potential difference on calomel reference electrodes were recorded. DC resistance (R_{DC}) was calculated from slope of current vs potential difference plot. This resistance comprises membrane resistance (R_m), boundary layer resistance (R_{bl}) and solution resistance (R_s). To eliminate solution resistance, DC measurement was repeated without membrane at the same conditions of investigated membrane. R_{m+dl} was then calculated by subtracting R_s from R_{DC}.

Resistance in AC mode

An advantage of using alternating current mode is to distinguish membrane resistance and boundary layer resistance. Following DC measurement, membrane resistance was characterized at same conditions in AC current ranged from 10^5 to 1 Hz. At high frequencies effect of boundary layer diminishes significantly. Thus, measured AC resistance (R_{AC}) represents R_{m+s}. A blank AC measurement at the same condition of tested membrane allows to obtain R_m by subtracting R_s from R_{AC}.

2.4.3. Morphology

Cross section of membranes were imaged by scanning electron microscopy (JSM-6010LA). A full cross section images at 1000 magnification were captured.

3. Results and discussion

3.1. FTIR

Electrophilic substitution of sulfonic group on PSf can be achieved up to DS=2 depending on the reagent ratio present in the reaction medium. As it is illustrated in Fig. 3, substitution mostly occurs on phenyl ether instead of phenyl sulfone due to electron-withdrawing character of SO_2 group [15].

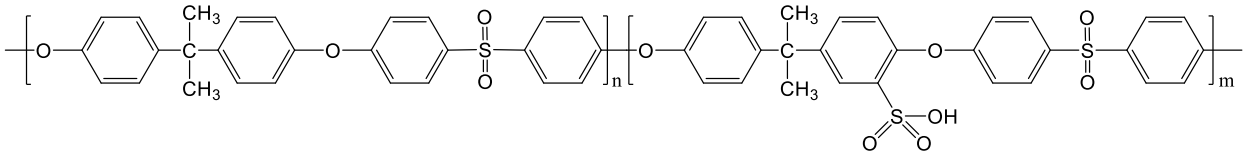

Figure 3. Molecular structure of sulfonated polysulfone

Sulfonation of polysulfone can be confirmed qualitatively by FTIR spectra. After chlorosulfonation of PSf, additional peaks were expected to show up near 1027 cm^{-1} and 1070 cm^{-1} related to symmetric and asymmetric O=S=O stretching of sulfonate group, respectively [14,23,24]. Fig. 4 demonstrates FTIR pattern of PSf and sPSf from 950 cm^{-1} to 1200 cm^{-1} where sPSf footprint fall into. Desired symmetric and asymmetric stretching sulfonate peaks were obtained at 1026 cm^{-1} and 1092 cm^{-1} in accordance with literature [14,23,24].

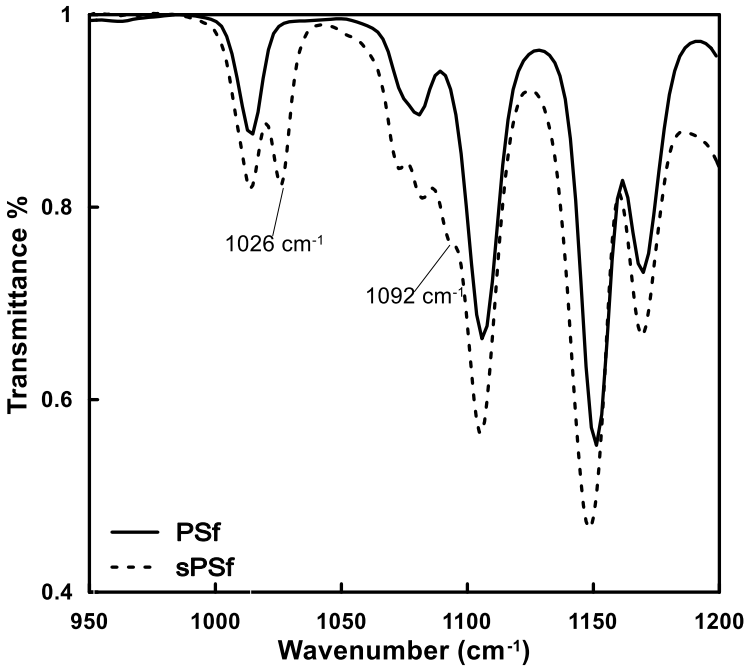

Figure 4. FTIR pattern of PSf and sPSf

3.2. ^{1}H NMR

DS of synthesized sPSf were decided quantitatively by applying Kopf's formula to ^{1}H NMR pattern. In the sulfonated polymer units, protons close to the sulfone group get split while non sulfonated units remain unchanged as it is illustrated in Fig. 5. Area (A) under related peaks allow us to calculate DS by the help of Kopf's formula.

$$DS = \frac{4 \times A(2'')}{A(3,3')} \tag{3}$$

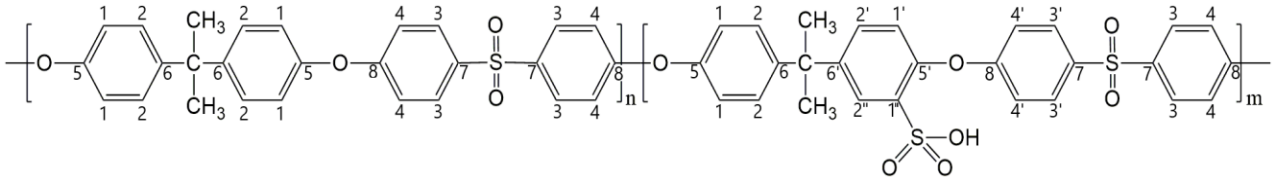

Figure 5. sPSf with numbered protons

Fig. 6 demonstrates obtained ^{1}H NMR pattern of sPSf-8. Since proton 2'' is a well-resolved singlet peak, it is considered as the reference peak and peak area of 2'' was assumed as 1.00. Relative areas for other characteristic peaks were calculated based on 2''.

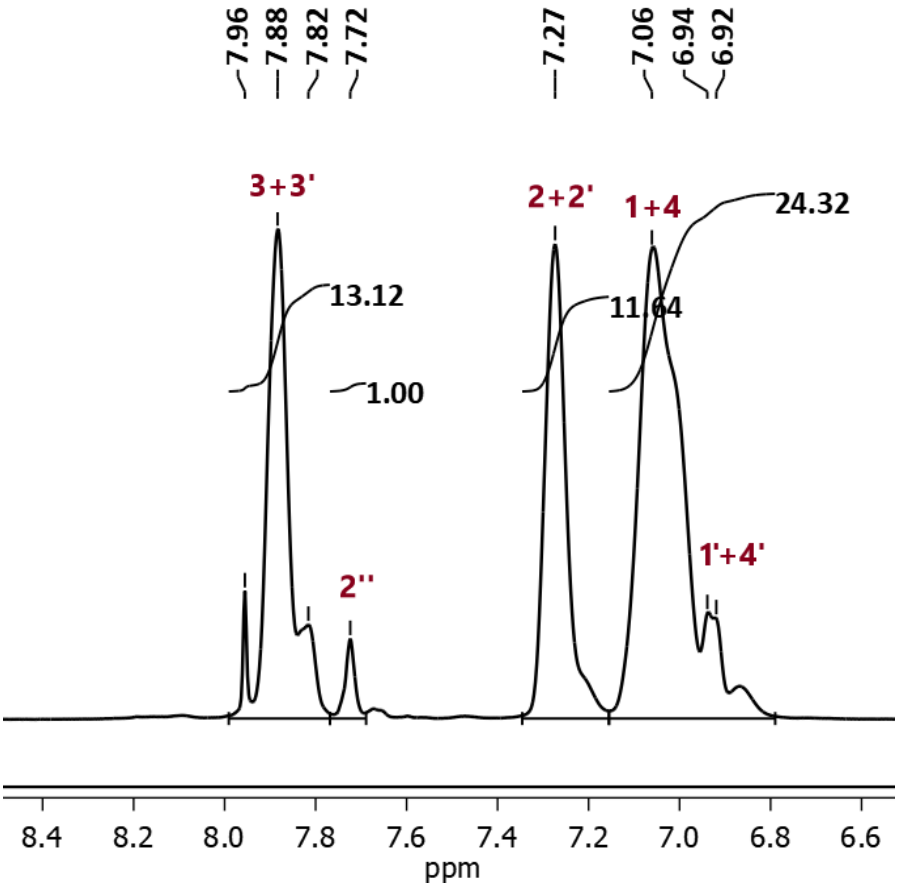

Figure 6. ^{1}H NMR pattern of sPSf-8

The sulfonation reaction takes place in DCM which is a solvent for the reagent PSF and a non-solvent for the product sPSF. This behavior of PSf can also be concluded theoretically by studying Hansen solubility parameters. According to theory, to have a soluble polymer in a particular solvent, they have to stand close in three dimensional space where dimensions are dispersion, hydrogen and polar forces. Table 2 compares Hansen solubility parameters of various polymers and solvents were used in this study. DS has drastic effect on hydrogen forces and polar forces while dispersive forces can be affected slightly. It is apparent from this table with increasing DS of PSf, the distance between DCM and the polymer increases. Therefore DCM shifts from being a solvent to non-solvent. This situation was also observed during the reaction. After half an hour of CSA addition, homogeneous reaction medium turned into a heterogeneous medium where

brownish sPSf slurry precipitated. Due to precipitation of polymer, DS is uncontrolled. Shorter chains in aqueous state has probably higher sulfonation degree. Addition to this, possible chain cleavage was reported by Baradie et al. in use of CSA which is a strong acid and causes hydrolysis of polymer chains [25]. Even though non-homogeneous reaction and chain cleavage, resulting polymers were mechanically stable enough to form self-standing membranes. In addition, despite the disadvantages, usage of CSA was favorable considering being cheap reagent and allowing an easy reaction.

Table 2. Hansen solubility parameters of some solvents and polymers used in this study [26,27]

Solvent or Polymer	δ_d ($MPa^{1/2}$)	δ_p ($MPa^{1/2}$)	δ_h ($MPa^{1/2}$)
DCM	18.2	6.3	6.1
NMP	18.0	12.3	7.2
DMF	17.4	13.7	11.3
IPA	15.8	6.1	16.4
PSf	18.2	4.3	6.9
sPSf (DS=0.30)	18.2	5.0	8.5
sPSf (DS=1.00)	18.1	6.0	11.0

In this study, sPSF were obtained with DS form 0.28 to 0.47. As shown in Fig. 7, DS of PSf can be controlled by arranging mole ratio of chlorosulfonic acid to polysulfone.

3.3. Membrane preparation

Wet phase inversion (PI) membranes were prepared from all sPSf presented in Fig. 7, as described previously in section 2.4. When water used as non-solvent instead of IPA, a gel like polymer precipitate was obtained and film formation was not possible for any sPSf. Although water is known as non-solvent for PSf from the previous studies, addition of sulfone groups to PSf was resulted a new polymer for which phase inversion parameters were altered. In this study, to be able to form a thin film in the precipitation bath, water was replaced with IPA. Furthermore, since the

final application of these membranes is water, after 10 min, membranes were immersed into water as second coagulation bath. After immersion into IPA, PI was resulted in white thin membrane films within approximately 2 min delay. However, membranes prepared with DS higher than 0.31 were turned into transparent film or lost their stand-alone film properties. White color of film is an indication of a porous membrane. Transition from white to transparent membrane can indirectly indicate transition from porous to dense membrane morphology. Possible explanations to change in film properties can be incomplete PI or swelling due to high ion exchange capacity. After this preliminary experiments, sPSf with 0.31 DS was determined as most convenient polymer to prepare PI membranes as explained in section 2.4. Further phase inversion parameters, co-solvent ratio and solvent type, were studied for this polymer.

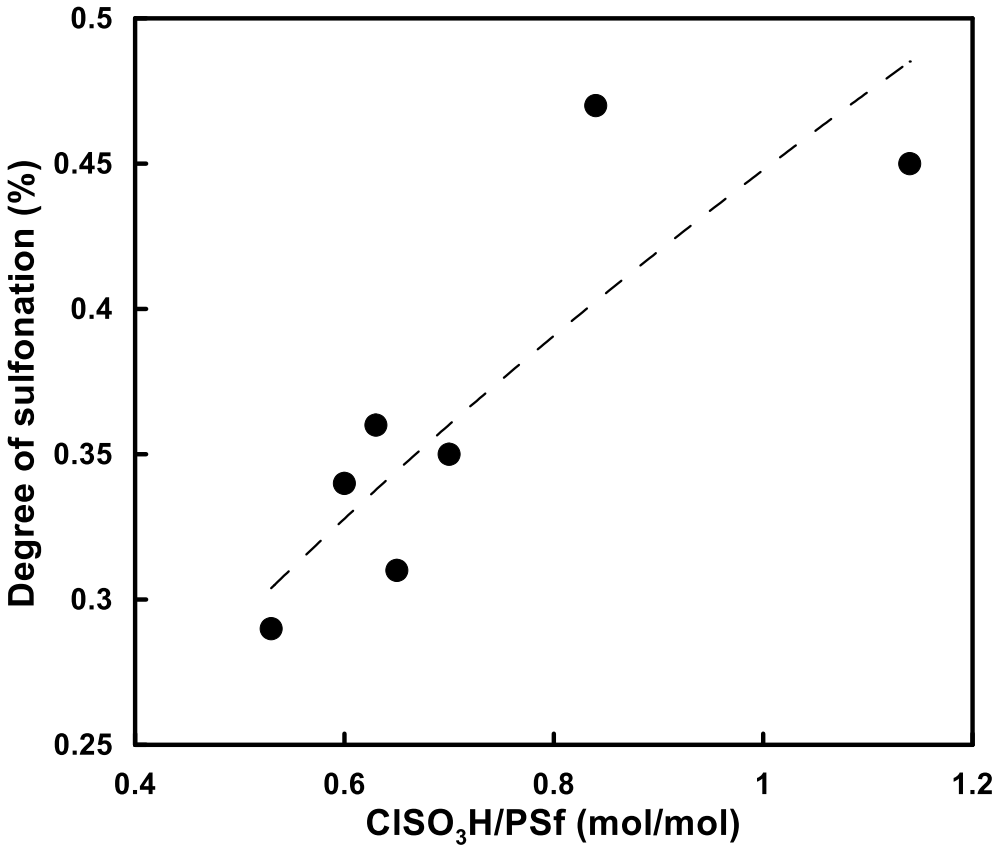

Figure 7. Relation between reagent ratios and sulfonation degree

3.4. Co-solvent addition

As it is stated previously, sPSf/DMF (or NMP)/IPA polymer/solvent/non-solvent system resulted in delayed demixing for wet phase inversion method due to poor miscibility of DMF and IPA. Based on our knowledge on demixing rate in the literature, instantaneous demixing results in porous membrane while delayed demixing may form completely dense or asymmetric morphology with thin dense top layer depending on delay duration. In this study, an asymmetric membrane with a top dense layer that can maintain the desired permselectivity and enhance the resistance of the membrane was aimed. There are various ways to promote demixing;

- the choice of the solvent/nonsolvent system;
- the polymer concentration;
- the composition of polymer solution;
- the composition of coagulation bath;
- the usage of additives;
- the temperature of the solution or the coagulation bath [28].

Based upon listed approaches, a parametric study on the choice of solvent/non-solvent system was conducted. In order to improve demixing rate, IPA was used as a co-solvent. During the selection of IPA as co-solvent, it is considered to avoid an extra chemical in the system. Cloud point experiments showed up to 33w/w % IPA addition can be tolerated by sPSf/DMF(or NMP)-IPA system. Therefore, membranes were prepared for following solvent/cosolvent ratios; 100/0, 90/10; 80/20, 70/30.

3.4.1. Characterization of membranes which DMF used as main-solvent

Membranes prepared without the co-solvent addition resulted with approximately 2 min delay on demixing. As expected, with introduction of IPA into dope solution decreased the delay and when IPA amount was 30 wt% and instantaneous demixing was observed. Poor miscibility of DMF and IPA system was enhanced by blending IPA with DMF in the solvent system.

Morphology of DMF membranes

Cross-sectional images of DMF membranes are illustrated in Fig. 8. It can be concluded up to 20w/w % IPA, membranes were formed with a dense top layer around 5 µm. When IPA concentration was higher than 20%, clear indication of dense top layer was not possible for the obtained images. In addition, it is difficult to correlate a trend between dense layer thickness and IPA concentration in the dope solution. However, images confirm porous layers of the membranes transform from well-defined pores to nodular, inter connected pores.

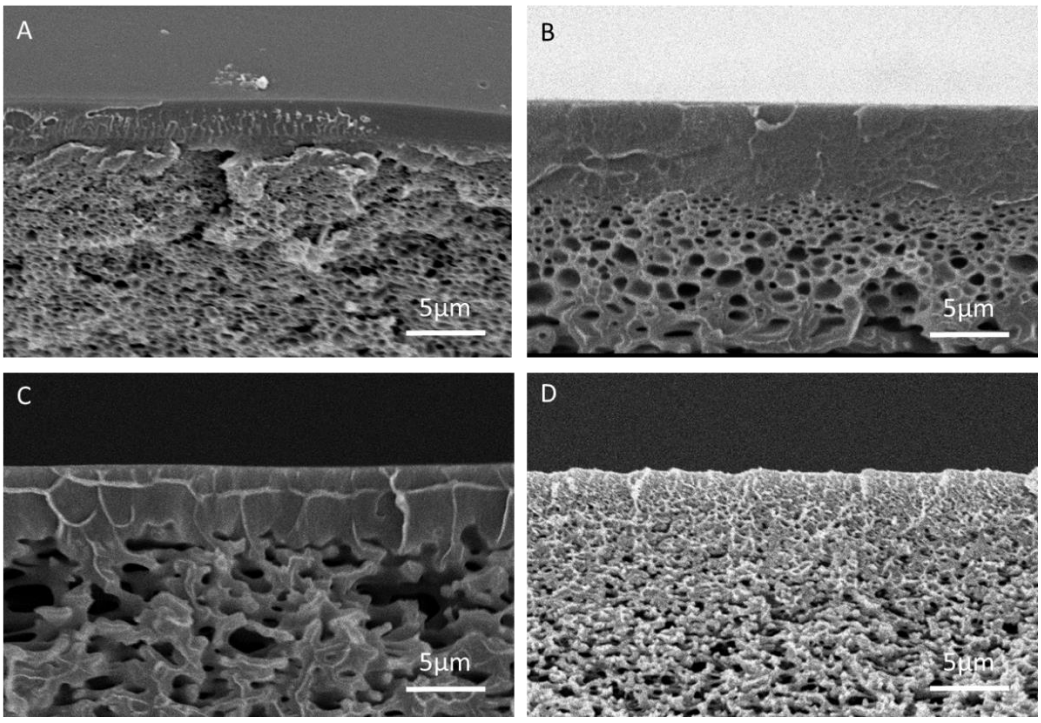

Figure 8. Cross section of membranes which solvent/co-solvent (DMF/IPA) ratio in dope solution: A) 100/0, B) 90/10, C) 80/20, D) 70/30

Electrochemical characterization of DMF membranes

Permselectivity of the DMF membranes were characterized in 0.1/0.5 M NaCl solution and membrane resistance were measured for 0.5/0.5 M NaCl solutions. The obtained results illustrated in Fig. 9. Membranes maintained permselectivity around 90% up to 20% IPA concentration and lost their selective properties for 30% IPA. The findings from electrochemical characterization are consistent with the cross-sectional images explained in the previous section. The membranes with the top dense layer were able to retain Cl^- ions, whereas the membrane with no visible dense layer was not selective against Cl^- ions. Moreover, probably ions were transported from large water channels without any preferential selection.

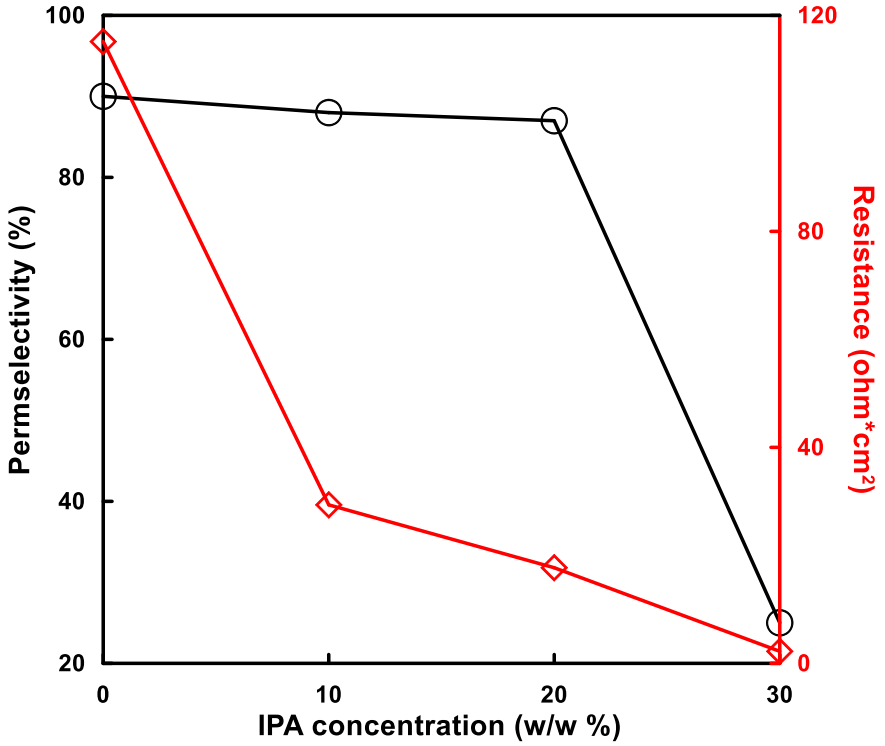

Figure 9. Electrochemical properties of membranes prepared by DMF

On the other side, resistance of membranes showed a decreasing trend for increasing IPA concentration. Even though thickness of top layers of the A-C membranes were not different significantly. Probably, porous layer of these membranes became more interconnected with

increasing IPA content in the dope solution. Therefore ions were transported freely across the porous layer. Lastly, the membrane with 30 % IPA lost its resistance drastically due to interconnected pores across the overall cross-section.

3.4.2. Characterization of membranes which NMP used as main-solvent

Likewise membranes prepared with DMF, IPA w/w percent in the solvent pair were changed from 0-30 % with an interval of 10 % for membranes prepared with NMP. Demixing properties are observed. Furthermore morphological and electrochemical characterization were completed.

Morphology of NMP membranes

Fig. 10 shows membranes prepared with NMP were porous. Cross-sectional images indicate starting from 10 % of IPA, fingerlike porous were formed and there is a positive correlation between size of the fingerlike structures and amount of the IPA in the dope solution. It can also be commented porous on the top layer become more nodular after 20% IPA in the dope solution. Compared to DMF membranes, there is no formation of visible dense top layer.

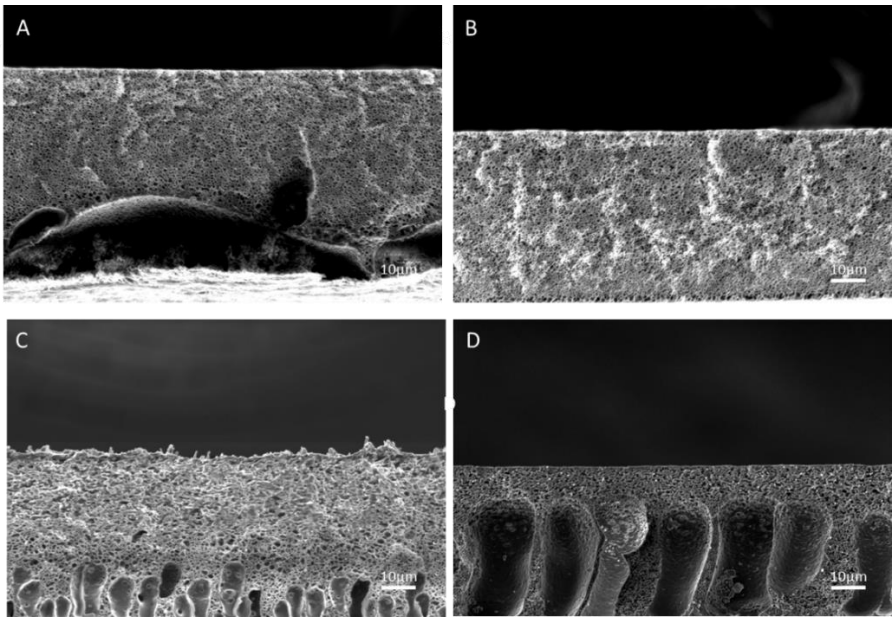

Figure 10. Cross section of membranes which solvent/co-solvent (NMP/IPA) ratio in dope solution: A) 100/0, B) 90/10, C) 80/20, D) 70/30

An unexpected membrane structure was obtained for the membrane had 0% IPA. Large cavity on the bottom surface can be due to a mistake during experimental procedure.

Electrochemical characterization of NMP membranes·

Membranes were characterized for permselectivity in 0.1/0.5 M NaCl solution and for ionic resistance in 0.5/0.5 M NaCl solution. The permselectivity and resistance results for NMP membranes are summarized in Fig. 11. Although there were no dense layer formed in the membranes, up to 20% IPA concentration, permslectivity of the membranes maintained over 80%. This high permslectivity can be explained by not having interconnected pores. Further increase in IPA concentration to 30% resulted with poor permselectivity because pores become nodular therefore large water channels were not able to retain co-ions.

Resistance of the membranes were resulted between 8.0 to 1.8 $\Omega \cdot cm^2$. It is hard to conclude there is a clear trend between IPA content and resistance. However, commenting on resistance results by taking into account SEM images can give a better understanding. SEM images clearly indicates ionic resistance is directly related to cavities in the membrane. Presence of large cavities and interconnected pores enhance the transport of the ions, so the resistance decreases.

3.5. RED performance of selected membrane

A convenient membrane for the RED application must have high permselectivity and low ionic resistance as well as cheap and stable for long time. Present commercial homogenous ED membranes has permselectivity >90% and resistance 1.5 to 3.0 $\Omega \cdot cm^2$. Considering resistance range of commercial IEMs, DMF membranes prepared in this study had significantly high resistance despite their comparable permselectivity. On the other hand, NMP membranes had promising performance. Particularly, membrane contains 20% IPA had the best electrochemical

properties. Therefore this membrane and commercial benchmark CMX provided by Ralex (α=0.99 and R=2.91 Ω·cm^2) were analyzed further for different concentrations of NaCl.

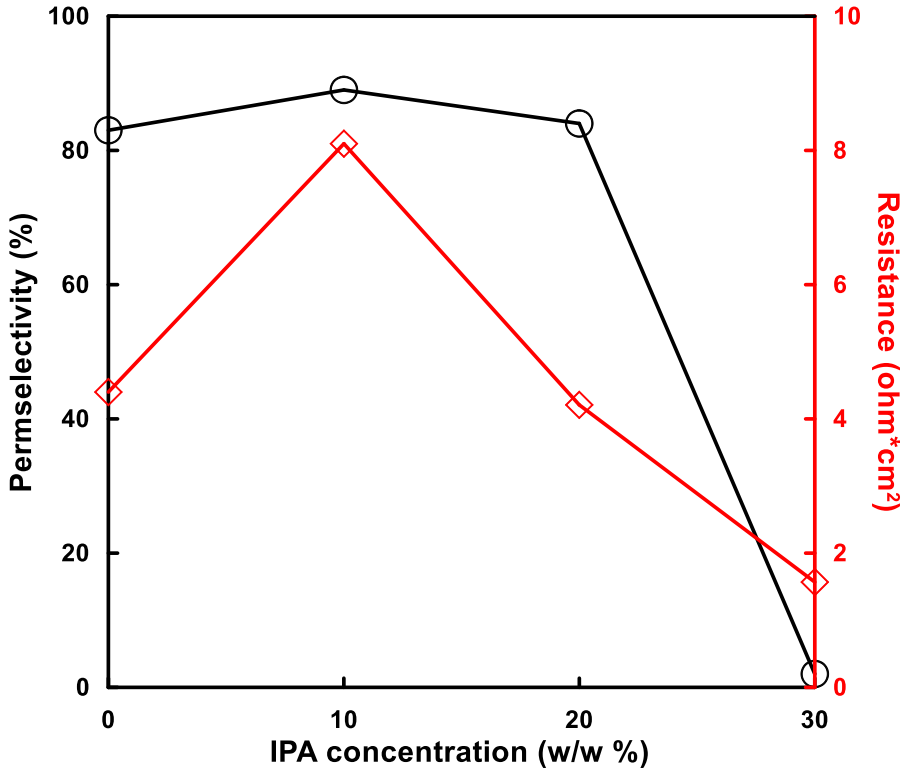

Figure 11. Electrochemical properties of membranes prepared by NMP

3.5.1. Permselectivity

To see the effect of different concentration around the membrane, alternative to 0.1/0.5 M NaCl solution, 0.1/1.0 and 0.5/1.0 M NaCl solutions were also studied. Permselectivity was also measured by reversing the concentration gradient in order to understand if membrane orientation has an effect on permselectivity due to asymmetric porosity, i.e. 0.1/0.5 M NaCl to 0.5/0.1 M NaCl.

From Fig. 12, we can see that response of the both membrane follows the same trend. Having more ions in the solutions reduce the co-ion exclusion capacity of the membranes. These results are consistent with the literature [29–31]. Zlotorowicz et al. explained permselectivity of membranes

decrease with increasing concentration of either solution. Furthermore, increasing concentration gradient would result in higher permselectivity where the highest concentration kept constant [29]. Effect of reversing concentration gradient around the membrane was negligible and insignificant regarding errors involved in the experiments.

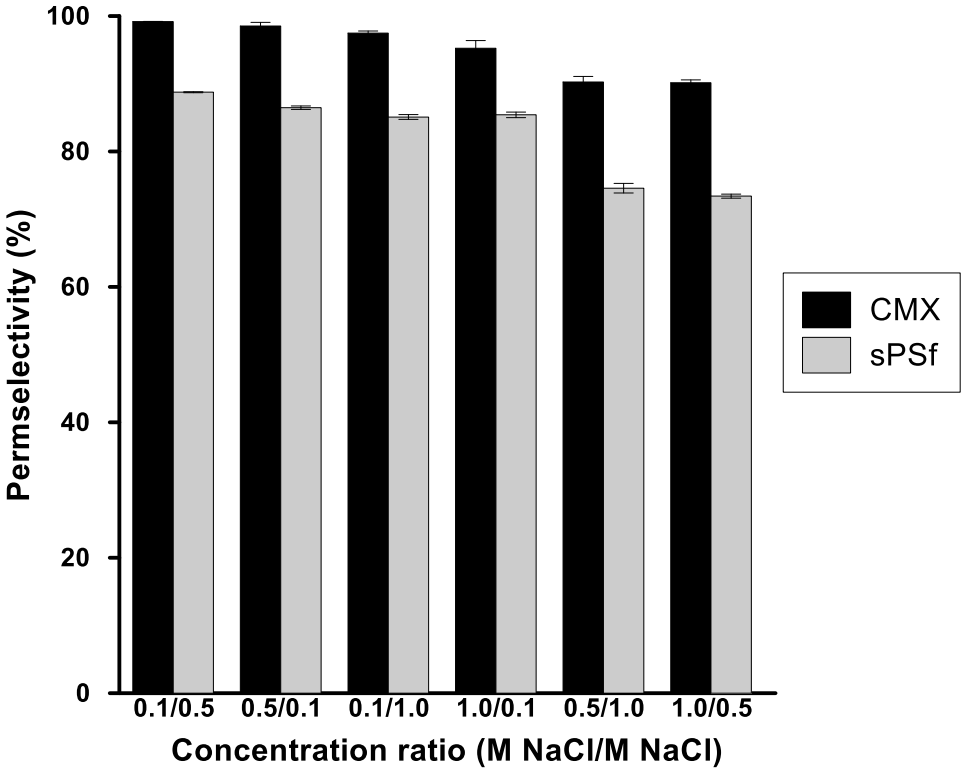

Figure 12. Permselectivity of CMX and sPSf at different concentrations

3.5.2. Non-gradient resistance

Typical solution pair to characterize ionic resistance is 0.5/0.5 M NaCl or KCl. In this study, experiments were performed with 0.1/0.1 M NaCl and 1.0/1.0 M NaCl in addition to 0.5/0.5 M NaCl. Ohmic and non-ohmic resistances are presented for CMX and sPSf membranes in Fig. 13. For sPSf membrane, both resistances were decreasing while for CMX membrane ohmic resistance remains constant and non-ohmic resistance decreases. The different trend on ohmic resistance of two membranes can be explained by membrane morphology. CMX has a dense structure whereas

sPSf membrane has asymmetric porous structure. Therefore probably resistance inside of the water channel across the sPSf contributes to membrane resistance. Resistance of these channels is dominated by the solution that is present in the channel. Increasing the concentration of this solution decreases the resistance of the channel so the resistance of the membrane. Since in a dense membrane (i.e CMX), water channels are limited compared to porous membrane, the ohmic resistance of the membrane will be decided by ion exchange material. Ohmic and non-ohmic resistances obtained in this study is comparable to the previous studies on resistance of CMX membranes [32,33].

Also, non-ohmic resistance of sPSf for all conditions are slightly higher. A possible explanation to this might be that an additional resistance of internal concentration polarization was occurred in the pores of sPSf due to poor flow conditions.

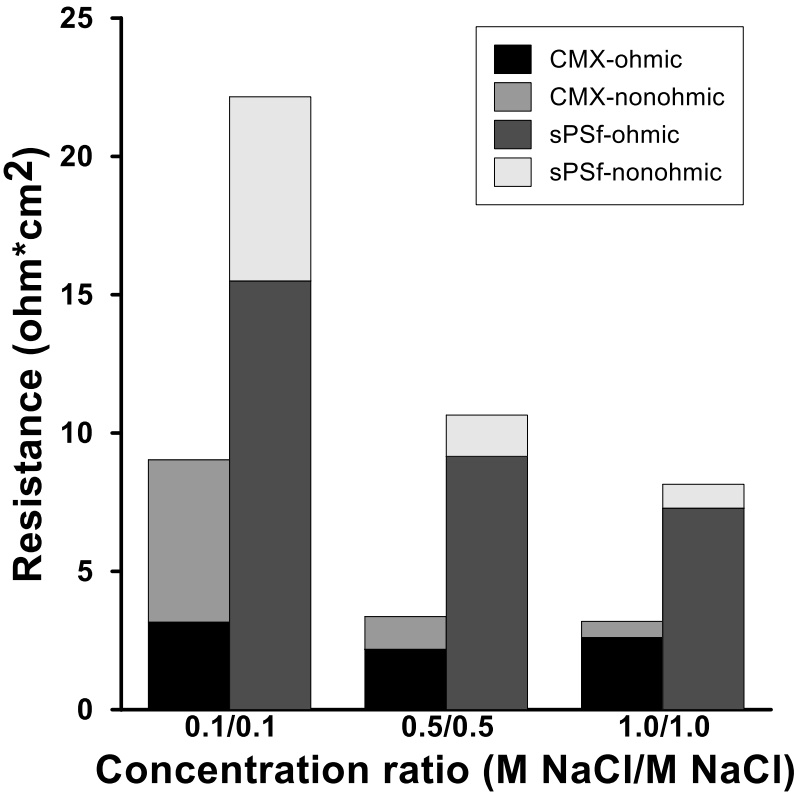

Figure 13. Resistance of CMX and M207 at different concentrations

3.5.3. Gradient resistance

Reverse electrodialysis harvest the energy of salinity gradient power. Therefore, better estimation can be made by measuring the membrane resistance when a gradient present across the membrane. In addition, non-ohmic resistance can be more realistic compared to the non-gradient resistance measurements.

All possible binary combinations of non-gradient solutions were tested as gradient solutions. The resistance of CMX and sPSf membranes are summarized in Fig. 14. For all cases, total resistance of CMX membrane is lower than sPSf membrane. From this data we can see total resistance and ohmic resistance of sPSf is decreasing with the increasing NaCl content, while, in same orientation of membrane, non-ohmic resistance do not differ significantly from 0.1/0.5 to 0.1/1.0 solution pair because non-ohmic resistance caused by 0.1 M NaCl is dominant. On the other side, no significant difference were found for CMX for 0.1/0.5 to 0.1/1.0 where resistance is halved for 0.5/1.0.

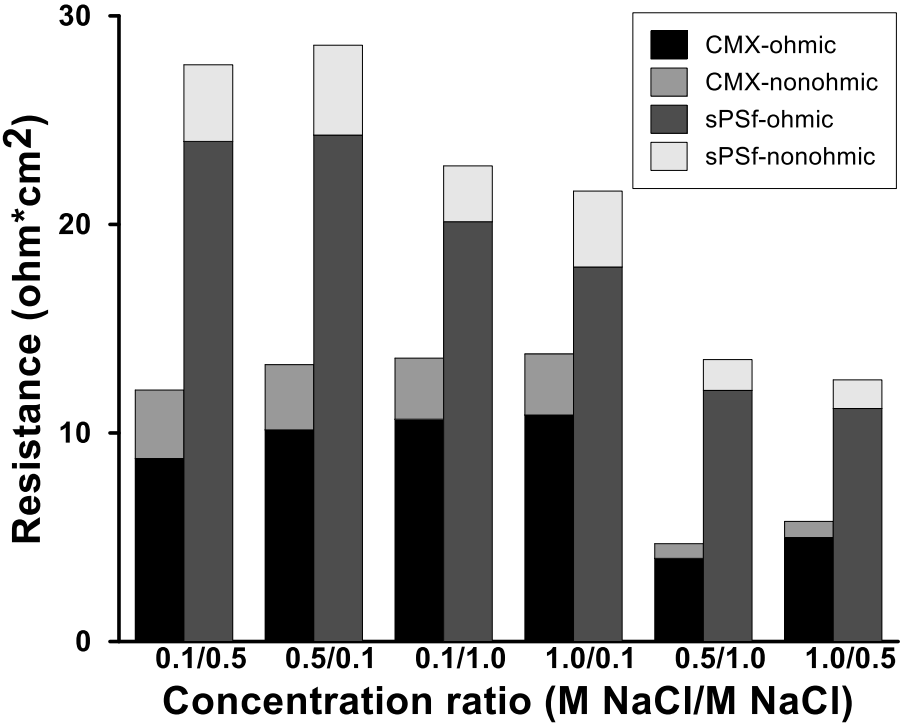

Figure 14. Resistance of CMX and M207 when concentration gradient is present

3.6. Theoretical power density calculation

Although sPSf membrane has lower permselectivity and higher resistance compared to benchmark CMX membrane, estimation of RED power potential is worthwhile. Previous studies, Dlugolecki et al., and Safaranova et al, estimated maximum power densities for artificial river water (~0.01 M NaCl)/seawater (0.5 M NaCl) solution pair [3,34]. Both studies used the resistance values measured in 0.5 M NaCl solution which can be a source of the error.

In this work, max power density was calculated by using more representative values for electrochemical properties.

$$P_{\max} = \frac{\left[\alpha \frac{RT}{F} \ln\left(a_c / a_d\right)\right]^2}{2\left(R_{CEM} + d/k_c + d/k_d\right)} \quad (3)$$

where α is permselectivity (-), a_c ionic activity of concentrated solution (-), a_d ionic activity of diluted solution (-), R_{CEM} is ionic resistance of CEM (Ωm^2), d is the thickness (m), k_c is the conductivity of concentrated solution (Ωm), k_d is the conductivity of diluted solution (Ωm), F is Faraday constant(96500 sA/mol), T is temperature (298 K) and R is universal gas constant (8.314 J/molK). Theoretical calculation was made for a half-cell. Half-cell includes half of the diluted compartment (100 μm), half of the concentrated compartment (100 μm) and CEM.

Summary of the power density calculation is presented in Fig. 15. Calculated power when sPSf membrane utilized was always resulted between half and one third of the CMX membrane. The highest power density was obtained for 0.1/1.0 M NaCl solution where the lowest was 0.5/1.0 M NaCl. Regarding orientation of membranes, sPSf was able to produce more power when the porous side of the membranes was in contact with the diluted compartment, on the other hand there was no clear trend for CMX membranes.

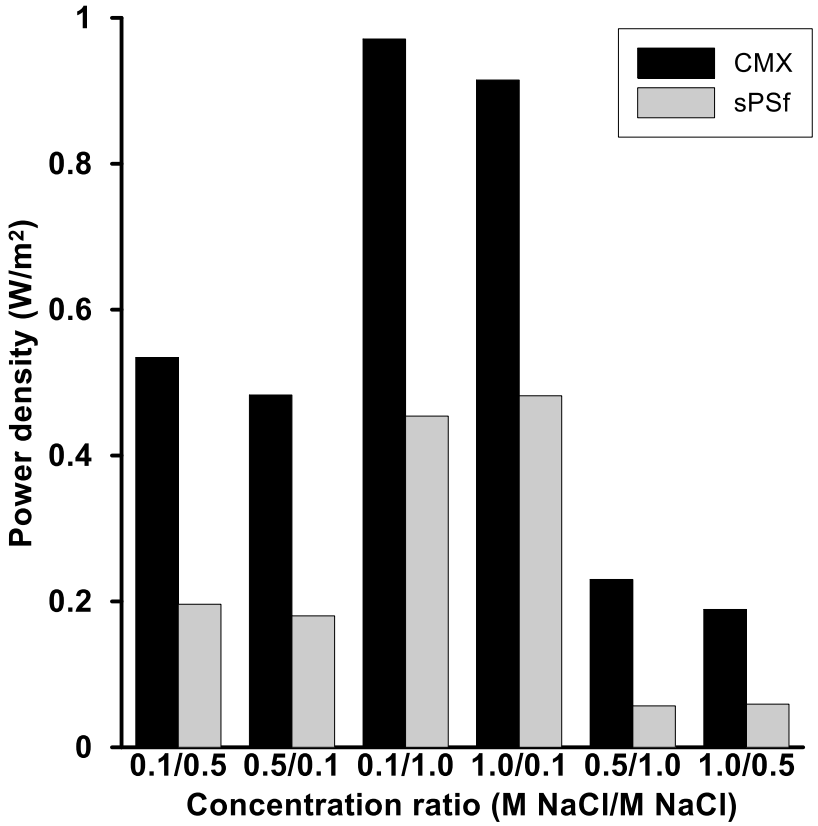

Figure 15. Theoretical power density of CMX and M207 at different concentrations

4. Conclusion and outlook

In this study, polysulfone (PSf) was successfully sulfonated to prepare cation exchange membrane for RED application. Among different DS, polymer with 0.31 DS was decided to continue with considering wet phase inversion membrane preparation easiness. The aim was to enhance electrochemical properties by preparing asymmetric phase inversion membranes. A parametric experimental work was completed by changing main solvent (NMP, DMF) and co-solvent (IPA) ratio in the polymer dope solution. Some obtained membranes were resulted in comparable electrochemical properties with commercial membranes. The most promising membrane was further characterized for different solution concentrations to estimate power generation potential under RED operating conditions. Lab-made membranes had comparable permselectivity whereas

poor conductivity. As a result, sPSf membrane was found not competitive from power generation point of view.

Although sPSf membranes were not competitive regarding power output, they can still be promising for the commercialization of RED. Membrane price is the biggest limitation on RED commercialization. For a feasible RED operation, cost of the membranes must be less than 5 €/m^2 [7,35]. Cheap sulfonation method, low sulfonation degree, less polymer consumption, well known phase inversion method can lower the price of sPSf membranes to desired value. Moreover, electrochemical properties can also be enhanced by investigation other phase inversion parameters.

5. References

[1] G.L. Wick, Power from salinity gradients, Energy. 3 (1977) 95–100.

[2] A.H. Avci, P. Sarkar, R.A. Tufa, D. Messana, P. Argurio, E. Fontananova, G. Di, E. Curcio, Effect of Mg^{2+} ions on energy generation by Reverse Electrodialysis, J. Memb. Sci. 520 (2016) 499–506.

[3] P. Dlugolecki, K. Nymeijer, S. Metz, M. Wessling, Current status of ion exchange membranes for power generation from salinity gradients, J. Memb. Sci. 319 (2008) 214–222.

[4] E. Guler, Y. Zhang, M. Saakes, K. Nijmeijer, Tailor-made anion-exchange membranes for salinity gradient power generation using reverse electrodialysis, ChemSusChem. 5 (2012) 2262–2270.

[5] R.E. Lacey, Energy by reverse electrodialysis, Ocean Eng. 7 (1980) 1–47.

[6] H. Strathmann, Electrodialysis, a mature technology with a multitude of new applications, Desalination. 264 (2010) 268–288.

[7] A. Daniilidis, R. Herber, D. a. Vermaas, Upscale potential and financial feasibility of a reverse electrodialysis power plant, Appl. Energy. 119 (2014) 257–265.

[8] J.W. Post, C.H. Goeting, J. Valk, S. Goinga, J. Veerman, H.V.M. Hamelers, P.J.F.M. Hack, Towards implementation of reverse electrodialysis for power generation from salinity gradients, Desalin. Water Treat. 16 (2010) 182–193.

[9] E. Güler, R. Elizen, D.A. Vermaas, M. Saakes, K. Nijmeijer, Performance-determining membrane properties in reverse electrodialysis, J. Memb. Sci. 446 (2013) 266–276.

[10] J.G. Hong, Y. Chen, Nanocomposite reverse electrodialysis (RED) ion-exchange membranes for salinity gradient power generation, J. Memb. Sci. 460 (2014) 139–147.

[11] H.-K. Kim, M.-S. Lee, S.-Y. Lee, Y.-W. Choi, N.-J. Jeong, C.-S. Kim, High power density of reverse electrodialysis with pore-filling ion exchange membranes and a high-open-area spacer, J. Mater. Chem. A. 3 (2015) 16302–16306.

[12] H. Strathmann, (2004). Ion exchange membrane separation processes. Amsterdam, The Netherlands: Elsevier.

[13] G. Maier, Meier-Haack. Jochen, Sulfonated Aromatic Polymers for Fuel Cell Membranes, Adv. Polym. Sci. 216 (2008) 1–62.

[14] R. Naim, A.F. Ismail, H. Saidi, E. Saion, Development of sulfonated polysulfone membranes as a material for Proton Exchange Membrane (PEM), Proc. Reg. Symp. Membr. Sci. Technol. (2004) 1–17.

[15] C. Iojoiu, M. Marøchal, F. Chabert, J. Sanchez, Mastering Sulfonation of Aromatic Polysulfones : Crucial for Membranes for Fuel Cell Application, Fuel Cells. 5 (2005) 344–354.

[16] J.F. Blanco, Q.T. Nguyen, P. Schaetzel, Sulfonation of polysulfones: Suitability of the

sulfonated materials for asymmetric membrane preparation, J. Appl. Polym. Sci. 84 (2002) 2461–2473.

[17] C. Hasiotis, V. Deimede, C. Kontoyannis, New polymer electrolytes based on blends of sulfonated polysulfones with polybenzimidazole, Electrochim. Acta. 46 (2001) 2401–2406.

[18] J. Quentin, (1973). U.S. Patent No. 3709841. Washington, DC: U.S. Patent and Trademark Office.

[19] N. Sivashinsky, G.B. Tanny, Ionic heterogeneities in sulfonated polysulfone films, J. Appl. Polym. Sci. 28 (1983) 3235–3245.

[20] C. Iojoiu, P. Genova-Dimitrova, M. Maréchal, J.Y. Sanchez, Chemical and physicochemical characterizations of ionomers, Electrochim. Acta. 51 (2006) 4789–4801.

[21] A. Noshay, L.M. Robeson, Sulfonated Polysulfone., J. Appl. Polym. Sci. 20 (1976) 1885–1903.

[22] R. C. Weast, M. J. Astle, W. H. Beyer, (1984). CRC Handbook of chemistry and physics. Boca Raton, FL. CRC Press, Inc.

[23] R.K. Nagarale, G.S. Gohil, V.K. Shahi, R. Rangarajan, Preparation and electrochemical characterization of sulfonated polysulfone cation-exchange membranes: Effects of the solvents on the degree of sulfonation, J. Appl. Polym. Sci. 96 (2005) 2344–2351.

[24] I.S. Byun, I.C. Kim, J.W. Seo, Pervaporation behavior of asymmetric sulfonated polysulfones and sulfonated poly(ether sulfone) membranes, J. Appl. Polym. Sci. 76 (2000) 787–798.

[25] B. Baradie, C. Poinsignon, J.. Sanchez, Y. Piffard, G. Vitter, N. Bestaoui, D. Foscallo, A. Denoyelle, D. Delabouglise, M. Vaujany, Thermostable ionomeric filled membrane for H2/O2 fuel cell, J. Power Sources. 74 (1998) 8–16.

[26] L. Yang, H. Fang, Y. Yi-Jun, Estimation of hansen parameters of PES, PSF and their sulfonated products with various degrees of sulfonation by group contribution method, Journal of Functional Polymers. 14 (2001) 214-220.

[27] C.M. Hansen, (2013). Hansen Solubility Parameters A User's Handbook. Boca Raton, FL. CRC Press, Inc.

[28] M. Mulder, (1996). Basic principles of membrane technology. Dordrecht, The Netherlands, Kluwer Academic Publishers.

[29] A. Zlotorowicz, R. V Strand, O.S. Burheim, S. Kjelstrup, The permselectivity and water transference number of ion exchange membranes in reverse electrodialysis, J. Memb. Sci. 523 (2017) 402–408.

[30] H.L. Yeager, B. O'Dell, Z. Twardowski, Transport Properties of Nafion Membranes in Concentrated Solution Environments, J. Electrochem. Soc. 129 (1982) 85–89.

[31] F.A. Siddiqi, S. Pratap, Studies of membrane phenomena-II Determination of membrnae potentials and evaluation of the membrane fixed charge density and permselectivity of parchment-supported silver iodide membrane, J. Electroanal. Chem. 23 (1969) 147–156.

[32] A.H. Galama, N.A. Hoog, D.R. Yntema, Method for determining ion exchange membrane resistance for electrodialysis systems, Desalination. 380 (2016) 1–11.

[33] A.H. Galama, D.A. Vermaas, J. Veerman, M. Saakes, H.H.M. Rijnaarts, J.W. Post, K. Nijmeijer, Membrane resistance: The effect of salinity gradients over a cation exchange membrane, J. Memb. Sci. 467 (2014) 279–291.

[34] E.Y. Safronova, D.V. Golubenko, N.V. Shevlyakova, M.G. D'yakova, V.A. Tverskoi, L. Dammak, D. Grande, A.B. Yaroslavtsev, New cation-exchange membranes based on cross-linked sulfonated polystyrene and polyethylene for power generation systems, J. Memb. Sci. 515 (2016) 196–203.

[35] J.W. Post, C.H. Goeting, J. Valk, S. Goinga, J. Veerman, H.V.M. Hamelers, P.J.F.M. Hack, Towards implementation of reverse electrodialysis for power generation from salinity gradients, Desalin. Water Treat. 16 (2010) 182–193.

CHAPTER 5:

IMMERSION PRECIPITATION CATION EXCHANGE MEMBRANE PREPARATION BY SULFONATED POLYETHERSULFONE FOR REVERSE ELECTRODIALYSIS

Abstract

Reverse Elecrodialysis (RED) is a promising sustainable membrane based technology that can harvest mixing energy of solutions. However, commercially available membranes cannot meet the needs of this process. In this work, to overcome the membrane related problems in RED, sulfonated polyethersulfone membranes were produced by solvent evaporation and wet phase inversion methods. Effect of co-solvent, evaporation time, coagulation bath composition and concentration were investigated to optimize the membrane electrochemical properties. Optimized membrane was further characterized for different feed solutions. In addition, it was compared with CMX by Neosepta and custom-made membrane prepared by solvent evaporation. Based on the electrochemical properties, theoretical maximum power density of the three membrane were estimated.

1. Introduction

Salinity gradient power (SGP) has regained its attention in last decade after introduced in 1954 by Pattle et al. for the first time [1]. Having theoretical potential energy between 0.23- 3.13 TW, SGP is a promising alternative renewable energy towards the targets on lowering greenhouse gases emission [2]. River mouths, where two solutions with different salinity meet, are considered the largest SGP sources. However, salt domes, salt lakes, brines of natural and oil gas fields, brines of desalination units (e.g., reverse osmosis and membrane distillation) are more energy intensive SGP effluents [3,4].

Among several approaches, pressure retarded osmosis (PRO) and reverse electrodialysis (RED) are promising membrane based technologies can extract the SGP [5,6]. Having a direct generation of electricity from salinity gradients makes RED application noticeable [7]. As it is illustrated in Fig. 1, a typical RED unit consist of alternatively arranged anion exchange membranes (AEM) and cation exchange membranes (CEM) which are separated by spacers to create water channels. By pumping saline solutions between channels, required electrochemical potential gradient can be created to drive the ions from high to low concentration. Due to charged nature of membranes, ions can only diffuse through the oppositely charged membranes (i.e., positive ions can diffuse through CEM which contains negative fixed moieties in their backbone). By utilizing electrodes at the both end of the RED stack, ionic flux in the membranes can be converted to electronic flux by the help of redox reaction [8].

Ion exchange membranes (IEM) are one of the performance determining elements in RED. IEMs utilized in other electromembrane process are designed to satisfy the requirements of the particular application. For example, permselectivity is essential for purification applications, i.e. electrodialysis, whilst chemical and thermal stability of membranes are more important for the

chlor-alkali production [9]. On the other hand, most of the membranes investigated for RED were commercial electrodialysis membranes (ED) due to similarity of two process [10,11]. Although there are similarities, needs of the RED differ from needs of the ED. In order to maintain permselectivity in ED membranes, membranes have high charge density and mostly reinforced with another more stable material. Even though reinforced material helps sustaining dimensional stability, it causes relatively thicker membranes. Moreover, ED membranes are designed for severe conditions such as high current density and extreme pH conditions. However, RED conditions are rather mild [12]. Process solutions are close to neutral pH and mechanical pressure is only applied to overcome pressure loss across the inlet and outlet of compartments.

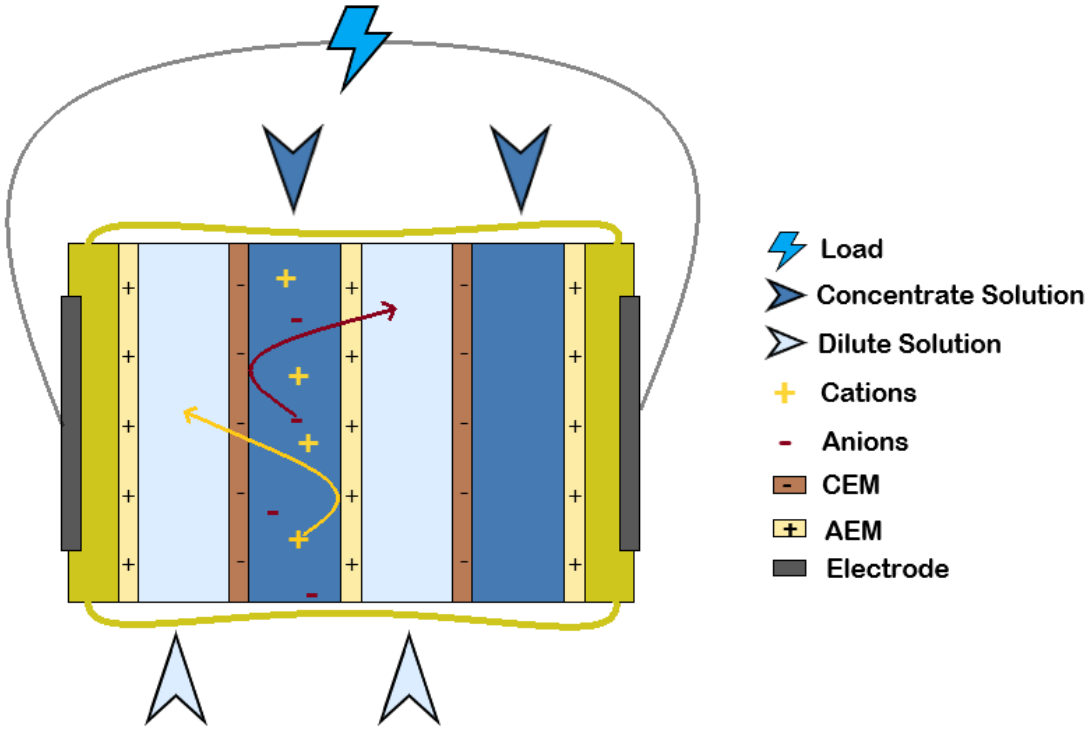

Figure 2. Schematic of RED Unit

The biggest problem in front of commercialization of the RED application is the absence of IEMs designed for needs of RED. A feasible RED membrane must have an optimized permselectivity, resistance, mechanical stability, chemical stability and price. Post et al. (2009) studied the

requirements of a RED membrane for river and seawater solution pair. For a cost effective operation, a membrane must have permselectivity must be higher than 95%, resistance less than 3 $\Omega \cdot cm^2$, mechanical stability sufficient to construct the stack, lifetime at least 5 years and price maximum 2 € $/m^2$ [13].

There are two types of membranes presents in the market. Heterogeneous membranes have high selectivity, mechanical stability and low price whereas have high resistance (>10 $\Omega \cdot cm^2$). On the other hand, homogeneous membranes have high mechanical and electrochemical properties but they are not cost efficient for RED (>100 € $/m^2$ membrane) [14]. Among these limiting parameters against commercialization, price of the membrane is the most challenging one for the near future [12–15].

Several studies have been made to prepare IEMs for RED. One of the notable work conducted by Guler et al. (2013) investigated the tailor-made IEMs prepared by using sulfonated polyetheretherketone (SPEEK) and polyepichlorohydrin (PECH). After electrochemical characterization of custom-made membranes with different thickness and commercial membranes (i.e. CMX and AMX) were completed, membranes were tested in artificial seawater and river water conditions in a lab scale RED stack. Superior amount of experimental power density, 1.28 W/m^2, was obtained when stack utilized with SPEEK/PECH membrane couple where the max power density obtained with commercial membrane was 1.19 $W \cdot m^{-2}$ for FKD/FAD membranes [16]. In another work, Hong et al. (2014), novel composite membranes were prepared by embedding Fe_2SO_4-SO_4^{2-} charged inorganic particles into PPO as organic polymer matrix. Membranes properties were characterized for different loading ratio and finally they are tested in the RED stack. The best gross power density was obtained as 1.30 $W \cdot m^{-2}$ for 0.7 wt% loading [17]. Recently, Kim et al. (2015) lab-made AEM and CEM were prepared by pore filling method.

Physicochemical and electrochemical characterization of the membranes revealed the membranes had comparable permselectivity and mechanical stability, whereas at least 4 times less areal resistance were obtained compared to commercial membranes used it the study (e.g. FKS and FAS from FumaTech GmbH, Germany, CMX and AMX from Takuyama Com, Japan, CMV and AMV from Asahi Glass Co. Ltd, Japan). Moreover, 2.5 $W \cdot m^{-2}$ gross power density was reported for lab-made IEMs. This value was 25% higher than best performing commercial membrane pair (AMX/CMX) tested in RED stack [18].

As it is discussed previously, several studies designed lab-made RED membrane by using solvent evaporation and pore filling methods [16–18]. Immersion precipitation is a well-established method that most commercial membrane are produced [19]. From dense membranes to membranes with 90 % porosity can be produced by using immersion precipitation. In this study, sulfonated polyethersulfone (SPES) CEM membranes were prepared by using immersion precipitation method. Effect of evaporation step, composition of coagulation bath, composition of the polymer solution on electrochemical properties were discussed. Based on characterization results, best performing membrane was further characterized for different solution and theoretical power density was calculated.

2. Experimental

2.1. Materials

Sulfonated polyethersulfone (SPES) with 1.19 $meq \cdot g^{-1}$ ion exchange capacity (IEC) and 119000 $g \cdot mol^{-1}$ molecular weight was provided by Konishi Chemical Ind. Co. Ltd. Polyethersulfone (PES) was purchased from BASF, Germany. Neosepta CMX cation exchange membranes were purchased from Astom Corp. Ltd., Japan.

1-Methyl-2-pyrrolidinone (NMP, 99%) and acetone (99%) were supplied from Acros, The Netherlands. Technical isopropanol were purchased from Boom lab, The Netherlands.

NaCl was purchased from AkzoNobel, The Netherlands and anhydrous Na_2SO_4 were purchased from Merck.

2.2. Membrane Preparation

Two phase inversion method were used to prepare CEMs; solvent evaporation and immersion precipitation.

For solvent evaporation method, NMP based solutions prepared with 20 wt% polymer concentration. SPES was blended with PES to have a range of IEC from 0.60 to 1.19 meq/g with 0.12 meq·g^{-1} incremental. Polymer solutions were cast on a glass plate by a casting bar which has 500 µm opening. After casting, films were dried under inert N_2 atmosphere at 70 ^{o}C for 2 days. At the end of 2 days, membrane were able to peel off easily in demi-water. Samples were kept in demi water until further usage.

For membranes prepared by immersion precipitation, IEC capacity of the polymer blend was arranged to 1.07 meq·g^{-1} which corresponds 9/1 as SPES/PES ratio. The same polymer concentration of solvent evaporation method, 20 wt%, was used but this time acetone was added to dope solution as a co-solvent. I-propanol and NaCl solution were used as precipitation baths in sequence. Following phase inversion process parameters were studied and tabulated in Table 1:

- Co-solvent ratio
- Evaporation time (ET)
- Time in first immersion bath
- Concentration of second immersion bath

Table 1. The phase inversion conditions of membranes prepared by immersion precipitation

Membrane	NMP/Acetone ratio	Evaporation time (min)	Time in i-propanol	Concentration of second bath (M NaCl)
M1	90/10	-	10	2
M2	70/30	-	10	2
M3	90/10	5	10	2
M4	90/10	-	60	2
M5	90/10	-	10	5.4
M6	70/30	-	10	5.4
M7	90/10	5	10	5.4
M8	90/10	-	60	5.4

2.3. Membrane Characterization

2.3.1. Permselectivity

Two compartment cell (Fig. 2) was operated at 25 ^{o}C to determine the membrane potential. Before measurements, membranes were conditioned overnight in low concentrated test solution. Then, membrane was fitted in between compartments and 3 different combinations of 3 solution with different concentration, 0.1 M NaCl, 0.5 M NaCl and 1.0 M NaCl in this case, were recirculated through the compartments at a flow rate 900 ml·min^{-1}. Potential difference over the electrodes was recorded until constant values were obtained. Finally, membrane permselectivity was calculated from the ratio between the measured membrane potential (V) to theoretical membrane potential (V) which represents 100% permselectivity.

$$\alpha(\%) = \frac{\Delta V_{measured}}{\Delta V_{theoretical}} 100\% \qquad (1)$$

$\Delta V_{theoretical}$ can be calculated by the Nernst equation:

$$\Delta V_{theoretical} = \frac{RT}{zF} \ln\left(\frac{C_2 \gamma_2}{C_1 \gamma_1}\right) \qquad (2)$$

In which R is the gas constant (J·mol^{-1}K^{-1}), T the temperature (K), z the electrochemical valence (-), F the Faraday constant (96485 s·A·mol^{-1}), C_1 and C_2 the concentrations of the two solutions

(mol·l^{-1}) and γ_1 and γ_2 the activity coefficients of the two solutions. Table 2 presents calculated theoretical membrane potentials for different solution pairs by using eq. 2.

Table 2. Activity coefficient and theoretical membrane potential of solution pairs [20].

Concentration (M NaCl)	Activity coefficient (-)	Test solution pair (M NaCl/M NaCl)	Theoretical ΔP (mV)
0.1	0.778	**0.1/0.5**	37.9
0.5	0.681	**0.1/1.0**	54.8
1.0	0.657	**0.5/1.0**	16.9

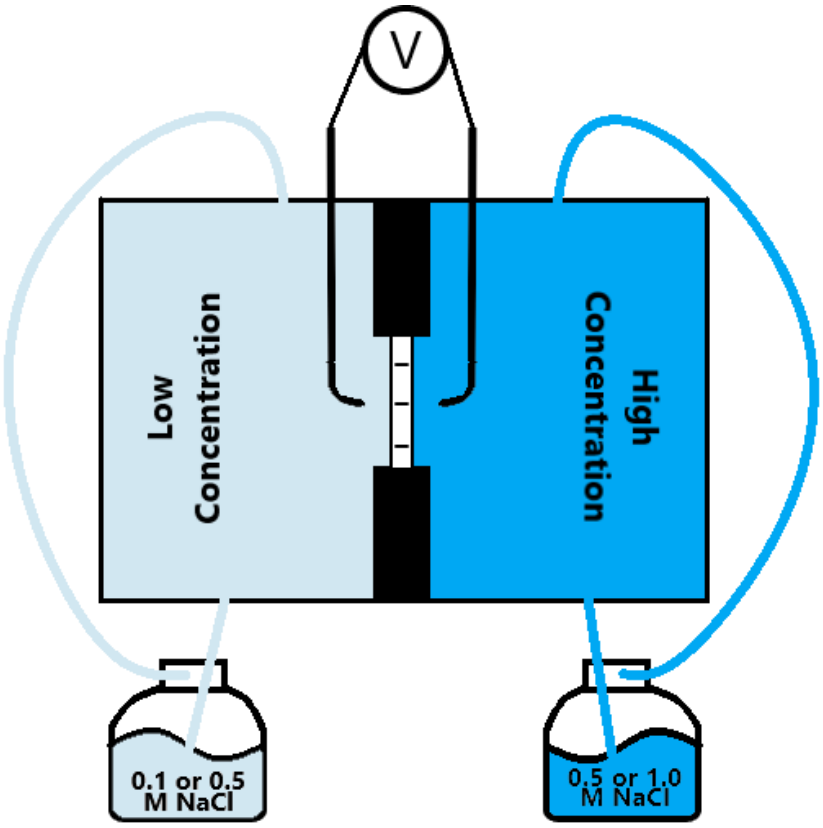

Figure 2. Two compartment permselectivity characterization setup

2.3.2. Resistance

Ionic resistance of sPES membranes were characterized in various NaCl solutions by using six compartment cell as it was described elsewhere[10]. Fig. 3 illustrates resistance measurement setup supported with 2 calomel electrodes in the compartment 3, 4 and two working electrodes in

the compartment 1, 6. Prior to measurement, membranes were conditioned overnight in the test solution which has lower concentration. Three feed (electrolyte, shielding and test) solution were warmed up to 25 ^{o}C. Membrane under investigation was fitted between compartment 3 and 4 while four CMX membranes were utilized to separate other compartments. CMX membranes which has 99% permselectivity for 0.1/0.5 M NaCl solution were preferred to reduce possible co-ion leakage from neighboring compartments. 1.0 M Na_2SO_4 electrolyte solution was fed into compartment 1 and 6 to avoid dangerous chemical production, i.e. Cl_2 in use of NaCl, on the electrode surface. In compartment 2 and 5, fed shielding solution was at same concentration of electrolyte solution due to inconsistent results obtained at low concentration (i.e. 0.1 M NaCl solution) in use of 0.1 M test solution in compartment 3 and 4.

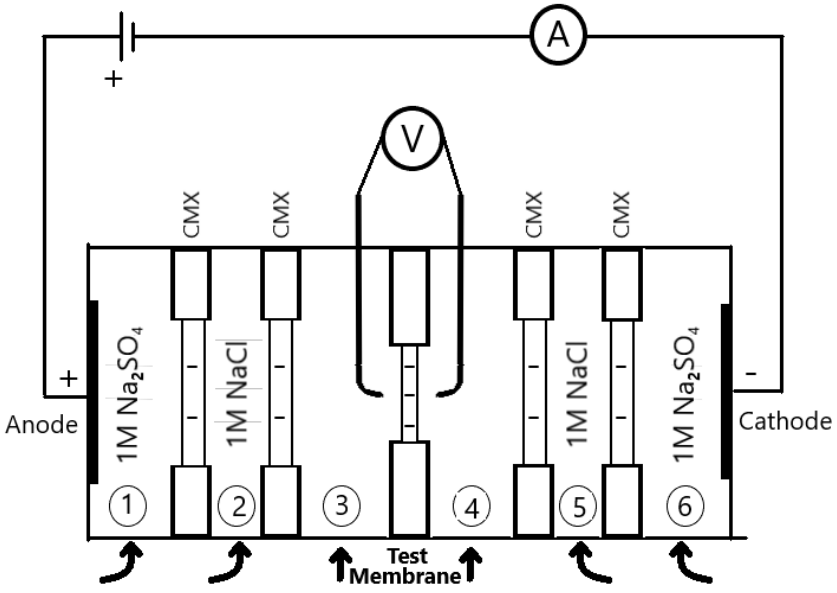

Figure 3. 6-compartment resistance characterization cell

In the first part of the experiments compartment 3 and 4 was fed with the same concentration: 0.1, 0.5, 1.0 M NaCl. This mode will be called as non-gradient resistance characterization later on. In the second mode concentration gradient has been created around the membrane by using different feed solutions in compartment 3 and 4. Gradient resistance characterization feed solution were

0.1/0.5, 0.1/1.0 and 0.5/1.0 M NaCl. Following this, test membranes were flipped to see if membrane orientation has an effect on resistance. Masterflex peristaltic pump with CT numbers 19347 were operated to feed the solutions at 270 $ml \cdot min^{-1}$ flowrate.

Membrane resistance characterization were carried out for DC and AC current mode.

Resistance in DC mode

DC current ranged 0-15 mA applied through working electrodes and corresponding potential difference on calomel reference electrodes were recorded. DC resistance (R_{DC}) was calculated from slope of current vs potential difference plot. This resistance comprises membrane resistance (R_m), boundary layer resistance (R_{bl}) and solution resistance (R_s). To eliminate solution resistance, a blank DC measurement was repeated at the same conditions of investigated membrane. R_{m+dl} was then calculated by subtracting R_s from R_{DC}.

Resistance in AC mode

An advantage of using alternating current mode is to distinguish membrane resistance and boundary layer resistance. Following DC measurement, membrane resistance was characterized at same conditions in AC current ranged from 10^5 to 1 Hz. At high frequencies effect of boundary layer diminishes significantly. Thus, measured AC resistance (R_{AC}) represents R_{m+s}. A blank AC measurement at the same condition of tested membrane allows to obtain R_m by subtracting Rs from R_{AC}.

2.3.3. Morphology

Cross section of membranes were imaged by scanning electron microscopy (JSM-6010LA). Top layer cross section image at 4000 magnification were captured for wet phase inversion membranes.

3. Results and Discussion

3.1. Membranes by solvent evaporation

Solvent evaporation is one of the simplest technique to prepare dense membranes on a suitable support e.g. metal, glass, porous or non-porous support [19]. Most of the commercial cation exchange membranes are produced as dense homogeneous membranes by functionalized polymeric materials. These membranes have permselectivity higher than 90%, areal resistance between 1-5 $\Omega \cdot cm^2$, IEC between 1.1-2.5 $meq \cdot g^{-1}$, swelling degree up to 30% and thickness between 30-200 µm [9,10,21]. All these parameters are interrelated to each other. For example high IEC capacity means high permselectivity and low resistance up to some content. Beyond this content, increasing IEC leads high swelling which reduces the functional group per unit and creates larger channels so permselectivity and resistance decrease.

In this study, membranes were prepared by solvent evaporation for different IEC. IEC of the polymers were arranged by blending SPES and PES. SPES/PES blend ratio was gradually varied from 100/0 to 50/50 so various IEC from 1.19 to 0.60, respectively. Final membranes resulted in yellowish transparent color with 50-75 µm wet thickness. Permselectivity and areal resistance characterization of the membranes were illustrated in Fig. 4. Membrane permselectivity were tested in 0.1/0.5 M NaCl solution at 25 ^oC and areal resistance was measured in 0.5/0.5 M NaCl solution as a common method in literature. Resistance measurements were corrected for the membrane thickness to have a better trend independent to thickness. From the permselectivity vs. IEC data in Fig. 4, it is apparent permselectivity remained constant around 95% for the given IEC range. Cassady et al. (2016) investigated permselectivity of SPES membranes for different IEC. In that work, decreasing permselectivity was measured for increasing IEC caused by increasing water uptake of polymer [22]. One explanation to the contradictory trends is the difference in IEC

of the polymers. Related to swelling, water channels get enlarge in the membrane and membrane lose its efficient exclusion properties against negative ions. Probably in the range 0.60-1.19 meq/g, due to low swelling degree, permselectivity of the membranes remained constant.

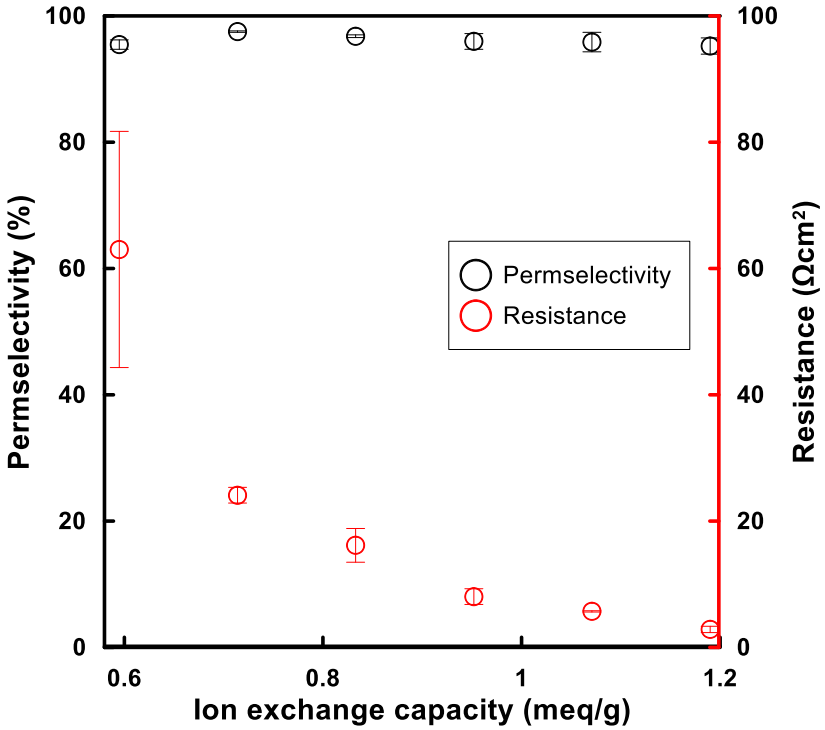

Figure 4. IEC vs. permselectivity and IEC vs resistance.

On the other side, areal resistance of the CEMs exponentially increased with the decreasing IEC. Membranes prepared with 1.19, 1.07 and 0.95 meq·g^{-1} IEC were resulted in a good conductive membranes comparable to commercial CEMs. When a polymer had less IEC than 0.95 meq·g^{-1}, resistance of the membranes were significantly higher.

3.2. Membranes by immersion precipitation

The main purpose of this study was to investigate the potential of the wet phase inversion membranes, however numerous parameters have effect on final membrane properties (i.e. polymer selection). Because the ultimate application of designed membrane is RED, permselectivity, resistance and observable mechanical properties of dense membranes were considered for the

selection of the SPES/PES ratio for immersion precipitation method. Even though dense membrane with 1.19 meq·g^{-1} resulted in with superior electrochemical performance, membranes prepared with this IEC were mechanically weak. Therefore, SPES/PES ratio has been decided as 90/10 which corresponds to 1.07 meq·g^{-1} IEC. Methodology of the wet phase inversion membranes produced with this ratio is described in Table 1. Effect of co-solvent ratio, evaporation time, time in first coagulation bath, concentration of second coagulation bath on electrochemical properties were observed.

It is possible to distinguish the membranes into two categories considering measured electrochemical properties (Fig. 5). This categorization also coincides with concentration of the second bath. When Fig. 5 analyzed carefully, it is clearly visible M1-M4 and M5-M8 fit to different trends. It is also worth to note that dense membrane stands on the same line with the membranes immersed into 5.4 M NaCl as second bath. During the preliminary experiments, also demineralized water was tested as the second bath in which peeling off the membrane from glass surface was not possible. This indicates demineralized water was not a good non-solvent. However, after addition of NaCl in the second coagulation bath, membranes easily peeled off from the glass surface. This was probably due to enhanced interaction between present charges in the membrane and the bath. Moreover, the white color of the membranes turned to half transparent after immersion into the second bath. The change in the color from white to transparent can indicate morphology change from porous to dense.

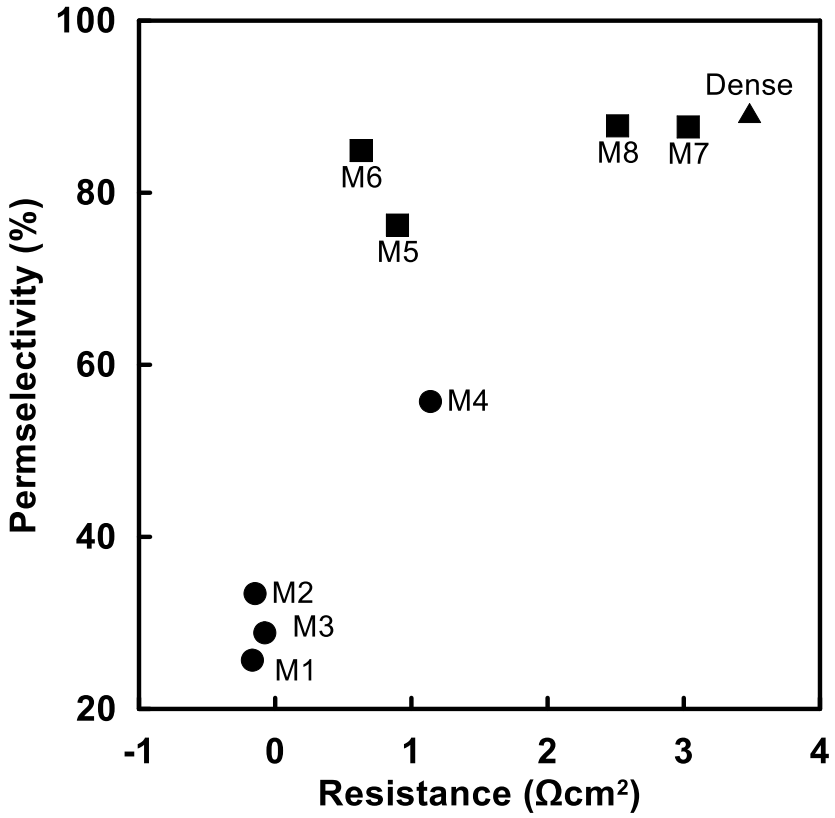

Figure 5. Electrochemical properties of wet phase inversion membranes and dense membrane prepared with the polymer has 1.07 meq/g IEC.

The densification of the membranes can also be followed from the wet thickness of the membranes (Table 3). Wet thickness of M1-M4 membranes were significantly higher than the M5-M8 membranes. High ion concentration in the coagulation bath has a shielding effect on the fixed charges of the membranes. When coagulation bath is ion-free, electrostatic interactions between the fixed groups force to have a stretched polymer orientation. On the other hand, ions in the coagulation bath screen the fixed charges of the polymer. Consequently, repulsive interaction decreases and polymer chains get rearranged from soluble state to insoluble state [23–25]. A visual indication to denser membranes in 5.4 M NaCl solution is the cross section of the membranes. SEM images (Fig. 6) clearly show porosity gets lower or diminishes when saturated NaCl solution used as coagulation bath.

Table 3. Thickness of membranes prepared and characterized in this study

Membrane	Wet thickness (μm)	Membrane	Wet thickness (μm)	Membrane	Wet thickness
M1	101±1	**M6**	49±0	***D3**	69±5
M2	86±2	**M7**	58±1	***D4**	64±3
M3	93±1	**M8**	56±2	***D5**	64±3
M4	90±1	***D1**	63±6	***D6**	71±1
M5	57±1	***D2**	74±13	**CMX** [10]	140-200

*"D" stands for Dense membranes in Fig. 4 and IEC decreases with ascending numbers

Although the effect of co-solvent ratio was not as significant as the effect of second bath concentration, membranes permselectivity improved slightly while areal resistance remained constant. From Fig. 5, it can be concluded M2 and M6 respond similarly to solvent/co-solvent ratio change from 90/10 to 70/30. Solvents like acetone and THF are well known co-solvents that delay the demixing and give denser membrane morphology [19]. Likewise, membrane wet thickness (Table 3) and cross section images (Fig. 6) reveal membranes from M1 to M2 and M5 to M6 are getting denser.

It is possible to have dense top layer when ET applied in use of a volatile co-solvent (i.e. acetone). In this study, enhancing permselectivity was aimed by applying adding 5 min ET step before immersion into IPA bath. Two different behavior was observed for electrochemical properties of M3 and M7. Fig. 5 shows that there has been an increase in both permselectivity and resistance of M7 where electrochemical properties of M3 were similar to M1. It is hard to explain this trends by analyzing SEM images and thickness as well. Wet thickness of the membranes indicates a slightly denser M3 and same thickness of M7. In the same way, cross section of the membranes overlaps with thickness results. A possible explanation for this might be that for M7, a really thin dense layer was formed but at 5000 magnification it was not possible to distinguish.

Wet phase inversion membranes can get their last form less than seconds by instantaneous demixing or it can endure minutes depending on thermodynamic and kinetic properties such as miscibility of solvent and non-solvent. To understand if our solvent/polymer/non-solvent system membranes gets their ultimate structure in the first coagulation bath, membranes were exposed to the IPA bath 10 min and 60 min. Fig. 5 illustrates clearly, both M4 and M8 have completely different electrochemical properties from M1 and M5, respectively. While permselectivity of both membrane enhanced, conductivities were decreased. SEM images (Fig. 6) show membrane macro porous has increased whereas wet thickness (Table 3) was slightly less or similar. It can be indicated dense part of the membrane have shrunk in to smaller volume. Therefore, eventually more compact dense layer was obtained.

Overall, these results based on investigated parameters indicate that concentration of second bath and time in first bath had the biggest impact on membrane electrochemical properties.

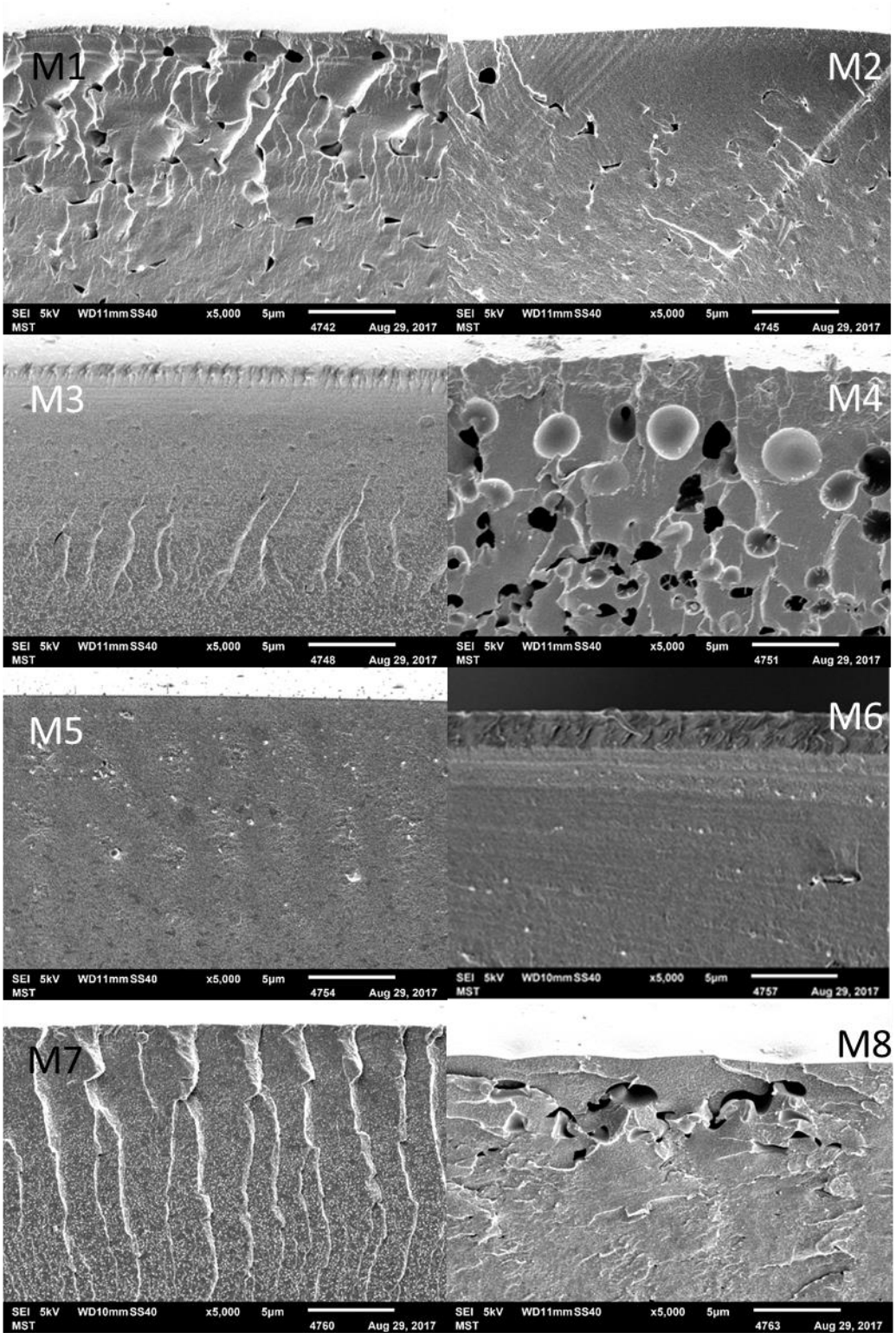

Figure 6. Top layer cross section of wet phase inversion membranes

3.3. RED performance of selected membranes

Regarding the electrochemical properties of the wet phase inversion membranes, M6 was selected to continue further characterization to estimate RED performance in different concentrations. Additionally, D2 (dense membrane prepared with same IEC of M6) and CMX (a commercial benchmark membrane) were tested to have a comparable study.

3.3.1. Permselectivity

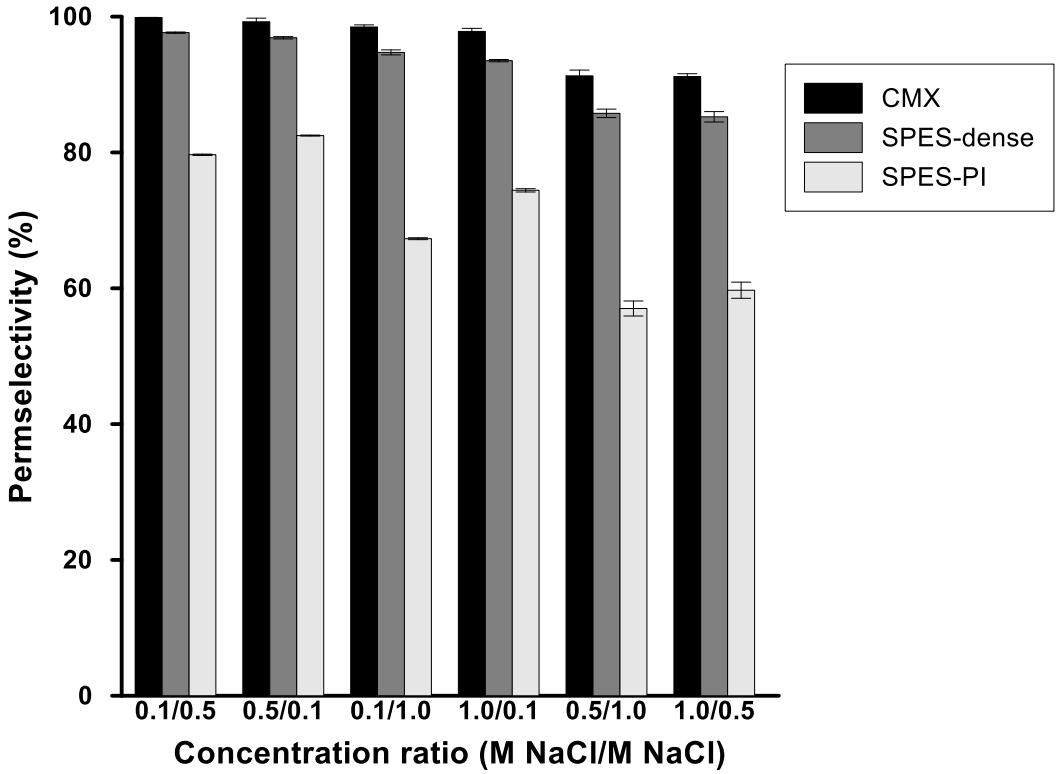

Figure 7. Permselectivity of CMX, D2 and M6

0.1/0.5 M NaCl solution pair can be accepted as standard in the permselectivity measurement of IEMs. However, previous studies showed that permselectivity of a membrane strongly related to concentration of test solutions. Membranes tested in diluted environment resulted in with a permselectivity close to ideal [26]. Therefore, in addition to standard test solutions, CEMs were tested in 0.1/1.0 and 0.5/1.0 M NaCl solution pairs.

Fig. 7 compares the permselectivity data of CMX, D2 and M6. For all concentrations, CMX resulted in superior where M6 had the lowest selectivity. Due to dense nature of CMX and D2, permselectivity loss were limited when higher NaCl content was tested (i.e. 0.5/1.0 M NaCl). Characterizations were repeated by reversing direction of the concentration gradient. Probably due to asymmetric structure of the M6 membranes, there was a notable difference on permselectivity, while dense membranes, CMX and D2, had the same permselectivity.

3.3.2. Non-gradient resistance

The areal resistance of membranes were characterized in 0.1, 0.5 and 1.0 M NaCl solutions. When membranes were in 0.1 M NaCl, non-ohmic resistance of the membranes were dominant. By increasing concentration, non-ohmic resistance diminished and ohmic resistance of the membranes became dominant. For the membranes with denser structure, CMX and D2, over a concentration of 0.1 M NaCl, membranes ohmic resistance were independent from concentration. However, resistance at 0.1 M NaCl resulted in with a higher ohmic resistance. This results are in line with the literature data. Dlugolecki et al. (2010) reported 0.1 M as a critic concentration where membrane resistance become concentration dependent [27]. Similarly, Galama et al. (2014) concluded 0.3 M of external ionic solution concentration is the lower limit where membrane resistance is independent of solution around [28]. On the other hand, in contrast to CMX and D2, resistance of M6 was dependent on concentration of ionic solution, even for greater values than 0.5 M NaCl. The difference can be explained by structural difference of the membranes. Because CMX and D2 membranes has well packed polymeric structure compared to M6, ionic solution occupy larger volume in M6 membranes. Therefore, more notable amount of contribution by ionic solution is expected.

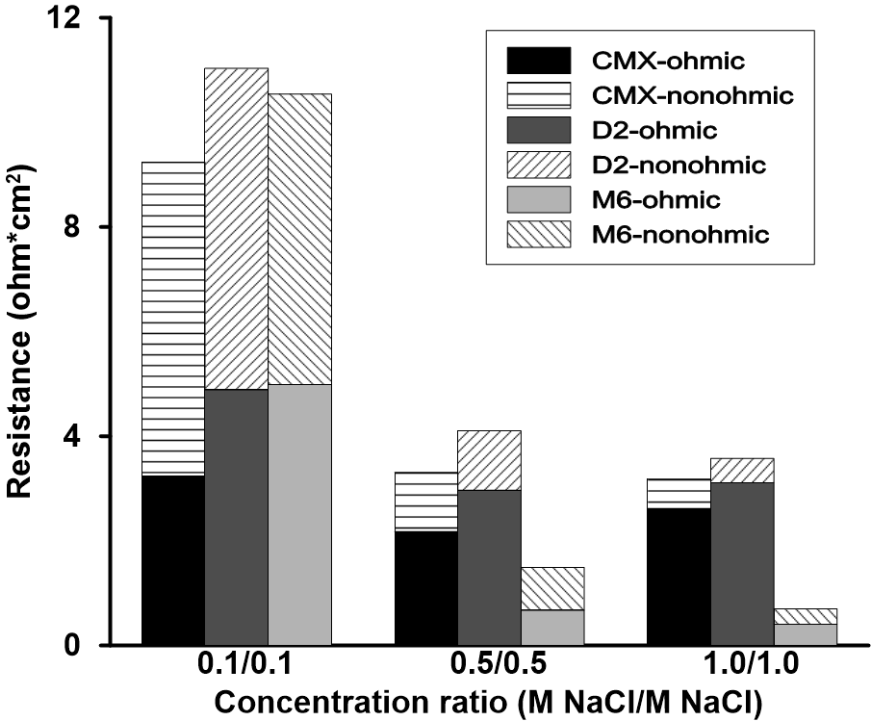

Figure 8. Resistance of CMX, D2 and M6 under non-gradient conditions

3.3.3. Gradient resistance

Due to simplicity of the method, areal resistance of membranes are characterized in 0.5/0.5 M NaCl in most of the previous study. However, IEMs expose to different ionic solutions in the real applications. Solutions can be diluted or concentrated, can contain other ions or organic compounds. Therefore in this part of the study, membrane ohmic and non-ohmic resistance were measured in case of different concentrations were fed left and right face of the membrane. Characterization were completed for all combinations of 0.1 M NaCl, 0.5 M NaCl and 1.0 M NaCl solutions.Having gradient during resistance measurement, helps to better representation of RED solutions which are never at the same concentrations.

Fig. 9 compares the areal resistance of membranes by giving details about ohmic and non-ohmic contribution. Membranes in 0.5/1.0 M NaCl solution were more conductive while 0.1/0.5 and 0.1/1.0 M NaCl solution pair resulted without a significant difference due to fact that resistance of

the membranes are decided by the lowest external ionic concentration [28]. In particular, M6 membranes had the superior conductivity except in case of 0.1/0.5 M NaCl where D2 had the highest total resistance. It is worth to say that, in gradient resistance characterization ohmic resitance were dominant over non-ohmic resistance. Moreover, the resistance difference caused by membrane orientation was probably due to large experimental error.

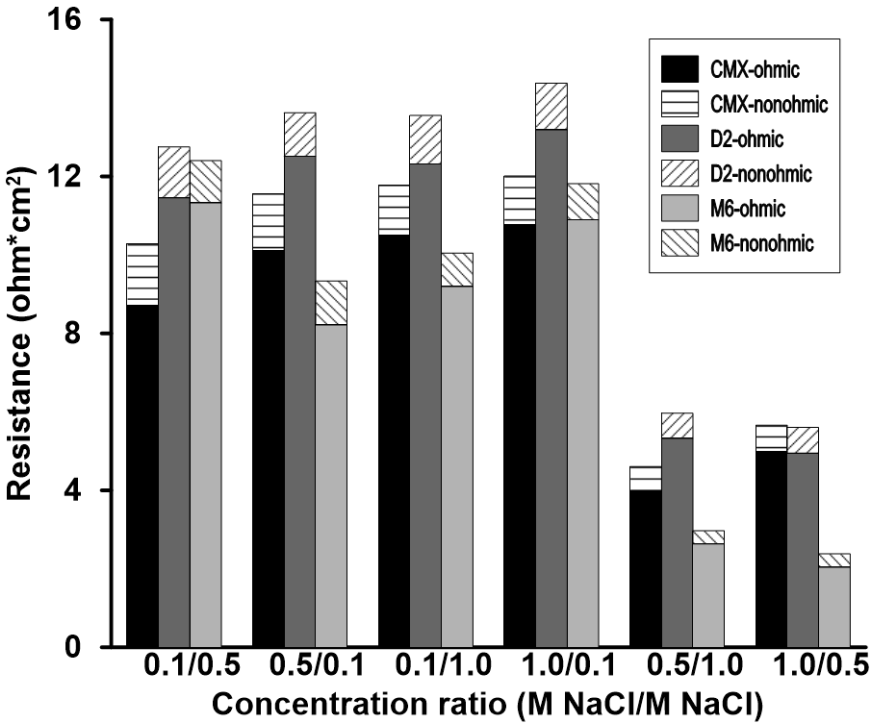

Figure 9. Resistance of CMX, D2 and M6 membranes under gradient conditions

3.3.4. Theoretical power density calculation

Having membrane resistance and permselectivity allows to calculate theoretical power density (P_d).

$$P_{\max} = \frac{\left[\alpha \frac{RT}{F} \ln\left(a_c / a_d\right)\right]^2}{2\left(R_{CEM} + d/k_c + d/k_d\right)} \quad (3)$$

where α is permselectivity (-), α_c ionic activity of concentrated solution (-), α_d ionic activity of diluted solution (-), R_{CEM} is ionic resistance of CEM ($\Omega \cdot m^2$), d is the thickness (m), k_c is the

conductivity of concentrated solution ($\Omega \cdot m^2$), k_d is the conductivity of diluted solution ($\Omega \cdot m$), F is Faraday constant(96500 $s \cdot A \cdot mol^{-1}$), T is temperature (298 K) and R is universal gas constant (8.314 $J \cdot mol^{-1}K^{-1}$). Theoretical calculation was made for a half-cell. Half-cell includes half of the diluted compartment (100 µm), half of the concentrated compartment (100 µm) and CEM.

Fig. 10 shows maximum P_d generated theoretically from the electrochemical characterization data. Out of two membrane orientation, only the superior one is reported. As it is expected, higher P_d was calculated for higher concentration ratio due to large driving force. For each solution pair, descending P_d value was CMX>D2>M6. Although M6 membranes had better conductivity, because of its low permselectivity, generated power density lower than D2 and CMX. The highest P_d value was obtained for custom made membrane was 0.82 $W \cdot m^{-2}$ for 0.1/1.0 M NaCl solutions were fed at 25 ^oC.

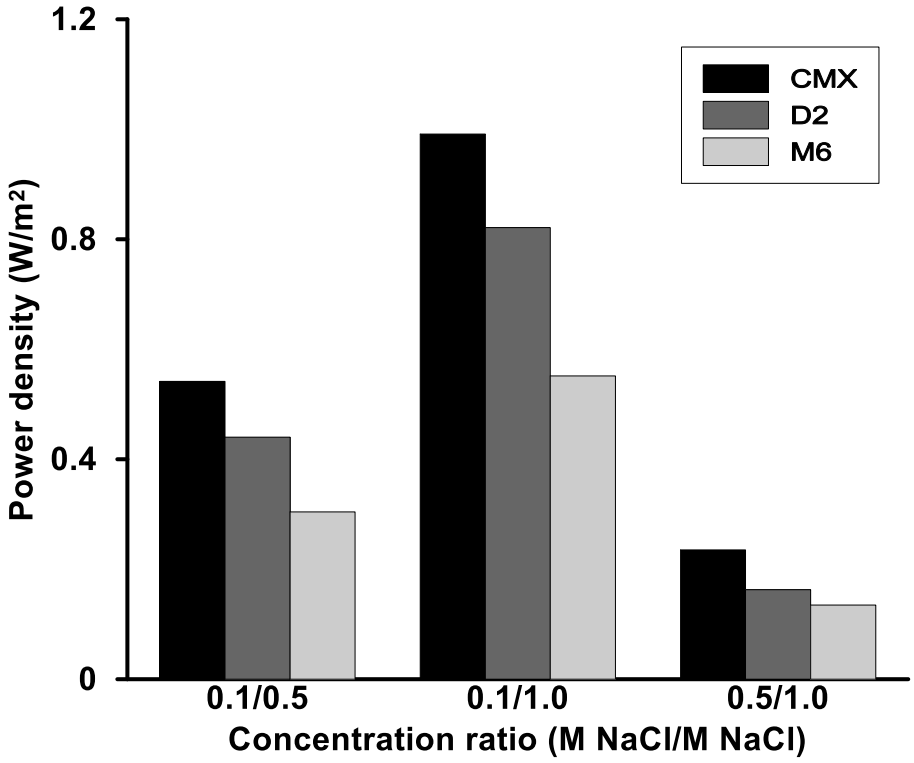

Figure 10. Theoretical power density of CMX, D2 and M6

4. Conclusion and outlook

In this study, SPES/PES with 1.07 meq·g^{-1} IEC capacity were used to prepare membranes by solvent evaporation and wet phase inversion methods. To our knowledge, for the first time SPES custom made membranes were prepared and characterized for RED potential.

Effect of various phase inversion parameters were investigated. Based on electrochemical characterization, cross section images and membrane thicknesses, a detailed discussion was conducted on impact of the membrane properties. Regarding the RED requirements, best performed membrane, M6, were further characterized to predict theoretical maximum power density. 0.82 and 0.55 W·m^{-2} power density obtained as maximum for D2 and M6, respectively, when 0.1 and 1.0 M solutions were fed.

Besides having novel custom-made RED membranes, membrane material and technique used in this study can be an answer to problems against RED commercialization. The price of the IEMs seems the most challenging limitation towards the commercialization. SPES membranes was functionalized from PES which is well known and cheap hydrocarbon polymer. In addition to that, wet phase inversion is well established technique and produced membranes less packed compared to dense membranes. Therefore, a cheap production line can be created by using less raw material. This study is promising to decrease membrane price to the targeted value which is less than 5 €/m^2.

5. References

[1] R.E. Pattle, Production of electric power by mixing fresh and salt water in the hydroelectric pile, Nature. 174 (1954) 660–660.

[2] O.A. Alvarez-Silva, A.F. Osorio, C. Winter, Practical global salinity gradient energy potential, Renew. Sustain. Energy Rev. 60 (2016) 1387–1395.

[3] R.A. Tufa, E. Curcio, E. Brauns, W. van Baak, E. Fontananova, G. Di Profio, Membrane distillation and reverse electrodialysis for near-zero liquid discharge and low energy seawater desalination, J. Memb. Sci. 496 (2015) 325–333.

[4] R.E. Lacey, Energy by reverse electrodialysis, Ocean Eng. 7 (1980) 1–47.

[5] J.W. Post, H.V.M. Hamelers, C.J.N. Buisman, Energy Recovery from Controlled Mixing Salt and Fresh Water with a Reverse Electrodialysis System, Environ. Sci. Technol. 42 (2008) 5785–5790.

[6] S. Chou, R. Wang, L. Shi, Q. She, C. Tang, A.G. Fane, Thin-film composite hollow fiber membranes for pressure retarded osmosis (PRO) process with high power density, J. Memb. Sci. 389 (2012) 25–33.

[7] B.E. Logan, M. Elimelech, Membrane-based processes for sustainable power generation using water., Nature. 488 (2012) 313–319.

[8] R.A. Tufa, E. Curcio, W. van Baak, J. Veerman, S. Grasman, E. Fontananova, G. Di Profio, Potential of brackish water and brine for energy generation by salinity gradient power-reverse electrodialysis (SGP-RE), RSC Adv. 4 (2014) 42617–42623.

[9] R.K. Nagarale, G.S. Gohil, V.K. Shahi, Recent developments on ion-exchange membranes and electro-membrane processes, Adv. Colloid Interface Sci. 119 (2006) 97–130.

[10] P. Dlugolecki, K. Nymeijer, S. Metz, M. Wessling, Current status of ion exchange membranes for power generation from salinity gradients, J. Memb. Sci. 319 (2008) 214–222.

[11] J. Veerman, R.M. de Jong, M. Saakes, S.J. Metz, G.J. Harmsen, Reverse electrodialysis: Comparison of six commercial membrane pairs on the thermodynamic efficiency and power density, J. Memb. Sci. 343 (2009) 7–15.

[12] E. Guler, Y. Zhang, M. Saakes, K. Nijmeijer, Tailor-made anion-exchange membranes for salinity gradient power generation using reverse electrodialysis, ChemSusChem. 5 (2012) 2262–2270.

[13] J.W. Post, C.H. Goeting, J. Valk, S. Goinga, J. Veerman, H.V.M. Hamelers, P.J.F.M. Hack, Towards implementation of reverse electrodialysis for power generation from salinity gradients, Desalin. Water Treat. 16 (2010) 182–193.

[14] M. Turek, B. Bandura, Renewable energy by reverse electrodialysis, Desalination. 205 (2007) 67–74.

[15] A. Daniilidis, R. Herber, D.A. Vermaas, Upscale potential and financial feasibility of a

reverse electrodialysis power plant, Appl. Energy. 119 (2014) 257–265.

[16] E. Güler, R. Elizen, D.A. Vermaas, M. Saakes, K. Nijmeijer, Performance-determining membrane properties in reverse electrodialysis, J. Memb. Sci. 446 (2013) 266–276.

[17] J.G. Hong, Y. Chen, Nanocomposite reverse electrodialysis (RED) ion-exchange membranes for salinity gradient power generation, J. Memb. Sci. 460 (2014) 139–147.

[18] H.-K. Kim, M.-S. Lee, S.-Y. Lee, Y.-W. Choi, N.-J. Jeong, C.-S. Kim, High power density of reverse electrodialysis with pore-filling ion exchange membranes and a high open area spacer, J. Mater. Chem. A. 3 (2015) 16302–16306.

[19] M. Mulder, (1996). Basic principles of membrane technology. Dordrecht, The Netherlands, Kluwer Academic Publishers.

[20] W.M. Haynes, (2016) CRC Handbook of Chemistry and Physics (internet version 2016), 96th ed., Taylor and Francis Group.

[21] J.G. Hong, B. Zhang, S. Glabman, N. Uzal, X. Dou, H. Zhang, X. Wei, Y. Chen, Potential ion exchange membranes and system performance in reverse electrodialysis for power generation: A review, J. Memb. Sci. 486 (2015) 71–88.

[22] H.J. Cassady, E.C. Cimino, M. Kumar, M.A. Hickner, Specific ion effects on the permselectivity of sulfonated poly(ether sulfone) cation exchange membranes, J. Memb. Sci. 508 (2016) 146–152.

[23] L. Burlamacchi, M.F. Ottaviani, E.M. Ceresa, M. Visca, Stability of colloidal TiO2 in the presence of polyelectrolytes and divalent metal ions, Colloids Surface 7 (1983) 165-182.

[24] V.A. Izumrudov, M.Y. Gorshkova, I.F. Volkova, Controlled phase separations in solutions of soluble polyelectrolyte complex of DIVEMA (copolymer of divinyl ether and maleic anhydride), Eur. Polym. J. 41 (2005) 1251–1259.

[25] K.S. Khairou, W.M. Al-Gethami, R.M. Hassan, Kinetics and mechanism of sol-gel transformation between sodium alginate polyelectrolyte and some heavy divalent metal ions with formation of capillary structure polymembranes ionotropic gels, J. Memb. Sci. 209 (2002) 445–456.

[26] A. Zlotorowicz, R. V Strand, O.S. Burheim, S. Kjelstrup, The permselectivity and water transference number of ion exchange membranes in reverse electrodialysis, J. Memb. Sci. 523 (2017) 402–408.

[27] P. Długołęcki, B. Anet, S.J. Metz, K. Nijmeijer, M. Wessling, Transport limitations in ion exchange membranes at low salt concentrations, J. Memb. Sci. 346 (2010) 163–171.

[28] A.H. Galama, D.A. Vermaas, J. Veerman, M. Saakes, H.H.M. Rijnaarts, J.W. Post, K. Nijmeijer, Membrane resistance: The effect of salinity gradients over a cation exchange membrane, J. Memb. Sci. 467 (2014) 279–291.

CHAPTER 6:

CONCLUSION AND OUTLOOK

1. General Conclusion

This PhD dissertation investigates two major challenges against commercialization of salinity gradient power – reverse electrodialysis process. The first challenge is performance reduction of RED under real operating solutions such as river and seawater collected directly from the sources. The second challenge is absence of ion exchange membranes designed for the needs of RED.

The largest salinity gradient power source is where river meets with the sea. Although most RED studies considers river water as 1 g NaCl and seawater as 35 g NaCl in one liter solution, natural river and seawater are composed of more complex ionic compounds. Total multivalent ions (e.g. Mg^{2+}, Ca^{2+} and SO_4^{2-}) can be present more than 10%. It is known these ions have decreasing effect on Nernst potential and conductivity of the membranes[1,2]. Therefore, in chapter 2, effect of real sea and river water has been investigated. In addition to real solutions, artificial equivalent solutions were tested to have a comparable study. At 20 ^oC and 20 $l \cdot h^{-1}$, 0.29 $W \cdot m^{-2}$ power density was obtained for real solution which was the half of power density obtained by artificial solutions. In case of increased temperature or increased flow rate, difference was more prominent. For example, at 60 ^oC, real solutions yielded 0.46 $W \cdot m^{-2}$ whereas artificial solutions produced 1.41 $W \cdot m^{-2}$ (the highest power density recorded in this experimental work). To enlighten and to understand deeply, ionic characterization of river water and impedance characterization of ion exchange membranes were completed. Ionic characterization revealed major multivalent ions (SO_4^{2-} and Mg^{2+}) transported against the concentration gradient which cause a reduction on produced power. Having multivalent ions in the solution also affected ion exchange membranes which are key components of the process. In particular, resistance of Fuji-CEM-80050 was three-fold when it is tested in real seawater solution. A possible explanation is that Mg^{2+} and Ca^{2+} has higher affinity to the membrane fixed group than Na^+. The increase in resistance of CEMs takes

place due to crosslinking two fixed charge group and neutralizing these charged groups (anionic groups) by divalent cations.

Using brine/seawater solution can increase the generated power by reducing dominance of low compartment cell resistance. In a seawater desalination process, brine effluent is more concentrated but has same ion ratio (i.e. Na^{+}/Mg^{2+}) with the seawater. In chapter 3, effect of Mg^{2+} on open circuit voltage, membrane resistance, ion transport and power generation has been studied. 0.5 m/ 4.0 m solutions were mimicked by using different ratios of NaCl to $MgCl_2$. 1.06 $W \cdot m^{-2}$ maximum gross power density was produced when operating pure NaCl solution. Introduction of 10 % molal $MgCl_2$ resulted in 60% reduction of power density, 20 % decrease of open circuit voltage and 3 folded cation exchange membrane resistance. Moreover, an extra contribution to the decreasing trend caused by the uphill transport of the Mg^{2+} ions where the concentration was between 0 to 30 %.

Mg^{2+} is the second most abundant cation in the natural solutions. Divalent cations (i.e. Mg^{2+}) typically bind more strongly to sulfonate groups than monovalent ions. This higher affinity can create a reduction effect by screening the functional charged groups on membrane. Similarly, due to high affinity, counter-ion/fixed charged group condensation may weaken the Donnan exclusion capability of the membrane and increase the ohmic resistance[3].

In most of the reverse electrodialysis study, due to similarities to electrodialysis, commercial ED membranes were utilized in the RED stacks although RED requirements are different. Optimization of membrane mechanical and electrochemical properties can help step forward on commercialization of RED. Therefore, chapter 4 and 5 were dedicated to investigate wet phase inversion membrane production for cation exchange membrane preparation. In both study, polymer backbone has been chosen as well-known polymers as polysulfone and polyethersulfone.

To be able commercialize the reverse electrodialysis, membranes must be produced less than 5 euro/m^2. In chapter 4, cation exchange membranes were produced starting from bare polysulfone. Polymer was sulfonated with chlorosulfonic acid to be able to have a cation permselective material. Sulfonated polysulfone with 0.31 sulfonation degree has been chosen to prepare cation exchange membranes by using wet phase inversion method. The main purpose of choosing this method was to reduce the resistance of the membrane by creating a thin layer asymmetric membrane. To optimize the electrochemical properties, various phase inversion parameters was applied; solvent type, co-solvent ratio. Membrane prepared with NMP was shown superior electrochemical properties against membrane prepared with DMF. Cross section images indicated that using NMP as main solvent resulted in more open membrane structure. Best performing NMP membrane had 4 Ωcm^2 membrane resistance in 0.5 M NaCl and 85% permselectivity in 0.1/0.5 M NaCl. This electrochemical properties was comparable to performance of commercial ED membranes. Beside the electrochemical properties, membranes are promising by being cheaper. During functionalization, a cheap sulfonation method was used and sulfonation degree was quite low to the membranes with similar electrochemical properties. Wet phase inversion method is one of the well-established process which most of the current membranes are produced. Implementing wet phase inversion to cation exchange membrane preparation is also expected to reduce the cost of the membranes. In addition, thanks to porous membrane morphology, less material can be used to produce same membrane area. These membrane production strategy can be a cheaper alternative to have membranes under desired properties and cost.

In a similar study in chapter 5, cation exchange membranes were prepared by solvent evaporation and wet phase inversion method by using sulfonated polyethersulfone (SPES). The polymer with 1.19 meq/g ion exchange capacity was provided by Konishi (Japan). To prepare dense membrane

by solvent evaporation method, various SPES/PES ratios was studied considering tolerable electrochemical properties. 90/10:SPES/PES ratio was found suitable to further prepare wet phase inversion method. Co-solvent ratio, evaporation time, time in the first coagulation bath, concentration of second bath has been studied to form best performing cation exchange membrane. Superior electrochemical properties was obtained with 70/30 NMP/Acetone ratio in dope solution, 10 min in iso-propanol bath and 5.4 M NaCl as second bath concentration. Permselectivity of the membrane prepared by wet phase inversion was more sensitive to increasing salt concentration in the test solutions. Theoretical power density calculation revealed both membrane by solvent evaporation and phase inversion were competitive with the commercial ED membranes.

Overall, this study elucidated two very important challenges of the SGP-RED; (1) negative effect of using real solutions on RED performance and ion exchange membranes, (2) absence of ion exchange membranes for RED and alternative fabrication methods of cation exchange membrane.

2. Outlook

2.1. Strategies for complex solutions

It can be concluded using real solutions or complex solutions that contain other ions than Na^+ and Cl^- has a negative effect on generated RED power. One of the reason to this power reduction is increasing membrane resistance due to multivalent ions while another reason is reducing open circuit voltage because of multivalent ions.

Preparing a monovalent selective ion exchange membrane can be a good strategy to avoid penetration of multivalent ions into the membrane and screen the fixed charges. There were several attempts to prepare monovalent selective IEMs. In one of the recent work, Guler et al. (2014) prepared anion exchange membrane by coating its surface with very thin cation exchange

material[4]. In a prior study Guesmi et al. (2012) prepared monovalent selective membranes by size exclusion for different hydration radii of the ions[5]. During the membrane modification, membrane modification technique must be chosen carefully to avoid adding extra resistance by the modification itself (i.e. extra layer).

2.2. Membrane production by wet phase inversion

Removing most abundant multivalent ions (Mg^{2+}) before RED can be another strategy to avoid crucial effect of the multivalent ions. One such method must consider the extra energy load to the process. Therefore a self-driven process (i.e. Donnan dialysis) can be an option. By applying such a pretreatment, all negative effects of multivalent ions can be prevented.

Another deduction from the dissertation was fabrication of RED ion exchange membrane by wet phase inversion method can be a cheap alternative to the present production methods. Wet phase inversion is a well-established method and most of the membranes in the market is produced by this method. However, finding optimized form of the membrane by this method need a lot of research. By creating asymmetric structure in Chapter 4, membrane resistance was reduced more than an order of magnitude compared to dense form while only 10 % of permselectivity was lost. Further optimization is possible for the electrochemical properties of these membranes by reducing the thin layer thickness to the nanometer level. This can be achieved by investigating other phase inversion parameters. Moreover, more environmentally friendly solvents can be replaced instead of NMP, iso-propanol, etc.

Majority of the membranes in the market is prepared by the wet phase inversion. Implementing this method to ion exchange membrane fabrication for reverse electrodialysis can be breakthrough considering membrane cost. The proposed methods in this dissertation point out that same electrochemical properties can be achieved with even low sulfonation degree. It also underlines

that packaging is far less than dense membranes for the same unit area. Eventually, wet phase inversion membrane fabrication will benefit from less sulfonation agent consumption and less polymeric material consumption.

2.3. Integrated membrane application

RED can also be utilized in an integrated arrangement with other membrane based applications. For example, brine effluents of membrane distillation or reverse osmosis can be utilized to generate energy. Mixing these brine solutions with seawater will eliminate the high resistance of low concentration compartment when river water is used. Integration of membrane based technology helps to have energy efficient systems and use the waste streams that usually discharged to the closest basin.

Increasing number of desalination units can cause environmental problems where the brines are discharged. In these disposal regions, an instant salinity elevation can be expected. In a closed basins the effect can be higher due to poor dilution by convection. In such cases, some marine organisms that live in a stable salinity can get effected[6]. Integration of RED to the desalination process can reduce the salinity of bine before discharge and produce an extra energy than be used to power the desalination plant[7].

3. References

[1] R.A. Tufa, E. Curcio, W. van Baak, J. Veerman, S. Grasman, E. Fontananova, G. Di Profio, Potential of brackish water and brine for energy generation by salinity gradient power-reverse electrodialysis (SGP-RE), RSC Adv. 4 (2014) 42617–42623.

[2] D.A. Vermaas, J. Veerman, M. Saakes, K. Nijmeijer, Influence of multivalent ions on renewable energy generation in reverse electrodialysis, Energy Environ. Sci. 7 (2014) 1434.

[3] H.J. Cassady, E.C. Cimino, M. Kumar, M.A. Hickner, Specific ion effects on the permselectivity of sulfonated poly (ether sulfone) cation exchange membranes, J. Memb. Sci. 508 (2016) 146–152.

[4] E. Güler, W. van Baak, M. Saakes, K. Nijmeijer, Monovalent-ion-selective membranes for reverse electrodialysis, J. Memb. Sci. 455 (2014) 254–270.

[5] F. Guesmi, C. Hannachi, B. Hamrouni, Selectivity of anion exchange membrane modified with polyethyleneimine, Ionics (Kiel). 18 (2012) 711–717.

[6] Y. Fernández-torquemada, J.M. Gónzalez-correa, A. Loya, M. Ferrero, M. Díaz-valdés, J.L. Sánchez-lizaso, Dispersion of brine discharge from seawater reverse osmosis desalination plants, Desalin. Water Treat. 5 (2009) 137–145.

[7] R.A. Tufa, E. Curcio, E. Brauns, W. van Baak, E. Fontananova, G. Di Profio, Membrane distillation and reverse electrodialysis for near-zero liquid discharge and low energy seawater desalination, J. Memb. Sci. 496 (2015) 325–333.

ACKNOWLEDGEMENTS

First of all, I would like to express my gratitude towards my mother Seher Avci, my father Rustu Avci and my sister Zeynep Avci. From the beginning, they always did their best for me. I do and will appreciate their endless support always.

I would like to thank the EUDIME committee for giving me this unique opportunity which helped me broaden my perspective both scientifically and socially. I am grateful to Prof. Enrico Drioli who initiated such a program that connects people, universities, science and cultures.

I am thankful to guidance of my supervisors Prof. Efrem Curcio (University of Calabria), Prof. Ivo Vankelecom (KU Leuven) and Assoc. Prof. Wiebe de Vos. They have never denied their knowledge and assistance to me. Thanks to their critical comments and suggestions, I am able to finalize a complete and satisfactory work in my PhD.

I believe Prof. Efrem Curcio deserves a special paragraph. He listened my problems in this PhD adventure more than anybody. Besides his scientific contribution, I appreciate also his patience and friendship.

I also want to thank to my MSc supervisor Prof. Birgul Ersolmaz. She is the first person introduced me membranes. She always encouraged me to move forward in my research career.

Lastly, I want to name some special colleagues and friends made my PhD days better. Without Ramato Tufa, Khaled Amin, Patricia Ayala, Maxime Corvilain, Ozlem Haval Demirel, Timon Rijnaarts, this PhD would be incomplete.